Chronic p53-independent p21 expression deregulates replication licensing, leading to genomic instability

[1*]Panagiotis Galanos, [1,2*]Konstantinos Vougas, [3]David Walter, [2]Alexander Polyzos, [4]Apolinar Maya-Mendoza, [5]Emma J. Haagensen, [2]Antonis Kokkalis, [2]Fani-Marlen Roumelioti, [2]Sarantis Gagos, [6]Maria Tzetis, [7]Begoña Canovas, [7]Ana Igea, [8]Akshay K. Ahuja, [8]Ralph Zellweger, [1]Sofia Havaki, [6,9]Emanuel Kanavakis, [10]Dimitris Kletsas, [11]Igor B. Roninson, [12]Spiros D. Garbis, [8]Massimo Lopes, [7,13]Angel Nebreda, [2]Dimitris Thanos, [5]J. Julian Blow, [14]Paul Townsend, [3]Claus Storgaard Sørensen, [4,15,16**]Jiri Bartek, [1,2,14**]Vassilis G. Gorgoulis

1. Molecular Carcinogenesis Group, Department of Histology and Embryology, School of Medicine, University of Athens, 75 Mikras Asias Str, Athens, GR-11527, Greece.
2. Biomedical Research Foundation of the Academy of Athens, 4 Soranou Ephessiou St., Athens, GR-11527, Greece.
3. Biotech Research and Innovation Centre (BRIC), University of Copenhagen, Ole Maaloes Vej 5, Copenhagen, DK-2200, Denmark.
4. Genome Integrity Unit, Danish Cancer Society Research Centre, Strandboulevarden 49, Copenhagen, DK-2100, Denmark.
5. Centre for Gene Regulation & Expression, College of Life Sciences, University of Dundee, Dow Street, Dundee, DD1 5EH, UK.
6. Department of Medical Genetics, Medical School, University of Athens, Thivon & Levadias Str., Athens, GR-11527, Greece.
7. Institute for Research in Biomedicine (IRB Barcelona), Barcelona Institute of Science and Technology, 08028 Barcelona, Spain.

8. Institute of Molecular Cancer Research, University of Zurich, Winterthurerstrasse 190, Zurich, CH-8057, Switzerland.
9. Research Institute for the Study of Genetic and Malignant Disorders in Childhood, Aghia Sophia Children's Hospital, Thivon Str., Athens, GR-11527, Greece.
10. Laboratory of Cell Proliferation and Ageing, Institute of Biosciences and Applications, National Centre for Scientific Research 'Demokritos', Agia Paraskevi Attikis, PO Box 60228, Athens, GR-153 10, Greece
11. Center for Targeted Therapeutics, Department of Drug Discovery and Biomedical Sciences, South Carolina College of Pharmacy, University of South Carolina, Coker Life Science Building, 715 Sumter Street, Columbia, SC 29208, USA
12. Cancer and Clinical Experimental Science Units, Faculty of Medicine, Institute for Life Sciences, Center for Proteome Research, University of Southampton, University Road Southampton, Southampton, SO17 1BJ, UK
13. Institució Catalana de Recerca i Estudis Avançats (ICREA), 08010 Barcelona, Spain.
14. Faculty Institute of Cancer Sciences, University of Manchester, Manchester Academic Health Science Centre, Wilmslow Road, Manchester, M20 4QL, UK
15. Institute of Molecular and Translational Medicine, Faculty of Medicine and Dentistry, Palacky University, Hněvotínská, Olomouc, 1333/5 779 00, Czech Republic.
16. Science for Life Laboratory, Division of Translational Medicine and Chemical Biology, Department of Medical Biochemistry and Biophysics, Karolinska Institute, Stockholm, SE-171 77, Sweden.

* Authors equally contributed

** To whom correspondence should be addressed:

Jiri Bartek, E-mail: jb@cancer.dk; Tel.: +45 – 35257357

and Vassilis G. Gorgoulis, E-mail: vgorg@med.uoa.gr; or: vgorgoulis@gmail.com;

Tel.: 0030-2107462352

Key words: $p21^{WAF1/Cip1}$, p53, replication stress, senescence, oncogenes, genomic instability

Abbreviations:

aCGH: array Comparative Genomic Hybridization; BrdU: 5-bromo-2'-deoxyuridine; Cdc6: Cell division cycle 6; CDKI: Cyclin-dependent kinase inhibitor; Cdt1: Chromatin licensing and DNA replication factor 1; CRL4: Cullin4A-RING E3 ubiquitin ligase 4; DDR: DNA damage response; EdU: Ethynyl-deoxyUridine; EGF: Epidermal growth factor; EGR-1: Early growth response-1; EME1: Essential meiotic endonuclease 1; FGF2: Fibroblast growth factor-2; HJ: Holliday Junction; IPTG: Isopropyl β-D-1-thiogalactopyranoside; M/FISH: Multicoloured FISH; MCM 2-7: Mini-chromosome maintenance 2-7; MUS81: Methymethanesulphonate-MMS and ultraviolet-sensitive 81; NHEJ: Non-homologous end joining; ORC: Origin recognition complex; p21: $p21^{WAF1/Cip1}$; PFGE: Pulse field gel electrophoresis; PIP: PCNA-Interacting-Protein motif; RLFs: Replication licensing factors; Skp2: S-phase kinase-associated protein 2; SKY: Spectral karyotyping; TGF-β: Transforming growth factor-β; ssDNA: Single-stranded DNA; WGS: Whole genome sequencing.

ABSTRACT

The cyclin-dependent kinase inhibitor $p21^{WAF1/Cip1}$ (p21) is a cell-cycle checkpoint effector and inducer of senescence, regulated by p53. Yet, evidence suggests that, through a so-far obscure mechanism, p21 could also be oncogenic. We report that a subset of atypical cancerous cells strongly expressing p21 showed proliferation features. This occurred predominantly in p53-mutant human cancers suggesting p53-independent upregulation of p21 selectively in more aggressive tumour cells. Multifaceted phenotypic and genomic analyses of p21-inducible, p53-null, cancerous and near-normal cellular models showed that after an initial senescence-like phase, a subpopulation of p21-expressing proliferating cells emerged, featuring increased genomic instability, aggressiveness and chemo-resistance. Mechanistically, sustained p21-accumulation inhibited mainly the $CRL4^{CDT2}$ ubiquitin-ligase, leading to deregulated origin licensing and replication stress. Collectively, our data reveal tumour-promoting ability of p21 through deregulation of DNA replication licensing machinery, an unorthodox role to be considered in cancer treatment, since p21 responds to various stimuli including some chemotherapy drugs.

Numerous proteins involved in key cellular processes display bimodality in cancer, acting either as tumour suppressors or oncoproteins **(Supplementary Table S1)**. This phenomenon is commonly attributed to "cellular or environmental context". Elucidating the mechanism(s) underlying such context-dependent duality is essential for rational design of cancer therapy.

The cyclin-dependent kinase inhibitor (CDKI) $p21^{WAF1/Cip1}$ (p21) is a pivotal downstream effector of the tumour-suppressor p53, mediating mainly G1-phase arrest and cellular senescence in response to various stimuli.[1] Several studies suggest that p21 can also manifest oncogenic properties **(Supplementary Table S1)**. In some studies, p21's oncogenic function was credited to unconventional cytoplasmic localization of p21 which inactivates pro-apoptotic proteins.[2,3] Still, in most cases the underlying mechanism remains obscure. Notably, while p53 is frequently mutated in cancer,[4] *p21* is rarely affected genetically.[1,5] The latter would be logical if p21 operated exclusively within the p53 pathway. However, p21 is activated also by diverse p53-independent signals.[1]

Replication licensing ensures that genome replication takes place once per cell cycle,[6,7] due to the periodic expression of the replication licensing factors (RLFs) ORC, Cdt1 and Cdc6 that increase in late M to G1-phases and decrease in S/G2-phases.[8] Deregulation of the replication licensing process promotes genomic instability and tumorigenicity, mainly *via* unscheduled DNA re-replication.[9,10,11,12] Aberrant expression of RLFs occurs in diverse malignancies.[13,14] Here we present a pathophysiological mechanism demonstrating that protracted p21 expression, in a p53 loss-of-function environment, causes deregulation of the replication licensing machinery, replication stress and genomic instability.

RESULTS

A subset of atypical p21-expressing cells in advanced-stage tumours and preneoplastic lesions show signs of proliferation

In an array of human tumours we observed an intriguing relationship between p21 and the proliferation marker Ki67. While the anticipated mutually exclusive expression pattern of p21 and Ki67 was prevalent, consistent with p21's growth-inhibitory properties, there was a number of atypical cancer cells co-expressing p21 and Ki67 **(Fig. 1a-c)**. Atypical cancer cells commonly point to adverse prognosis.[15] Most of the carcinomas examined displayed p53 alterations.[13,14,16] In preneoplastic lesions with p53 aberrations we noticed a similar phenomenon **(Fig. 1d).**[17] The unexpected co-expression of p21 with Ki67 suggests either tolerance to high p21 levels, or selection under chronic p21 expression allowing for emergence of a subpopulation of p21-positive cells which regained proliferative capacity and possibly acquired enhanced aggressiveness.

p53-independent expression of p21 up-regulates replication licensing factors

To address the impact of constitutive p21 expression in a p53-deficient context we employed two doxycycline-inducible (Tet-ON) p21 expressing cellular systems: one recapitulating the cancerous stage, based on Saos2, a p53-null human osteosarcoma cell line (Saos2 $p21^{WAF1/Cip1}$ Tet-ON), and the other reflecting the precancerous stage by expressing the inducible module in the Li-Fraumeni-derived fibroblasts (MDAH041-Li-Fraumemi $p21^{WAF1/Cip1}$ Tet-ON)**(Fig. 1e).** The MDAH041 fibroblasts are p53-null human cells, considered "near"-normal, as they are

reminiscent of normal diploid cells when p53 is restored, suggesting their downstream functions are largely intact.[18]

To avoid heterogeneity of p21 expression in bulk cell cultures, we isolated p21-inducible clones that expressed p21 levels comparable to those observed *in vivo* and in cells exposed to genotoxic agents or p53-independent p21-inducing stimuli (like TGF-β)[1](**Fig. 1e)**. Apart from monitoring cell proliferation, transcriptome and proteome landscapes were examined at distinct time-points **(Fig. 1e)** after p21 induction to identify candidate pathways/networks that could over time exercise an "oncogenic" effect **(Supplementary Tables S2-S9)**. Representative high-throughput results were confirmed independently by quantitative real-time PCR and immunoblotting **(Fig. 2a, Supplementary Fig. S1ai-ii)**. As expected,[19] the p21-expressing clones reduced their growth rate and progressively acquired a senescent phenotype that peaked around day 10 **(Supplementary Fig. S1b, Video S1-S3)**. Consistent with such phenotypical changes, Gene-Ontology biological-process enrichment analyses revealed suppression of key "mitosis" factors **(Supplementary Fig. S1a, Tables S2-S9)**. Unexpectedly and counter-intuitively, the proteome analysis revealed prominent up-regulation of the RLFs: Cdt1, Cdc6 and ORC (p=1.5 x 10^{-6}); with Cdt1 protein increase being the earliest biochemical alteration among all measured parameters **(Supplementary Tables S2-S9)**. The increase of the RLFs was not accompanied by elevated mRNA, implying post-transcriptional regulation **(Fig. 2a)**. Similar results were observed in the Li-Fraumeni p21-inducible cells **(Fig. 2b)**. Notably, p21, Cdt1 and Cdc6 share the same E3 ubiquitin ligase, $CRL4^{CDT2}$.[8,20] Continuous p21 expression might saturate its enzymatic activity leading to Cdt1 and Cdc6 accumulation **(Fig. 2c)**. Consistently, SET8-methyltrasferase a known target of $CRL4^{CDT2}$,[21] was up-regulated after p21 induction **(Fig. 2c).** Shutting-off p21, after a

period of induction, led to an ubiquitylation-dependent decrease of Cdt1 **(Fig. 2d)**. Furthermore, transiently expressed mutant $p21^{PCNA}$, that avoids p21 degradation by $CRL4^{CDT2}$, did not augment Cdt1 and Cdc6 abundance **(Fig. 2e)**.[20] Also, induction of wild-type p21, but not the $p21^{PCNA}$ mutant, resulted in Cdt1 and Cdc6 accumulation **(Fig. 2f)**. Given that p21 has the strongest affinity amongst all PCNA interacting proteins (K_D ~2.5 nM)[22] these results strongly support a mechanism whereby excessive p21 saturates its own ubiquitin ligases allowing accumulation of other targets such as Cdt1 and Cdc6. The increase of G1-phase cells caused by p21 induction likely also contributed to the observed reduced RLF protein turnover, as RLFs are normally protected from degradation in G1 **(Fig. 2g)**. Moreover, Cdc6 accumulation under conditions of blocked protein synthesis was not further enhanced upon proteasome inhibition, suggesting reduced protein turnover of Cdc6 **(Fig. 2h)**, possibly also due to reduced activity of APC^{Cdh1}, another E3 ligase that targets Cdc6 for degradation.[23] Indeed, abundance of Cdh1/Fzr1, the substrate recognition and activating component of the APC was decreased **(Fig. 2i)**. Down-regulation of Cdh1/Fzr1 contributes to high E2F1 levels **(Fig. 2c, Supplementary Fig. S1ci-ii),**[24,25] thereby further boosting Cdt1 expression.[13] Enhanced Cdc6 stability was associated with Cdk2-mediated phosphorylation at Serine 54 (Cdc6-pS54) that protects Cdc6 from degradation **(Fig. 2h)**.[23] Despite p21-mediated Cdk2 activity decrease **(Supplementary Fig. S1ciii),** reduction of Cdh1/Fzr1 appears to tilt the balance in favour of Cdc6 accumulation (total and Cdc6-pS54)**(Fig. 2h)**. Notably, protein synthesis and proteasome inhibition did not restore Cdh1/Fzr1 protein levels implying regulation at the transcriptional level, a notion confirmed experimentally **(Fig. 2i)**.

Given that most clinical specimens with p21/Ki67-double-positive cells were p53-deficient, we examined whether p53 impacts the ability of p21 to regulate the

Cdt1 and Cdc6 levels, as previously suggested.[26] Indeed, p21 expression in p53-defective and p53-wild-type (wt-p53) cell types resulted in increased (**Figs. 2c;3a,d**), and suppressed (**Fig. 3b,c,e**) RLF abundance, respectively. It was suggested that p53 shields the organism from cells undergoing re-replication by triggering apoptosis.[26] Consistently, after p21 induction wt-p53 HT1080 p21-IPTG-ON cells experienced massive apoptosis, accompanied by a dramatic decrease of Cdt1 and Cdc6 **(Fig. 3e)**. Conversely, silencing of p53 suppressed apoptosis and allowed up-regulation of Cdt1 and Cdc6 **(Fig. 3e).** Similar results were obtained upon p53 restoration in the Saos2 cellular system (**Fig. 3c**).[27] Lastly, exposure to p53-independent p21-inducing stimuli such as TGF-β led to up-regulation of both RLFs (**Fig. 3d**).

Expression of p21 in p53-null cells triggers replication-stress in a Cdt1/Cdc6-dependent manner

Re-replication is a form of replication stress driven mainly by inappropriate expression of RLFs[6,8,9], leading to DNA damage and DNA damage response (DDR) activation.[6,9] Following p21 induction in both, Saos2 and Li-Fraumeni p21 Tet-ON cellular systems, chromatin loading of the MCM2-7 helicase complex increased robustly indicating that Cdt1 and Cdc6 up-regulation is functional **(Supplementary Fig. S1d)**. Flow cytometry analysis of cells double-stained for DNA content and DNA synthesis revealed a cell sub-population with DNA content greater than 4n, indicative of re-replication **(Fig. 3f-h; Supplementary Video S4).** Subsequently, DNA damage, assessed by the alkaline comet assay (total number of DNA lesions) and pulsed field gel electrophoresis (PFGE) was evident and accompanied by DDR, documented by H2AX phosphorylation (γH2AX) and increased 53BP1 foci formation **(Fig. 4a-c,d-e; Supplementary Fig. S1ei-iv)**. Strikingly, re-replication, DNA damage DDR

activation were Cdc6- and Cdt1-dependent, further suggesting that deregulated p21 causes replication stress associated with re-replication **(Fig. 4b,c,d,e).** Likewise, silencing of p21 alleviated DNA damage and DDR **(Supplementary Fig. S1eiii,eiv and S2ai-iii).** DNA damage reduction was negligible upon dNTPs supplementation, in contrast to the impact of Cdt1 and Cdc6 silencing **(Fig. 4d)**.[28] Finally, re-replication and DNA damage were significantly reduced when the $p21^{PCNA}$ mutant was employed, consistent with our model that excess p21 acts by suppressing PCNA-dependent ubiquitylation of Cdt1 and Cdc6 **(Fig. 2f,3h,4f; Supplementary Fig. S1ei,eii)**.[8]

It seems paradoxical that p21 could trigger replication stress, given its role as a potent cell-cycle inhibitor. Nevertheless, DNA combing showed that replication fork progression did not cease, but its speed was reduced **(Fig. 4g)**. In addition, replication fork asymmetry was observed, possibly related to the presence of DNA lesions impeding bi-directional fork movement **(Fig. 4g)**. Consistently, multi-parameter flow cytometry analysis of γH2AX, DNA content and DNA synthesis showed that, following p21 induction, DNA damage accumulated mainly in cells incorporating EdU, whereas depletion of Cdc6 and Cdt1 profoundly suppressed the accumulation of DNA damage in S phase **(Fig. 4h,i)**. Markedly, the cells expressing p21 demonstrated a focal PCNA pattern typical for early S phase **(Supplementary Fig. S2b)**,[29] suggesting that DNA damage occurs at a sensitive period when particularly active genes and early-replication fragile sites are replicated.[30]

p21-induced replication intermediates are processed by MUS81-EME1 and repaired by a Rad52-dependent mechanism

To further characterize p21-induced replication stress, we examined single-stranded DNA (ssDNA) formation, a common intermediate at replication-associated lesions. To this end, p21 expressing cells were incubated with BrdU under non-denaturating conditions, allowing anti-BrdU staining to selectively visualize ssDNA regions.[31] *In situ* analysis showed a strong correlation between the native BrdU staining and p21 expression **(Fig. 5a,b)** that was also associated with an increased number of foci formed by the ssDNA-binding protein RPA **(Fig. 5c)**. The ssDNA could occur either on the template or the newly synthesized (nascent) strand.[32-34] BrdU staining was absent upon short BrdU pulses, suggesting that the source of ssDNA is the template strand **(Supplementary Fig. S2c)**.

Next, we inspected replication intermediates *in vivo* by an established electron microscopy method.[35] Compared to wt-p53 U2OS cell line,[36] in unperturbed Saos2 cells we found pronounced accumulation of the so-called reversed forks (**Fig. 5di**), four-way DNA junctions that have been proposed to limit the amount of exposed ssDNA and thereby possibly mitigate the detrimental impact of gross replication stress.[36,37] Expression of p21 in the Saos2 cell model led to a marked accumulation of small replication bubbles (**Fig. 5dii**), decreased fork reversal and enhanced accumulation of ssDNA stretches at replication forks, with most small bubbles showing one side entirely single-stranded (hemireplicated)(**Fig. 5di,5diii**). Overall, these data are consistent with the notion that p21 expression in p53-defective cancer cells deregulates origin firing, leading to accumulation of ssDNA and increased replication stress.

Replication intermediates need to be resolved for replication to restart. After long periods of replication inhibition, DSBs generated by the structure-specific resolvase complex of MUS81-EME1 are required for replication restart.[32,38] We hypothesized

that sustained p21 expression may phenocopy the latter state. Indeed, MUS81-EME1 depletion caused a significant DNA damage decrease, inflicted by p21 expression, as well as reduction of EdU-positive cells harbouring signs of DNA damage **(Fig. 5e-g; Supplementary Fig. S2di-ii)**. MUS81-EME1 is considered a central player in oncogene-induced DNA damage response,[39,40] promoting homologous recombination (HR)-mediated repair of inactivated (collapsed) forks.[32] Surprisingly, we noticed that silencing of the HR recombinase Rad51 resulted in decreased γH2AX levels **(Fig. 5h)**. This finding implies a negative control over an alternative, Rad51-indepenent, repair process. Rad51 seems to exert such an effect preventing Rad52-dependent DNA repair.[41] Indeed, suppression of Rad52 was followed by increased γH2AX and cell death in both p21-induced models **(Fig. 5i,j,k)**, suggesting that Rad52 guided the repair process. Rad52 is possibly involved in error-prone microhomology-mediated repair pathways challenging genomic stability.[42,43] Interestingly, Rad51 levels were reduced upon p21 induction **(Fig. 5h; Supplementary Fig. S2diii).** Rad51 is in short supply and under stressful conditions, such as hypoxia, *Rad51* is repressed by E2F4/p130 complexes. Such complexes are recruited by p21 to mediate gene repression.[44] In accordance, the promoter of *Rad51* was occupied by E2F4 **(Fig. 5l)**, providing an explanation why Rad52 is chosen for repair in this setting.

Deregulated Cdt1 and Cdc6 link p53-independent p21 induction with senescence

Sustained p53-independent p21 expression triggered senescence, a well established antitumor barrier, in a Cdt1- and Cdc6-dependent manner **(Fig. 6a,b)**.[14,45] Consistently, no signs of senescence were observed when the $p21^{PCNA}$ inducible mutant was employed or p21 was silenced **(Fig 6c, Supplementary Fig. S2ai-iii)**. As p73, the p53 homologue, responds to DDR signaling,[46] we asked whether p73 could

operate downstream in the emerging p21–RLFs–DDR–signalling route. Indeed, p73 proved to be required for the p21-Cdt1/Cdc6-induced senescence **(Fig. 6d,e)**.

According to the oncogene-induced DNA damage concept for cancer development, the DDR-mediated anti-tumour barriers are breached at some point in tumours that progress, accompanied by genomic instability.[12] If this concept is applicable for chronic p53-independent p21 induction, then in due time the p21 expressing cells could bypass the senescence barrier generating more aggressive outgrowing clones. Cdc6 overexpression *per se* could contribute to senescence bypass by repressing the *INK4/ARF* locus,[47] encoding $p16^{INK4A}$, an indispensible factor of irreversible senescence.[48] Indeed, p21 activation led to down-regulation of both *INK4/ARF* products, $p16^{INK4A}$ and $p14^{ARF}$, undermining the durability of p21-mediated senescence **(Fig. 6f,g)**.

Senescence bypass, genomic instability and enhanced aggressiveness under protracted p21 expression

After 10 days of p21 induction in p53-deficient models the senescent phenotype gradually declined and a sub-population of proliferating p21-positive cells emerged **(Fig. 7a-e; Supplementary Video S5).** Likewise the mutually exclusive expression pattern of cyclin A-an established late S/G2 marker-[49,50] and p21 was reduced and replaced by a p21/cyclin A double-positive cell sub-population **(Fig. 7f)**. It appears that a fraction of p21 expressing cells evaded arrest/senescence, re-entering the cell cycle (*"escaped cells"*). Cdk2 activity and its stimulatory phosphorylation (p-T160) were concomitantly restored **(Fig. 7g; Supplementary Fig. S2ei)**. Notably, p21 expression in the "escaped" cells was similar to, or even higher than, that observed in

the initial phase of p21 induction, excluding the possibility that low p21 stoichiometric concentrations drive proliferation **(Fig. 7g; Supplementary Fig. S2eii-iii)**.[1] The "escaped" cells showed a dramatic reduction of p73 expression **(Fig. 7g,h).** There was no evidence of genetic or epigenetic inactivation of the *p73* locus but instead downregulation of EGR1, the main transcriptional activator of *TP73* **(Supplementary Figs. S2f,S3-5)**.[51] The nuclei in most "escaped" cells were larger than those in the cycling control cells **(Fig. 7i, Supplementary Video S5)**, a feature noticed also *in vivo* **(Fig. 1,7j; Supplementary Fig. S2g)**. Noticeably, *in vivo,* the cells displaying Ki67/p21 coexpression were also Cdc6 and/or Cdt1 positive **(Fig 7j; Supplementary Fig. S2g)**. DNA damage was also reduced in the "escaped" cells implying that a repair process took place **(Fig. 7k)**. The involvement of the MUS81-EME1 - Rad52 repair route **(Fig. 5e-k)** and the increased presence of micronuclei **(Fig. 8a)** that are considered surrogate markers of chromosomal instability, defective DDR and repair,[52] indicated, that such repair was error-prone. To gain a genome-wide view of this emerging scenario we performed aCGH, deep sequencing and M/FISH/SKY comparing the "escaped" and the un-induced cells (**Fig. 8; Supplementary Fig. S4-6, Tables S10-S12**). Cumulatively, the results from six independent biological replicates employing all three experimental procedures showed that the genomic landscape of the "escaped" cells acquired chromosomal aberrations, in the form of gains and losses (**Fig. 8b,c; Supplementary Fig. S4a-c,S5,S6, Tables S10-S12**), as well as novel translocations (**Fig. 8d,e,f; Supplementary Fig. S4c, Table S13-S15**). Notably, high frequency of microhomologies ($\geq$ 2 nucleotides)[42] was identified adjacent to the novel breakpoints in both systems, favoring a role of microhomology-mediated repair in p21-driven genomic instability **(Figure 8d,e; Supplementary Fig. S7, Table S16).** Interestingly

among the genetic lesions found were alterations reminiscent of chromoanasynthesis or chromothripsis (**Fig. 8b,c; Supplementary Table S10,S11**).[53] Given that the multifaceted chromosomal assessment showed concordant results **(Fig. 8d-g; Supplementary Fig. S4-S6)** and each experimental procedure took place at different time periods, we propose that p21 may steer a "deterministic" set of genetic events that may play a role in the behavior of the "escaped" cells. In line with this notion the transcriptome of the "escaped" cells **(Supplementary Fig. S3,S8)** demonstrated a specific non-random correlation with the genomic alterations found in these cells ($p<2.2*10^{-16}$ for the Saos2 and $p=0.0013$ for the Li-Fraumeni cells). Deregulation of the replication licensing machinery was the earliest biochemical event observed upon p21 induction, further suggesting that genomic instability "drove" the alterations in transcriptome landscapes of the "escaped" cells. While p21 is not a transcription factor it can modulate transcription in certain cases.[54] However, the fact that only 42 (7.6%) of the 553 genes and 538 (15%) of the 3507 genes found differentially expressed in the "escaped" Saos2 and Li-Fraumeni p21 Tet-ON cells, respectively, were detected in earlier time-points makes the latter scenario of more 'direct' transcriptional effects of p21 most unlikely **(Supplementary Fig. S8)**.

Importantly the "escaped" clones demonstrated enhanced anchorage-independent growth and were more invasive **(Fig. 8h,i,l)**. Furthermore, they tolerated treatment with genotoxic drugs doxorubicin and cisplatin much more efficiently, yet showed no significant difference in the response to taxol, a microtubule polymer stabilizer. The enhanced resistance to doxorubicin and cisplatin persisted even when p21 was switched off in the "escaped" cells for 10 days, documenting that this feature was a durable consequence, independent of any potential p21-mediated transient

transcriptional effect **(Fig. 8j,m)**. This chemoresistance effect was absent when p21 was silenced very early after p21 induction **(Supplementary Fig. S2ai-iii)**. A number of the transcriptionally altered genes connected with aggressive behaviour could help interpret the acquired aggressive phenotypic features **(Supplementary Fig. S3d,e, Table S17-S22)**. Furthermore, assessments of tumor-sphere formation and anchorage independent growth indicated that the "escaped" populations are enriched in cells with "stemness"-like features (**Fig. 8k, Supplementary Fig. S3d)**.

DISCUSSION

The present dataset demonstrates an unexpected p21-mediated oncogenic mechanism that is distinct from that reported for leukemia stem-cells.[55] It also explains why p21 is only transiently expressed during induction of senescence[48,56] and how p53 inactivation can tip the balance towards the p21's oncogenic function.

When free from influence of wt-p53, p21 induced by p53-independent signals causes deregulation of the replication licensing machinery triggering replication stress. We provide evidence that continuous production of p21 suppresses its degradation module, $CRL4^{CDT2}$, possibly by oversaturating it as p21 has the strongest PCNA-binding affinity **(Supplementary Fig. 8c)**,[22] thereby leaving their other targets, including Cdt1, Cdc6 and E2F1 unabated to perform their functions **(Supplementary Fig. 8c)**. Since Cdt1 expression is positively regulated by E2F1,[13] such feed-forward mechanism could further boost Cdt1 expression **(Supplementary Fig. 8c)**. Although $CRL4^{CDT2}$ seems to be the key player in this process, SCF^{Skp2} which also targets p21 and Cdt1 may also contribute.[1,22,57]

By up-regulating the pivotal replication licensing factors Cdt1 and Cdc6, the cells expressing p21 acquire the capacity to re-replicate (or "endo-reduplicate)", a phenomenon that we now explain mechanistically.[58] We show that p21-mediated genome re-replication eventually drives a chromosome-destabilizing process giving rise to descendant cells with more aggressive cancerous features **(Supplementary Fig. 8c)**. Re-replication is a form of replication stress that leads to replication fork stalling, collapse, DNA damage and eventually genomic instability.[8,9,59] Within this context, the p53 checkpoint was shown to limit re-replication, via eliminating re-replicating cells by apoptosis **(Fig. 3b)**.[26] The fact that the turn-over of p21, Cdt1 and Cdc6 is controlled by the same E3-ubiquitin ligase, $CRL4^{CDT2}$, underscores the

significance of p53 whose inactivation abolishes a cell-protective mechanism. Given that *p21* mutations are extremely rare events in cancer,[1,5] it is apparent that human cancers with mutant p53 are at risk of suffering additional deleterious, tumour heterogeneity-promoting genetic alterations by protracted operation of p21, induced through p53-independent signals **(Supplementary Fig. 1eiii-iv).**[1]

The ensuing involvement of MUS81-EME1 and the recombinase Rad52 point towards a replication-based error-prone DNA repair process.[39,40] Reduction of Rad51 elicits a switch from high-fidelity homologous recombination to a lower-fidelity repair process mediated by Rad52 that requires much less homology (micro-homology)**(Supplementary Fig. 8c)**.[41,42,60] The altered genomic landscape and the high frequency of micro-homologies found within and adjacent to the mapped breakpoints supports the latter scenario (**Supplementary Fig. S4-7**). Among the chromosomal aberrations observed, chromoanasynthesis results from replicative template-switching events **(Fig. 8b,c)**.[61] However, chromothripsis, another complex chromosomal rearrangement pattern noticed here **(Fig. 8b,c)**, is considered to be the outcome of NHEJ,[62] implying that other repair pathways, possibly non-replicative ones, may also contribute to the p21–driven genomic instability.

A question that always emerges is whether genomic alterations represent a passenger or a driver event. The strong correlation between the transcriptome and genome changes supports the latter possibility. Among the transcripts found deranged were growth factors and metalloproteinases that could account for the aggressive behavior of the "escaped" cells **(Supplementary Fig. S3; Table S17-S22)**. Notably, ID1 shown to antagonize the suppressive effects of $p16^{INK4A}$ and p21,[63] was up-regulated in the "escaped" cells **(Supplementary Fig. S3).**

Collectively, p21-driven genomic instability constitutes part of a selection trajectory to promote survival and long-term cancer evolution,[64] as illustrated mainly by the increased aggressiveness and resistance of the "escaped" cells to genotoxic agents. This tumour evolutionary scenario involves a combination of p53 defects permissible for passage through a reversible senescence phase **(Fig. 6f,g)**[48,57] that "conceals" an underlying replication stress-based/error-prone repair route that over time ensures that the "fittest and more adapted cancer cells" emerge.[10] Our results highlight the "dark side" of p21 that should be taken into consideration when designing therapeutic strategies, particularly for p53-deficient tumours, as agents used in clinical oncology, such as dexamethazone, can induce p21 in a p53-independent manner with potential detrimental effects to patients.[65]

METHODS

Methods and any associated references are available in the online version of the paper.

Acknowledgements. We would like to thank Drs A. Kotsinas, K. Evangelou, T. Liloglou and A. Georgakilas for their valuable support to this work. We would like to thank Prof A. Dutta for kindly providing the vectors with wt and PIP mutated domain of $p21^{WAF1/Cip1}$, Dr G. Blandino for the H1299 $p21^{WAF1/Cip1}$–Ponesterone-ON cells and Dr Z. Lygerou for the secondary antibodies employed in the IF analyses. We thank Mr. Roger Allsopp, Mr. Derek Coates, the Wessex Cancer Trust and Medical Research, U.K., and the University of Southampton "Annual Adventures in Research" fund for their support of the proteomics infrastructure and its use for this study. We are also indebted to the PRIDE team for the proteomics data processing−repository assistance. This work received funding from the European Union's Seventh Framework Programme (project INsPiRE), the Greek GSRT program of Excellence II (Aristeia II) the Hellenic Association for Molecular Cancer Research (HAMCR), and partial funding from the Research Institute for the Study of Genetic and Malignant Diseases in Childhood, "Aghia Sophia" Childrens Hospital, Athens, Greece, the Danish National Research Foundation (Center of excellence project CARD), the Lundbeck Foundation and the Danish Council for Independent Research.

AUTHOR CONTRIBUTIONS

PG, KV and DW: cell culture and manipulations, siRNA/plasmid/viral transfections/transductions/infections, immunoblots, cell growth, RT-PCR, ChIP, Comet, IHC and IF assays. DW and CSS: PFGE analysis. AMM and JB: DNA fiber

spreading assay. AKA, RZ, SH, ML: electron microscopy (EM) and cell culture for EM. EJH and JJB: FACS analyses. BC, AI and AN: video laps analyses. DK: MTT, soft agar, invasion and kinase assays. FMR and SG: molecular cytogenetic analyses. AP, AK and DT: deep and RNA sequencing. MT and EK: aCGH analyses. KV, SDG and PT: proteomic analysis. IR: Data analysis and cell line production. KV and AP: transcriptomic and bioinformatic analyses. JJB, CSS, AN and JB: data analysis and interpretation, and assistance in manuscript preparation. VGG: experimental design, guidance, manuscript preparation and writing.

COMPETING FINANCIAL INTERESTS

The authors declare no competing financial interests.

In the memory of Ioannis Terrovitis

REFERENCES

1. Abbas, T. & Dutta, A. p21 in cancer: intricate networks and multiple activities. *Nat Rev Cancer* **9,** 400-414 (2009).

2. Roninson, I.B. Oncogenic functions of tumour suppressor p21(Waf1/Cip1/Sdi1): association with cell senescence and tumour-promoting activities of stromal fibroblasts. *Cancer Lett* **179,** 1-14 (2002).

3. Pateras, I.S., Apostolopoulou, K., Niforou, K., Kotsinas, A. & Gorgoulis, V.G. p57KIP2: "Kip"ing the cell under control. *Mol Cancer Res* **7,** 1902-1919 (2009).

4. Rivlin, N., Brosh, R., Oren, M. & Rotter, V. Mutations in the p53 tumor suppressor gene: important milestones at the various steps of tumorigenesis. *Genes Cancer* **2,** 466-474 (2011).

5. Warfel, N.A. & El-Deiry, W.S. p21WAF1 and tumourigenesis: 20 years after. *Curr Opin Oncol* **25,** 52-58 (2013).

6. Abbas, T., Keaton, M.A. & Dutta, A. Genomic instability in cancer. *Cold Spring Harb Perspect Biol* **5,** a012914 (2013).

7. Blow, J.J. & Dutta, A. Preventing re-replication of chromosomal DNA. *Nat Rev Mol Cell Biol.* **6,** 476-486 (2005).

8. Petrakis, T.G. *et al*. Exploring and exploiting the systemic effects of deregulated replication licensing. *Semin Cancer Biol* **pii:** S1044-579X(15)30003-1 (2015) [Epub ahead of print].

9. Blow, J.J. & Gillespie, P.J. Replication licensing and cancer--a fatal entanglement? *Nat Rev Cancer* **8,** 799-806 (2008).

10. Negrini, S., Gorgoulis, V.G. & Halazonetis, T.D. Genomic instability-an evolving hallmark of cancer. *Nat Rev Mol Cell Biol* **11,** 220-228 (2010).

11. Halazonetis, T.D., Gorgoulis, V.G. & Bartek, J. An oncogene-induced DNA damage model for cancer development. *Science* **319,** 1352-1355 (2008).

12. Sideridou, M. *et al*. Cdc6 expression represses E-cadherin transcription and activates adjacent replication origins. *J Cell Biol* **195,** 1123-1140 (2011).

13. Karakaidos, P. *et al*. Overexpression of the replication licensing regulators hCdt1 and hCdc6 characterizes a subset of non-small-cell lung carcinomas: synergistic effect with mutant p53 on tumor growth and chromosomal instability-evidence of E2F-1 transcriptional control over hCdt1. *Am J Pathol* **165,** 1351-1365 (2004).

14. Liontos, M. *et al*. Deregulated overexpression of hCdt1 and hCdc6 promotes malignant behavior. *Cancer Res* **67,** 10899-10909 (2007).

15. Rosai, J.R. & Ackerman's Surgical Pathology. Elsevier, London, UK (2011).

16. Velimezi, G. *et al*. Functional interplay between the DNA-damage-response kinase ATM and ARF tumour suppressor protein in human cancer. *Nat Cell Biol* **15,** 967-977 (2013).

17. Cooks, T. *et al*. Mutant p53 prolongs NF-κB activation and promotes chronic inflammation and inflammation-associated colorectal cancer. *Cancer Cell* **23,** 634-646 (2013).

18. Agarwal, M.L., Agarwal, A., Taylor, W.R. & Stark, G.R. p53 controls both the G2/M and the G1 cell cycle checkpoints and mediates reversible growth arrest in human fibroblasts. *Proc Natl Acad Sci U S A* **92,** 8493-8497 (1995).

19. Bates, S., Ryan, K.M., Phillips, A.C. & Vousden, K.H. Cell cycle arrest and DNA endoreduplication following p21Waf1/Cip1 expression. *Oncogene* **17,** 1691-1703 (1998).

20. Havens, C.G. & Walter, J.C. Mechanism of CRL4(Cdt2), a PCNA-dependent E3 ubiquitin ligase. *Genes Dev* **25,** 1568-1582 (2011).

21. Jørgensen, S. *et al*. SET8 is degraded via PCNA-coupled CRL4(CDT2) ubiquitylation in S phase and after UV irradiation. *J Cell Biol* **192,** 43-54 (2011).

22. Gibbs, E. *et al*. The influence of the proliferating cell nuclear antigen-interacting domain of p21(CIP1) on DNA synthesis catalyzed by the human and Saccharomyces cerevisiae polymerase delta holoenzymes. *J Biol Chem* **272,** 2373-2381 (1997).

23. Duursma, A. & Agami, R. p53-Dependent regulation of Cdc6 protein stability controls cellular proliferation. *Mol Cell Biol* **25,** 6937-6947 (2005).

24. Peart, M.J. *et al*. APC/C(Cdc20) targets E2F1 for degradation in prometaphase. *Cell Cycle* **9,** 3956-3964 (2010).

25. Budhavarapu, V.N. *et al*, Regulation of E2F1 by APC/C Cdh1 via K11 linkage-specific ubiquitin chain formation. *Cell Cycle* **11**, 2030-2038 (2012).

26. Vaziri, C. *et al*. A p53-dependent checkpoint pathway prevents rereplication. *Mol Cell* **11,** 997-1008 (2003).

27. Gorgoulis, V.G. *et al*. p53 activates ICAM-1 (CD54) expression in an NF-kappaB-independent manner. *EMBO J* **22,** 1567-1578 (2003).

28. Bester, A.C. *et al*. Nucleotide deficiency promotes genomic instability in early stages of cancer development. *Cell* Apr **145,** 435-446 (2011).

29. Essers, J. *et al*. Nuclear dynamics of PCNA in DNA replication and repair. *Mol Cell Biol* **25,** 9350-9359 (2005).

30. Barlow, J.H. *et al*. Identification of early replicating fragile sites that contribute to genome instability. *Cell* **152,** 620-632 (2013).

31. Beck, H. *et al*. Regulators of cyclin-dependent kinases are crucial for maintaining genome integrity in S phase. *J Cell Biol* **188,** 629-638 (2010).

32. Petermann, E. & Helleday, T. Pathways of mammalian replication fork restart. *Nat Rev Mol Cell Biol* **11,** 683-687 (2010).

33. Neelsen, K.J. *et al*. Deregulated origin licensing leads to chromosomal breaks by rereplication of a gapped DNA template. *Genes Dev* **27,** 2537-2542 (2013).

34. Couch, F.B. *et al*. ATR phosphorylates SMARCAL1 to prevent replication fork collapse. *Genes Dev* **27,** 1610-1623 (2013).

35. Neelsen, K.J. *et al*. Visualization and interpretation of eukaryotic DNA replication intermediates in vivo by electron microscopy. *Methods Mol Biol* **1094,** 177-208 (2014).

36. Zellweger, R. *et al*. Rad51-mediated replication fork reversal is a global response to genotoxic treatments in human cells. *J Cell Biol* **208,** 563-579 (2015).

37. Neelsen, K.J. & Lopes, M. Replication fork reversal in eukaryotes: from dead end to dynamic response. *Nat Rev Mol Cell Biol* **16,** 207-220 (2015).

38. Hanada, K. *et al*. The structure-specific endonuclease Mus81 contributes to replication restart by generating double-strand DNA breaks. *Nat Struct Mol Biol* **14,** 1096-1104 (2007).

39. Neelsen, K.J., Zanini, I.M., Herrador, R. & Lopes, M. Oncogenes induce genotoxic stress by mitotic processing of unusual replication intermediates. *J Cell Biol* **200,** 699-708 (2013).

40. Murfuni, I. *et al*. The WRN and MUS81 proteins limit cell death and genome instability following oncogene activation. *Oncogene* **32,** 610-620 (2013).

41. Wu, Y., Kantake, N., Sugiyama, T. & Kowalczykowski, S.C. Rad51 protein controls Rad52-mediated DNA annealing. *J Biol Chem* **283,** 14883-14892 (2008).

42. Ottaviani, D., LeCain, M. & Sheer, D. The role of microhomology in genomic structural variation. *Trends Genet* **30,** 85-94 (2014).

43. Iraqui, I. *et al*. Recovery of arrested replication forks by homologous recombination is error-prone. *PLoS Genet* **8,** e1002976 (2012).

44. Benson, E.K. *et al*. p53-dependent gene repression through p21 is mediated by recruitment of E2F4 repression complexes. *Oncogene* **33**, 3959-3969 (2014)

45. Bartkova, J. *et al*. Oncogene-induced senescence is part of the tumorigenesis barrier imposed by DNA damage checkpoints. *Nature* **444,** 633-637 (2006).

46. Liontos, M. *et al*. Modulation of the E2F1-driven cancer cell fate by the DNA damage response machinery and potential novel E2F1 targets in osteosarcomas. *Am J Pathol* **175,** 376-391 (2009).

47. Gonzalez, S. *et al*. Oncogenic activity of Cdc6 through repression of the INK4/ARF locus. *Nature* **440,** 702-706 (2006).

48. Beauséjour, C.M. *et al*. Reversal of human cellular senescence: roles of the p53 and p16 pathways. *EMBO J* **22,** 4212-4222 (2003).

49. Woo, R.A. & Poon, R.Y. Cyclin-dependent kinases and S phase control in mammalian cells. *Cell Cycle* **2,** 316-324 (2003).

50. Pines, J. & Hunter, T. Human cyclins A and B1 are differentially located in the cell and undergo cell cycle-dependent nuclear transport. *J Cell Biol* **115,** 1-17 (1991).

51. Yu, J. *et al*. A network of p73, p53 and Egr1 is required for efficient apoptosis in tumor cells. *Cell Death Differ* **14,** 436-446 (2007).

52. Terradas, M., Martín, M., Tusell, L. & Genescà, A. DNA lesions sequestered in micronuclei induce a local defective-damage response. *DNA Repair (Amst)*. **8,** 1225-1234 (2009).

53. Holland, A.J. & Cleveland, D.W. Chromoanagenesis and cancer: mechanisms and consequences of localized, complex chromosomal rearrangements. *Nat Med* **18,** 1630-1638 (2012).

54. Perkins, N.D. *et al*. Regulation of NF-kappaB by cyclin-dependent kinases associated with the p300 coactivator. *Science* **275,** 523-527 (1997).

55. Viale, A. *et al*. Cell-cycle restriction limits DNA damage and maintains self-renewal of leukaemia stem cells. *Nature* **457**, 51-56 (2009).

56. Shay, J.W. & Roninson, I.B. Hallmarks of senescence in carcinogenesis and cancer therapy. *Oncogene* **23,** 2919-2933 (2004).

57. Nishitani, H. *et al*. Two E3 ubiquitin ligases, SCF-Skp2 and DDB1-Cul4, target human Cdt1 for proteolysis. *EMBO J* **25**, 1126-1136 (2006).

58. Niculescu, A.B. *et al*. Effects of p21(Cip1/Waf1) at both the G1/S and the G2/M cell cycle transitions: pRb is a critical determinant in blocking DNA replication and in preventing endoreduplication. *Mol Cell Biol*. **18,** 629-643 (1998).

59. Porter, A.C. Preventing DNA over-replication: a Cdk perspective. *Cell Div* **3,** 3 doi: 10.1186/1747-1028-3-3 (2008).

60. Hastings, P.J., Ira, G. & Lupski, J.R. A microhomology-mediated break-induced replication model for the origin of human copy number variation. *PLoS Genet* **5,** e1000327 (2009).

61. Zhang, C.Z., Leibowitz, M.L. & Pellman, D. Chromothripsis and beyond: rapid genome evolution from complex chromosomal rearrangements. *Genes Dev* **27,** 2513-2530 (2013).

62. Stephens, P.J. *et al*. Massive genomic rearrangement acquired in a single catastrophic event during cancer development. *Cell* **144,** 27-40 (2011).

63. Sikder, H.A., Devlin, M.K., Dunlap, S., Ryu, B. & Alani, R.M. Id proteins in cell growth and tumorigenesis. *Cancer Cell* **3,** 525-530 (2003).

64. Burrell, R.A., McGranahan, N., Bartek, J. & Swanton, C. The causes and consequences of genetic heterogeneity in cancer evolution. Nature **501,** 338-345, (2013).

65. Cha, H.H. *et al*. Glucocorticoids stimulate p21 gene expression by targeting multiple transcriptional elements within a steroid responsive region of the p21waf1/cip1 promoter in rat hepatoma cells. *J Biol Chem* **273,** 1998-2007 (1998).

66. Georgakopoulou, E.A. *et al*. Specific lipofuscin staining as a novel biomarker to detect replicative and stress-induced senescence. A method applicable in cryo-preserved and archival tissues. *Aging (Albany NY)* **5,** 37-50 (2013).

Figure legends

Figure 1. The p21 and Ki67 are co-expressed in a subset of atypical cells of high grade/poorly differentiated, advanced human carcinomas and precancerous lesions. Serial-section immunohistochemical (IHC) analysis and double immunofluorescent (IF) analysis showed co-expression of p21 and the mitotic marker Ki67 in a subset of large cancer cells with giant nuclei in **(a)** head and neck squamous cell carcinomas, **(b)** lung squamous cell carcinomas (inset depicts in higher magnification, a large atypical cell with p21/Ki67 co-expression), **(c)** urothelial carcinomas and **(d)** colon precancerous lesions (dysplasia-associated lesions or masses – DALMs), obtained from patients with ulcerative colitis, that are known to exhibit early p53 aberrations.[17] **(e)** Cellular models used to recapitulate the *in vivo* observations. Timeline of p21 induction in Li-Fraumeni $p21^{WAF1/Cip1}$ Tet-ON and Saos2 $p21^{WAF1/Cip1}$ Tet-ON cells, showing time points where main biochemical and phenotypical events occur. IHC and IF: Black and white thin arrows denote p21 and Ki67 co-expressing cells, respectively; IF: white and yellow thick arrows depict cells with mutual exclusive p21 and Ki67 expression, respectively. Scale bars in IHC panels: 50 μm, IF panels: 50 μm. Uncropped images of blots are shown in **Supplementary Fig. S9**.

Figure 2. Prolonged stimulation of p21 up-regulates and stabilizes the Replication Licensing Factors (RLFs), Cdc6 and Cdt1, at the protein level. (a) Upper panel: Heat-maps of transcriptomic and proteomic analyses, at days 2 and 4, after p21 induction in Saos2 $p21^{WAF1/Cip1}$ Tet-ON cells. Set of significant overexpressed and underexpressed genes are shown, respectively. Lower panel:

Schematic representative significant genes that are up-regulated and down-regulated, along with their biochemical function, at day 4 of $p21^{WAF1/Cip1}$ induction. **(b)** p21 induction in Li-Fraumeni $p21^{WAF1/Cip1}$ Tet-ON cells leads to Cdt1 and Cdc6 upregulation only at protein level. Lower panel: Real-time RT-PCR performed at depicted time points showing no changes in transcriptional levels of same factors (p = NS, *t*-test, error bars indicate SDs, n=3 experiments). **(c)** Cdt1 stabilization possibly via suppression of $CRL4^{CDT2}$ ubiquitin ligase complexe due to overabundance of p21 (see text for details). **(d)** Ubiquitinilation-dependent decrease of Cdt1 levels upon switching-off p21. Doxycycline induced Saos2 $p21^{WAF1/Cip1}$ Tet-ON cells were subsequently shut-off for the indicated time points and treated also with 30μM MG132 (* $p < 0.0001$, *ANOVA*, error bars indicate SDs, n=3 blots). **(e)** Saos2 cells were transfected with wild-type $p21^{WAF1/Cip1}$ and a specific $p21^{WAF1/Cip1}$ mutant [$p21^{PCNA}$: harboring Q144, M147, F150 substitutions to A in its PCNA-interacting-protein (PIP) degron motif- see panel below] abrogating its interaction with PCNA. (Empty vector: pMSCV, $p21^{WAF1}$: pMSCV-$p21^{WAF1/Cip1}$, $p21^{PCNA}$: pMSCV-$p21^{PCNA}$). **(f)** Induction of $p21^{PCNA}$ abrogated upregulation of Cdt1 and Cdc6 in Li-Fraumeni cells. Panel below (e) and (f) presents p21 protein structure and domains. Location of mutations in the PIP motif of $p21^{PCNA}$ is also depicted. **(g)** Cdt1 and Cdc6 reduced turnover due to the cell cycle profile imposed by constitutive p21 expression. **(h)** Stabilization of Cdc6 by p21 over-expression. **(i)** Real-time RT-PCR assessment of Cdh1/Fzr1 in induced and non-induced Saos2 and Li-Fraumeni $p21^{WAF1/Cip1}$ Tet-ON cells [* $p = 0.02108$ (Saos2), * $p = 0.00479$ (Li-Fraumeni), *t*-test, error bars indicate SDs, n=3 experiments]. Actin and vinculin serve as loading controls, GAPDH serves as a normalizing housekeeping gene; h: hours; MG132: proteasome inhibitor; CHX: cycloheximide. Uncropped images of blots are shown in **Supplementary Fig. S9**.

Figure 3. The status of p53 defines the ability of p21 to regulate the levels of Cdt1 and Cdc6. Immunoblots (IBs) for Cdt1 and Cdc6 in **(a)** H1299 $p21^{WAF1/Cip1}$–Ponasterone-ON and **(b)** HT1080 $p21^{WAF1/Cip1}$–IPTG-ON cells challenged with $p21^{WAF1/Cip1}$. **(c)** IBs for Cdt1 and Cdc6 in Saos2 p53 Tet-ON cells upon p53 induction. Histogram illustrates apoptosis as assessed by flow cytometry analysis (FACS) after p53 induction (* $p < 0.01$, *t*-test, error bars indicate SDs, n=3 experiments). **(d)** IBs for Cdt1 and Cdc6 in Saos2 cells treated with TGF-β (see also **Supplementary Fig. S1eiii-iv**). **(e)** FACS of HT1080 $p21^{WAF1/Cip1}$–IPTG-ON cells showed that induction of apoptosis as well as Cdt1 and Cdc6 expression are p53-dependent upon p21 expression. Corresponding IBs for p53, Cdt1 and Cdc6 in the manipulated HT1080 $p21^{WAF1/Cip1}$–IPTG-ON cells. **(f-h)** FACS analysis of (f) Saos2- and (g) Li-Fraumeni-$p21^{WAF1/Cip1}$ Tet-ON cells showed an accumulation of cells with >4N DNA content (re-replication) after p21 induction that is Cdt1 and Cdc6 dependent (* $p < 0.0001$, *ANOVA*, error bars indicate SDs, n=5 experiments). Similar analysis using (h) the $p21^{PCNA}$ mutant (see panel under **Fig. 2e,f**) abrogated re-replication (p = NS, *t*-test, error bars indicate SDs, n=5 experiments). Actin serves as a loading control. Ctl: control short-hairpin RNA; d: days; h: hours. Uncropped images of blots are shown in **Supplementary Fig. S9**.

Figure 4. Sustained p21 expression triggers replication stress and DNA damage accumulation in a Cdt1/Cdc6-dependent manner in S-phase. (**a)** PFGE depicts DNA damage upon prolonged p21 expression. **(b)** Assessment of DNA breaks with comet assays in Saos2 $p21^{WAF1/Cip1}$ Tet-ON induced for the indicated time points and

after Cdc6, Cdt1 siRNA silencing or both. Red lines in inset magnifications depict comet (moment) tails. Scale bars: 50μm. **(c)** p21 expression, in cells with non-functional p53, activated the DDR pathway in a Cdc6 and Cdt1-dependent manner (* $p < 0.0001$, *ANOVA*, error bars indicate SDs, n=3 experiments). Scale bars: 7.5μm. **(d-f)** p21–dependent Cdc6 and Cdt1 overexpression produces DNA damage and activation of the DDR pathway in a Cdc6 and Cdt1-reliant manner in Li-Fraumeni $p21^{WAF1/Cip1}$ Tet-ON cells as assessed by comet assay (d) and immunofluorescence analysis of DDR markers (e) (* $p < 0.0001$, *ANOVA* (d,e), p = NS, *t*-test (f), error bars indicate SDs, n=3 experiments) Scale bars: 50μm (d,f), 7.5μm (e). Comet assays using $p21^{PCNA}$ demonstrated absence of DNA damage (f). Red lines in inset magnifications label comet (moment) tails. Scale bars: 50μm. **(g)** Reduced replication fork speed and replication fork asymmetry upon sustained p21 expression (* $p < 0.001$, $p < 0.002$, t-test, ± indicate SDs). Saos2 $p21^{WAF1/Cip1}$ Tet-ON non-induced cells versus induced ones for 96h and after 20min consecutive labeling pulses of CIdU (red) and IdU (green) were subjected to DNA fiber spreading analysis. **(h-i)** Protracted p21 expression inflicts DNA damage in S-phase in (h) Saos2 $p21^{WAF1/Cip1}$ Tet-ON and (i) Li-Fraumeni $p21^{WAF1/Cip1}$ Tet-ON cells. FACS of p21-induced cells for 96h and co-stained for γH2AX/Propidium Iodide (PI), with or without anti-Cdc6/Cdt1 siRNA targeting, and p21-induced cells for the indicated time points and co-stained for EdU/γH2AX. Histograms for γH2AX/PI depict counts in rectangular areas (both dashed and not) (* $p < 0.0001$, *ANOVA* and *t*-test respectively, error bars indicate SDs, n=5 experiments). Actin, H2AX and vinculin serve as loading controls; Ctl: control siRNA; d: days; h: hours; NS: non-significant. Uncropped images of blots are shown in **Supplementary Fig. S9**.

Figure 5. Extended p21 over-expression mediates replication intermediate lesions accumulation that are processed by MUS81-EME1 and repaired by a Rad52-dependent mechanism. (a-c) Single-stranded DNA production in p21 over-expressing cells. Scale bars: 25μm. **(d)** i) Electron micrograph of a representative reversed replication fork from p21-induced Saos2 cells. Relevant portions of the molecules are magnified in the insets. Bars: (main images) 100 nm; (insets) 50 nm. Histogram depicts frequency of reversed replication forks in cells with or without p21 induction (brackets: total number of analyzed molecules, above each column: percentage of reversed forks). Similar results were obtained in at least one independent experiment. ii) Electron micrograph of a representative replication bubble with one side entirely single-stranded in p21-induced Saos2 cells. Bar, 100 nm. Histogram depicts frequency of replication bubbles in p21-induced vs non-induced Saos2 cells (brackets: total number of analyzed molecules; above each column: percentage of replication bubbles). Similar results were obtained in at least two independent experiments. iii) Electron micrograph of a representative replication fork in p21-induced Saos2 cells. Black arrow points an ssDNA region at the fork. Relevant portion of the molecule is magnified in the inset. Bars: (main image) 100 nm; (inset) 100 nm. Graphical distribution of ssDNA length at the junction (black arrow) in Saos2 $p21^{WAF1/Cip1}$ Tet-ON and OFF cells. Only molecules with detectable ssDNA stretches are included in the analysis. The lines show the median lengths of the ssDNA regions at the fork in the specific set of analyzed molecules (*, $p \leq 0.1$; **, $p \leq 0.01$; ***, $p \leq 0.001$; ****, $p \leq 0.0001$, Mann–Whitney *t*-test) (brackets: total number of analyzed molecules) (P: parental duplex, D: daughter duplexes, R:

regressed arm). **(e-g)** p21 mediated DNA damage is processed by MUS81 resolvase (* $p < 0.0001$, *ANOVA*, error bars indicate SDs, n=3-comet, n=5-FACS experiments). Red lines in inset magnifications label comet (moment) tails. Scale bars: 50μm. FACS of Saos2 $p21^{WAF1/Cip1}$ Tet-ON induced cells for 96h and co-stained for EdU/γH2AX, with or without anti-*MUS81* silencing (f). **(h)** Silencing of *Rad51* resulted in decreased γH2AX levels (* $p < 0.01$, t-test, error bars indicate SDs, n=3 experiments). **(i-k)** Suppression of *Rad52* was followed by increased γH2AX expression and cell death (j) (* $p < 0.0001$, *ANOVA*, error bars indicate SDs, n=3 IBs, n=3 FACS experiments). **(l)** *Rad51* promoter is occupied by E2F4 upon p21 induction as assessed by chromatin immunoprecipitation (* $p < 0.000913$, *t*-test, error bars indicate SDs, n=3 experiments). Actin and H2AX serve as loading controls; Ctl: control siRNA; h: hours. Uncropped images of blots are shown in **Supplementary Fig. S9**.

Figure 6. Deregulated up-regulation of Cdc6 / Cdt1 links p53-independent activation of p21 with senescence. (a-c) Sustained p21 expression triggers senescence in (a) Saos2 $p21^{WAF1/Cip1}$ Tet-ON (Scale bars: 20 μm) and (b) Li-Fraumeni $p21^{WAF1/Cip1}$ Tet-ON cells (Scale bars: 10 μm) (error bars indicate SDs, n=3 experiments). (c) Induction of $p21^{PCNA}$ expression in Li-Fraumeni cells does not yield similar results (error bars indicate SDs, n=3 experiments). Cells grown on coverslips were stained to assess the senescent phenotype applying the Sudan Black-B protocol and SA-b-gal.[66] (Scale bars: 10 μm) **(d-e)** IBs depict p73 status upon siRNAs targeting *Cdc6* and *Cdt1*, as well as the efficiency of anti-*p73* treatment in (d) Saos2 $p21^{WAF1/Cip1}$ Tet-ON and (e) Li-Fraumeni $p21^{WAF1/Cip1}$ Tet-ON cells. **(f-g)** Sustained p21 expression reduces $p14^{ARF}$ and $p16^{INK4A}$ protein levels in (f) Saos2 $p21^{WAF1/Cip1}$

Tet-ON and (g) Li-Fraumeni p21$^{WAF1/Cip1}$ Tet-ON cells. Actin serves as loading control; Ctl: control siRNA; h: hours. Uncropped images of blots are shown in **Supplementary Fig. S9**.

Figure 7. Prolonged p21 expression, in cells with p53 loss of function, overrides the senescence barrier. (a-b) Morphological features observed by inverted-phase contrast microscope of escaped cells (20 days of p21 expression) in (a) Saos2 p21$^{WAF1/Cip1}$ Tet-ON and (b) Li-Fraumeni p21$^{WAF1/Cip1}$ Tet-ON cells. Scale bars: 15μm **(c-d)** BrdU incorporation is restored to almost similar levels to non-induced cells after bypass of senescence in (c) Saos2 p21$^{WAF1/Cip1}$ Tet-ON and (d) Li-Fraumeni p21$^{WAF1/Cip1}$ Tet-ON cells (error bars indicate SDs, n=3 experiments). Scale bars: 50μm. **(e)** EdU incorporation increases in p21$^{WAF1/Cip1}$ expressing cells after 20 days of continuous induction (error bars indicate SDs, n=5 experiments). **(f)** Appearance of a significant sub-population of Cyclin A and p21 positive cells at 20 days of induction. Double IF analysis of induced cells for Cyclin A and p21 at indicated time points (error bars indicate SDs, n=3 experiments). Scale bars: 50μm. **(g-h)** Restoration of Cdk2 activity and reduction of p73 levels [(g) Saos2 p21$^{WAF1/Cip1}$ Tet-ON and (h) Li-Fraumeni p21$^{WAF1/Cip1}$ Tet-ON cells] in cells "escaping" senescence (see also **Supplementary Fig. S2e**). **(i)** Escaped cells depict larger nuclei than non-induced ones (staining with DAPI). Histogram depicts average values in the OFF versus ON groups, after 20 days (* $p < 0.0001$, *t*-test, error bars indicate SDs, n=3 experiments). Scale bars: 7.5μm. **(j)** Serial-section immunohistochemical (IHC) analysis showed co-expression of p21, Ki67 and Cdc6 in atypical cancer cells in clinical samples (see also **Supplementary Fig. S2g**). (Scale bars: 50μm). **(k)** DNA damage was significantly

reduced in escaped cells. Comet assays showed DNA breaks in cells induced for the indicated time points (error bars indicate SDs, n=3 experiments). Red lines in magnifications of insets label comet (moment) tails (TM) for length comparison. (Scale bars: 50μm). Actin serves as loading control; h: hours. Uncropped images of blots are shown in **Supplementary Fig. S9**.

Figure 8. p21 expressing cells that have overridden (escaped) the senescence barrier demonstrate genomic instability and aggressive behaviour. (a) Increased frequency of micronuclei in "escaped" cells. Arrows depict micronuclei (* p = 0.0098, *t*-test, error bars indicate SDs, n=3 experiments). **(b-c)** High resolution array-Comparative Genomic Hybridization (aCGH) analysis between "escaped" p21 expressing (b) Saos2- and (c) Li-Fraumeni-p21$^{WAF1/Cip1}$ Tet-ON cells and non-induced ones at 30 days. Blue and red coloured regions along the chromosome ideograms depict genome gains and losses, respectively. Upper (b-c) insets depict narrow subchromosomal areas exhibiting alternating regions of gains or losses with retention regions in between (in blue and red shadowed rectangles, respectively), possibly indicating events of chromoanasynthesis and chromothrypsis, respectively. **(d-e)** Circos diagrams depicting novel (d: N=175 and e: N=44) chromosomal rearrangements in "escaped" Saos2 (d) and Li-Fraumeni (e) p21$^{WAF1/Cip1}$ Tet-ON expressing cells, respectively, revealed by whole-genome sequencing (human chromosomes are located at the perimeter). A representative breakpoint is also shown. **(f-g)** Representative results showing the high correlation between the aCGH, deep sequencing (Next Generation Sequencing: NGS) and cytogenetic analyses results in "escaped" p21 cells. Dashed-white rectangles denote gains or losses, while yellow

ones depict translocations. **(h,i,l)** Escaped Saos2 p21$^{WAF1/Cip1}$ Tet-ON cells (45 days of p21 expression) form more and larger colonies than cells with non-induced (OFF) p21 in soft agar assay (h). Escaped (i) Saos2- and (l) Li-Fraumeni- p21$^{WAF1/Cip1}$ Tet-ON cells also display invasion capability (p = 0.00373, p = 0.034, p = 0.000314 (h,i); p = 0.0015 (l), *t*-test, error bars indicate SDs, n=3 experiments). **(j,m)** Escaped (j) Saos2 p21$^{WAF1/Cip1}$ Tet-ON and (m) Li-Fraumeni p21$^{WAF1/Cip1}$ Tet-ON cells (at 20d) exhibit increased genotoxic drug tolerance. Histogram depicting increased IC_{50} values by escaped cells upon treatment with Doxorubicin and Cis-platinum (p = 0.91, p < 0.0001, p = 0.013 (j); p = 0.38, p = 0.0005, p = 0.0001 (m); *ANOVA*, error bars indicate SDs, n=3 experiments). **(k)** Escaped Saos2 p21$^{WAF1/Cip1}$ Tet-ON cells (20d) demonstrate cancer stem cell-like traits as assessed by tumorsphere formation assay coupled to soft agar growth (p = 0.0045, p = 0.0151, *t*-test, error bars indicate SDs, n=3 experiments).

Supplementary materials legends

Supplemental Figure legends

Suppl. Figure 1. (a) Representative factors affected by p21$^{WAF1/Cip1}$ induction at transcriptional and translational level. Representative real-time RT-PCR analyses to validate the high-throughput expression results (see also **Fig. 2**) ($p < 0.01$, t-test, error bars indicate SDs, n=3 experiments). **i.** Mitotic factors: PLK1, AURKB, BUB1, BUB1B, KIF23 and the pro-apoptotic factor GLIPR1 along with the suppressor of the p21$^{WAF1/Cip1}$ mediated effects ID1 are transcriptionally downregulated at the indicated time points in Saos2 p21$^{WAF1/Cip1}$ Tet-ON induced cells. Growth factor IGFBP5, the ion channel encoding gene TRPM8 and the poly-A binding protein PABPC1L are upregulated. PBGD: Porphobilinogen deaminase (house-keeping gene) **ii.** Representative immunoblots that validate the proteome. Actin serves as a loading control. (PLK1: Polo-like kinase-1; AURKB: Aurora kinase B; BUB1: budding uninhibited by benzimidazoles 1 homolog; KIF23: kinesin family member 23; GLIPR1: Glioma pathogenesis related 1; ID1: inhibitor of DNA binding 1; IGFBP5: insulin-like growth factor binding protein 5; TRPM8: transient receptor potential cation channel subfamily M member 8; PABPC1L: poly(A) binding protein, cytoplasmic 1-like; TOP2A: topoisomerase 2A)

(b) Timeline of senescence appearance in Saos2 p21$^{WAF1/Cip1}$ Tet-ON and Li-Fraumeni p21$^{WAF1/Cip1}$ Tet-ON induced cells. Activation of the senescence barrier occurs at approximately day 3 of induction in both cellular systems and increases gradually, reaching its highest value at around day 10, while no signs of senescence are evident in untreated cells grown for the same time period (as corresponding graphs depict). p21$^{WAF1/Cip1}$ was confirmed by western blot (upper right panel).

(c) i. E2F1 is upregulated while Chk1 is activated upon prolonged $p21^{WAF1/Cip1}$ induction. Lysates from Saos2 $p21^{WAF1/Cip1}$ Tet-ON cells, after treatment with 1μg /ml Doxycycline for the depicted time points, were separated by SDS-PAGE and immunoblotted to detect the indicated proteins (n=3 experiments). **ii.** Silencing of Cdh-1/FZR-1 leads to increase in E2F1 expression in the p53 null H1299 cells. **iii.** A decline of Cdk2 activity is observed following $p21^{WAF1/Cip1}$ induction. Histogram depicting decreased Cdk2 activity at days 4 after $p21^{WAF1/Cip1}$ induction.

(d) MCM2-7 chromatin loading is increased following $p21^{WAF1/Cip1}$ induction in Saos2 and Li-Fraumeni cells. i. Diagram describing cell fractionation experimental algorithm. **ii-iii.** All fractions were separated by SDS-PAGE and were analyzed by IB in Saos2 cells (ii) and Li-Fraumeni cells (iii). Lamin-B serves as fractionation control, while β-tubulin as loading control (n=3 experiments). **iv.** FACS analysis of MCM2 chromatin loading in induced Saos2 $p21^{WAF1/Cip1}$ Tet-ON cells versus non-induced (red dots, -ve: control experiment with no MCM2 antibody; blue dots, +ve: experiment with MCM2 antibody) (* $p < 0.05$, ** $p < 0.01$, *** $p < 0.005$, t-test, error bars indicate SDs, n=3 experiments).

(e) Re-replication and DNA damage was significantly lesser in Saos2 cells infected with $p21^{PCNA}$ mutant. i. Comet assays showed DNA breaks in cells infected with the indicated constructs (see also **Fig. 4b,d,f**) ($p < 0.0001$, *ANOVA*, error bars indicate SDs, n=3 experiments). Red lines in magnifications of insets label comet (moment) tails for length comparison. **ii.** FACS analysis of the corresponding treatments. **iii.** DNA damage is $p21^{WAF1/Cip1}$ dependent in Saos2 cells treated with TGF-β (n=3 experiments). **iv.** $p21^{WAF1/Cip1}$ dependent DNA damage, in Saos2 cells treated with TGF-β, is exerted via

Cdc6/Cdt1 mediated replication stress. (Empty vector: pMSCV, $p21^{PCNA}$: mutant $p21^{WAF1/Cip1}$ harboring Q144, M147, F150 substitutions to A in its PIP degron motif)

Suppl. Figure 2. (a) Silencing of $p21^{WAF1/Cip1}$ in induced (ii.) Saos2- and (iii.) Li Fraumeni- $p21^{WAF1/Cip1}$ Tet-ON cells alleviates replication stress, DNA damage, senescence induction and enhanced resistance to chemotherapeutic drugs. Timeline of the experimental procedure is also depicted (i.). cells (p = NS, t-test or *ANOVA*, error bars indicate SDs, n=3 experiments) Bars: 20μm (IF), 30μm (comet)

(b) PCNA staining patterns reveal that sustained $p21^{WAF1/Cip1}$ expression, in cells with non-functional p53, "traps" cells mainly in early S-phase. IF analysis for assessing PCNA staining patterns in non-induced and 96h induced cells. Histograms depict average of observed patterns in the induction conditions employed (n=3 experiments). Scale bars: 10 μm.

(c) Absence of nascent ssDNA in Saos2 $p21^{WAF1/Cip1}$ Tet-ON expressing cells. $p21^{WAF1/Cip1}$ expression was induced for 96h with 1μg/ml doxycycline. The newly synthesized DNA was labeled for 20 min with 10 μM BrdU. 2 mM HU and 5 μM ATRi were added after the BrdU pulse as indicated for 2 h. After the indicated treatments, cells were fixed and stained with antibodies against BrdU without DNA denaturation to selectively detect nascent-strand ssDNA (n=3 experiments). Bars: 40μm.

(d) $P21^{WAF1/Cip1}$ mediated DNA damage is processed by MUS81 resolvase. i. IF staining of DDR markers (53BP1 and γH2AX) in Saos2 $p21^{WAF1}$ Tet-ON induced cells for 96h, with or without anti-*MUS81* siRNA targeting. Histogram depicts quantification of 53BP1 and γH2AX foci/cell (p < 0.01, t-test, error bars indicate SDs, n=3

experiments). Bars: 20μm. **ii.** DNA damage assessed by comet assay after prolonged expression in Li-Fraumeni $p21^{WAF1}$ Tet-ON cells ($p < 0.01$, t-test, error bars indicate SDs, n=3 experiments). Bars: 50μm. **iii.** Silencing of the homologous repair recombinase *Rad51* resulted in decreased γH2AX levels in Li-Fraumeni $p21^{WAF1}$ Tet-ON cells ($p < 0.0001$, *ANOVA*, error bars indicate SDs, n=3 experiments).

(e) Sustained expression of $p21^{WAF1/Cip1}$ in cells with non-functional p53 leads to restoration of Cdk2 activity in "escaped" cells. i. Following an initial decline (days 2-12) Cdk2 activity is increased in "escaped" cells (after day 20) ($p < 0.01$, t-test, error bars indicate SDs, n=3 experiments). **ii.** Expression levels of $p21^{WAF1/Cip1}$ in the "escaped" (i) Saos2 and (ii) Li-Fraumeni $p21^{WAF1}$ Tet-ON cells were similar or even higher sometimes (see **Fig. 7g**) to those observed in the initial phase of $p21^{WAF1/Cip1}$ induction (n=3 experiments).

(f) Potential mechanisms involved in p73 down regulation in the "escaped" Saos2- and Li-Fraumeni-p21 cells. (see Fig 7g) i. Absence of p73 promoter methylation and genetic loss at *TP73* locus (1p36.33) (**see Supplementary Fig. S5, S6; Supplementary Table 4)**. Representative result from real-time PCR followed by high resolution melting (HRM) analysis is depicted (n=3 experiments). Ctl DNA: SssI methylated and unmethylated control DNA. **ii.** Bioinformatic analysis employing Ingenuity software revealed potential factors that regulate p73 expression and activity. EGR-1 (Early Growth Response-1) is a potent transcriptional up-regulator of p73.[51] In turn, p73 can also transcriptionally induce EGR-1exprresion, forming a positive feed-back loop. HECW2 (HECT, C2 αnd WW Domain Containing E3 Ubiquitin Protein Ligase 2) expression stabilizes p73 protein levels via mono-ubiquitination,[75] while PRKACB (Protein Kinase

A Catalytic Subunit β) decreases p73 transactivation and intramolecular interaction capacity.[76] **iii.** *TP73* gene locus organization and structure of p73 protein with HECW2 and PRKACB interacting domains. Yellow rectangles: transcribed non translated *TP73* exons; Blue rectangles: transcribed *TP73* exons; Green rectangle: P1 promoter of *TP73* gene; Blue ovals: EGR-1 biding sites. TDA: transactivation domain; DBD: DNA binding domain; OD: oligomerization domain; SAM: sterile alpha-motif domain. **iv-v.** Analysis of EGR-1, HECW2 and PRKACB expression status in "escaped" Saos2 $p21^{WAF1/Cip1}$ cells at mRNA (iv.) and protein (v.) level validated results obtained from high-throughput transcriptome analysis (**Supplementary Fig. S3**) (n=3 experiments). CREB phosphorylation was examined as a proof-of-concept for PRKACB activity. **vi.** Analysis of EGR-1 at mRNA and protein level in "escaped" Li-Fraumeni $p21^{WAF1/Cip1}$ cells (n=3 experiments). **vii.** Potential mechanism for p73 downregulation in "escaped" cells. Decreased levels of EGR-1 possibly represent the main reason for low p73 expression.[49] Additionally, high levels of PRKACB decreases p73 transactivation and intramolecular interaction abilities,[76] counteracting the ability of high HECW2 expression to stabilize p73 via mono-ubiquitination.[75] High PRKACB levels may contribute further to p73 down-regulation by interfering with the positive feed-back loop between ERG-1 and p73.[76] **(g)** Serial-section immunohistochemical (IHC) analysis showed co-expression of $p21^{WAF1/Cip1}$, Ki67 and Cdc6/Cdt1 in atypical cancer cells in head and neck carcinomas, urothelial carcinomas and precancerous lesions. Actin serves as a loading control.

Suppl. Figure 3. Differentially expressed genes whose expression status affects cancer according to literature in Saos2- and Li-Fraumeni-p21 cells. Expression status

of genes associated with cancer progression (see also **Supplemental Table 8**). **(a)** Timeline of experimental planning of transcriptome analyses. **(b)** Principal Component Analysis (PCA) of the differentially expressed genes depicting the majorly different gene expression signatures over the (19540 in Saos2- and 25376 in Li-Fraumeni cells) transcripts analysed. **(c)** Validation of representative factors in "escaped" (ON) cells versus non-induced (OFF) Saos2 and Li-Fraumeni cells. Representative real-time RT-PCR analyses, validating the high-throughput expression analysis ($p < 0.01$, t-test, error bars indicate SDs, n=3 experiments). **(d)** Relative expression levels given as log-2-ratios of differentially expressed genes ($p < 0.05$) of the "escaped" vs OFF-cells, whose expression status (up or down-regulated) is reported to promote carcinogenesis. Arrow (←) denotes genes conferring cancer stemness (see also **Supplemental Tables 8Aa, 8Ba**). Lysates from non-induced and escaped Saos2 $p21^{WAF1/Cip1}$ Tet-ON cells were immunoblotted to verify representatively the expression of the LGR5 cancer related stemness gene. **(e)** Differentially expressed genes whose expression status either promotes or suppresses cancer according to literature. Relative expression levels given as log-2-ratios of differentially expressed genes ($p < 0.05$) of the "escaped" vs OFF-cells. The lengths of the "encircled" lines depict the intensity of expression. Uncropped images of blots are shown in **Supplementary Fig. S9**.

Suppl. Figure 4. "Escaped" Saos2 $p21^{WAF1/Cip1}$ cells exhibit increased genomic instability relative to non-induced cells. (a) Timeline of experimental planning of genomic analyses. **(b)** Overview of all array-CGH (aCGH) analyses results. In total 41 aberrations were found involving all chromosomes (except 9, 12, 14 and 15). The

aberrations included 19 gains and 22 losses (**Supplemental Table 5**). The majority of aberrations were concentrated in chromosomes 3, 10 and X (**Supplemental Table 5**). [reference (Ref) genome is from un-induced (0 d) Saos2 $p21^{WAF1/Cip1}$ cells] **(c)** Novel clonal rearrangements distinguish the "escaped" Saos2 $p21^{WAF1/Cip1}$ (ON) from OFF cells [arrows indicate lost (in OFF cells) or rearranged (in "escaped"-ON cells) chromosomes]. The $p21^{WAF1/Cip1}$-OFF cells (control), were mainly hypotriploid (51-56 chromosomes) and shared most of the characteristic structural chromosome aberrations of the parental Saos2 cell line.[77] Compared to these cells, the "escaped" ones remained hypo-triploid but displayed at least 10 novel clonal structural or numerical aberrations affecting chromosomes 2, 3, 5, 8, 11, 13, 14, 20, 21 and X. Large portions of chromosomes X and 13 were lost in 90% of the "escaped" cells, confirming the aCGH findings. Furthermore, differential imbalances of chromosomes 5 and X between Saos2 $p21^{WAF1/Cip1}$ ON cells and the controls were observed. In "escaped" (ON) cells, an additional inverted duplication of 5p was also present in 90% of the examined nuclei. **(d)** The Saos2 $p21^{WAF1/Cip1}$ ON cells exert significantly higher rates (two fold) of random structural CIN/chromosome as compared to controls. (CIN:chromosomal instability) **(e)** Genomic distribution of breakpoints of random structural chromosome anomalies. Telomeric regions were found to be most frequently affected by fusions, translocations and tandem duplications of large chromosome segments. As unidentified ones were categorized the non-telomeric, non centromeric genomic rearrangements in which the cytogenetic bands of their breakpoints remained obscure. **(f)** "Escaped" Saos2 $p21^{WAF1/Cip1}$ cells exhibit increased karyotypic aberrations relative to non-induced cells. Comparative pseudo-colored M-FISH/SKY karyograms of 10 non-induced (OFF) Saos2 $p21^{WAF1/Cip1}$ cells

(588 chromosomes) and 10 “escaped” (ON) ones (639 chromosomes), for the evaluation of whole genome structural CIN at the 350 chromosome band level. Arrows (and dashed rectangles) indicate representative non-clonal random structural rearrangements (unique anomalies encountered in a single cell). The “escaped” $p21^{WAF1/Cip1}$ expressing cells (ON) displayed significantly higher rates of genome wide, random structural chromosomal rearrangements. *ON cells (upper panel):* Cells #1 and #7, from the Saos2 $p21^{WAF1/Cip1}$ OFF panel, represent a minor subclone (20%) of this population because they share a distinctive clonal rearrangement affecting a derivative chromosome X and a deletion of 12p. Cells #3 and #5, belong to a second subclone of the control cells that is characterized by a deletion of a rearranged chromosome 19. The remaining non-induced (OFF) $p21^{WAF1/Cip1}$ cells #2, #4, #6, #8 and #10, display a homogeneous karyotypic constitution and represent the major clone. Cell #9 is a polyploid product of whole genome endoreduplication of the major clone of Saos2 $p21^{WAF1/Cip1}$ OFF cells. *“Escaped”-OFF cells (lower panel):* Cells #1 and #6 differ from the majority of the “escaped” (ON) population as they share a clonal inverted duplication of the long arm of chromosome 21. In addition, cells #2, #4 and #9, have lost a marker translocation der(9)t(5;9) that was replaced by a deletion 9p and acquired clonally an extra translocated der(22)t(20;22). A unique subclonal finding in Cells #3 and #10, of the “escaped” (ON) cells is the persistence of der(9)t(5;9). Cells #5 and #7 represent two different endoreduplicated ON subclones, characterized by unique structural abnormalities of chromosomes 7, 15 and 6 respectively. The karyotypic constitution of cell #8, resembles that of the control population and justifies the presence of an additional subclone that does not exceed the 10% of the “escaped” (ON) cells. (CIN:chromosomal instability)

Suppl. Figure 5. Correlation between aCGH replicates and corroboration with the cytogenetically detectable novel clonal alterations in Saos2 p21 cells (* see also Fig. 8f). [reference (Ref) genome is from un-induced (0 d) Saos2 $p21^{WAF1/Cip1}$ cells]

Suppl. Figure 6. Correlation between aCGH and deep sequencing in Saos2 (a) and Li-Fraumeni (b) cells (Next Generation Sequencing: NGS) analyses. Data from all replicates for each application were averaged before comparison.

Suppl. Figure 7. Novel chromosomal rearrangements and microhomology regions related to breakpoints in (a) Saos2 and (b) Li-Fraumeni cells. Circos diagrams depicting novel chromosomal rearrangements in "escaped" Saos2 (a) and Li-Fraumeni (b) $p21^{WAF1/Cip1}$ Tet-ON expressing cells, respectively, revealed by deep sequencing (human chromosomes are located at the perimeter). Data from two biological replicates are depicted. Circos in the middle show shared chromosomal rearrangements by the two Saos2 (a) and Li-Fraumeni (b) $p21^{WAF1/Cip1}$ Tet-ON biological replicates. Breakpoints employing micro-homologies ≥ 4bp in Saos2 (a) and ≥ 3bp in Li-Fraumeni (b) $p21^{WAF1/Cip1}$ Tet-ON cells, respectively, are also presented below each circus diagram. Cytogenetic analyses (see also **Supplementary Fig S4**) confirming NGS data on breakpoints in the "escaped" Saos2 $p21^{WAF1/Cip1}$ Tet-ON expressing cells are also shown. Asterisk (a) denotes breakpoint that does not encompass a micro-homology. Continuous red line denotes position of breakpoints.

Suppl. Figure 8. Relative gene expression levels (log-2 ratios) at 12, 48, 96-hs after p21$^{WAF1/Cip1}$ -induction as well as "escaped" versus OFF cells in (a) Saos2 and relative gene expression levels (log-2 ratios) at 10 days after p21$^{WAF1/Cip1}$ -induction as well as "escaped" versus OFF in (b) Li-Fraumeni cells. (c) Proposed model. (a) A: Relative expression of all measured genes (19540) at each depicted time-point as compared to non-induced cells (OFF). The correlogram at the bottom which presents the Pearson correlation coefficient among the 4 datasets illustrates that the overall gene-expression of the "escaped" population is non-correlated (~0 correlation coefficient) to the three prior time points, which amongst them present a high degree of correlation. B: Relative expression of genes presenting differential expression ($p < 0.05$) in the "escaped" cells in relation to OFF (553 genes). The correlogram at the bottom illustrates the absence of correlation between the "escaped" population with the three early time points (12, 48, 96hs). C: Relative expression of commonly differentially expressed genes (42) ($p < 0.05$) at each time-point versus OFF. Special interest present the 16 out of 42 marked genes whose expression levels are reversed at the "escaped" population in comparison to the previous time-points.

(b) The same heatmaps are presented for Li-Fraumeni cells. A: Relative expression of all measured genes (25367) at each depicted time-point as compared to non-induced cells (OFF). B: Relative expression of genes presenting differential expression ($p < 0.05$) in the "escaped" cells in relation to OFF (3507 genes). C: Relative expression of commonly differentially expressed genes (538) ($p < 0.05$) at each time-point versus OFF. Special interest present the 154 out of 538 marked genes whose expression levels are reversed at the "escaped" population in comparison to 10-days.

(c) Proposed model depicting prolonged p53-independent p21 oncogenic action (for additional mechanistic explanations see discussion). Under "physiological" conditions, MDM2 degrades p53.[4,10] Dashed lines depict ineffective pathway.

Suppl. Figure 9. Unprocessed blots/gels employed in the current manuscript.

Supplementary References

75. Miyazaki, K. *et al*. A novel HECT-type E3 ubiquitin ligase, NEDL2, stabilizes p73 and enhances its transcriptional activity. *Biochem Biophys Res Commun* **308,** 106-113 (2003).

76. Hanamoto, T. *et al*. Identification of protein kinase A catalytic subunit beta as a novel binding partner of p73 and regulation of p73 function. *J Biol Chem* **280,** 16665-16675 (2005).

77. Sakellariou, D., Chiourea, M., Raftopoulou, C. & Gagos, S. Alternative lengthening of telomeres: recurrent cytogenetic aberrations and chromosome stability under extreme telomere dysfunction. *Neoplasia* **15,** 1301-1313 (2013).

Supplementary Table legends

Supplementary Table 1. Molecules involved in key cellular processes displaing bimodality in cancer.

Supplementary Table 2. Results from mRNA expression analysis on the Illumina whole-genome HumanHT-12 v4.0 arrays, showing gene transcripts affected at 12h, 48h and 96h upon sustained $p21^{WAF1/Cip1}$ induction in Tet-ON, Saos2-$p21^{WAF1/Cip1}$. Three biological replicates (n=3) were used for the analysis of each time point (0,12,48,96).

Supplementary Table 3. Results from mRNA expression analysis on the Illumina whole-genome HumanHT-12 v4.0 arrays, showing gene transcripts (from Table 2) responding early upon sustained $p21^{WAF1/Cip1}$ induction in Tet-ON, Saos2-$p21^{WAF1/Cip1}$. Three biological replicates (n=3) were used for the analysis of each time point (0,12,48,96).

Supplementary Table 4. Results from mRNA expression analysis on the Illumina whole-genome HumanHT-12 v4.0 arrays, showing gene transcripts (from Table 2) responding at intermediate time upon sustained $p21^{WAF1/Cip1}$ induction in Tet-ON, Saos2-$p21^{WAF1/Cip1}$. Three biological replicates (n=3) were used for the analysis of each time point (0,12,48,96).

Supplementary Table 5. Results from mRNA expression analysis on the Illumina whole-genome HumanHT-12 v4.0 arrays, showing gene transcripts (from Table 2) responding late upon sustained $p21^{WAF1/Cip1}$ induction in Tet-ON, Saos2-$p21^{WAF1/Cip1}$. Three biological replicates (n=3) were used for the analysis of each time point (0,12,48,96).

Supplementary Table 6. Results from proteomic analysis showing proteins affected at 12h, 48h and 96h upon sustained p21WAF1/Cip1 expression in Tet-ON, Saos2 $p21^{WAF1/Cip1}$. Two biological replicates (n=2) were used for the analysis of each time point (0,12,48,96).

Supplementary Table 7. Results from proteomic analysis showing proteins (from Table 6) responding early upon sustained p21WAF1/Cip1 expression in Tet-ON, Saos2 $p21^{WAF1/Cip1}$. Two biological replicates (n=2) were used for the analysis of each time point (0,12,48,96).

Supplementary Table 8. Results from proteomic analysis showing proteins (from Table 6) responding at intermediate time point upon sustained $p21^{WAF1/Cip1}$ expression in Tet-ON, Saos2 $p21^{WAF1/Cip1}$. Two biological replicates (n=2) were used for the analysis of each time point (0,12,48,96).

Supplementary Table 9. Results from proteomic analysis showing proteins (from Table 6) responding late upon sustained $p21^{WAF1/Cip1}$ expression in Tet-ON, Saos2 $p21^{WAF1/Cip1}$.

Two biological replicates (n=2) were used for the analysis of each time point (0,12,48,96).

Supplementary Table 10. Results from aCGH analysis in Li-Fraumeni p21$^{WAF1/Cip1}$ Tet-ON "escape" vs non-induced (OFF) cells (Agilent G3 CGH 1M arrays). "Escaped" cells acquired chromosomal aberrations, in the form of gains and losses that ranged in size from approximately 1.75Kb to 92Mb.

Supplementary Table 11. Results from aCGH analysis in Li-Fraumeni p21$^{WAF1/Cip1}$ Tet-ON "escape" vs non-induced (OFF) cells (Agilent G3 CGH 1M arrays). "Escaped" cells acquired chromosomal aberrations, in the form of gains and losses that ranged in size from approximately 1.26Kb to 48Mb.

Supplementary Table 12. Results from cytogenetic analysis in "escaped" (ON) Saos2 p21$^{WAF1/Cip1}$ cells depict the predominance of breakpoints of random re-arrangements in Fragile Sites (FSs).

Supplementary Table13. Chromosomal coordinates of breakpoints found by deep sequencing in Saos2 p21$^{WAF1/Cip1}$ Tet-ON.

Supplementary Table 14. Chromosomal coordinates of breakpoints found by deep sequencing in Li-Fraumeni p21$^{WAF1/Cip1}$ Tet-ON.

Supplementary Table 15. Shared breakpoints found in the Saos2 p21$^{WAF1/Cip1}$ Tet-ON (from Table 13) and Li-Fraumeni p21$^{WAF1/Cip1}$ Tet-ON (from Table 14), respectively.

Supplementary Table 16. Breakpoints with microhomologies (MHs) in Saos2 p21$^{WAF1/Cip1}$ Tet-ON (69% of total breakpoints) and Li-Fraumeni p21$^{WAF1/Cip1}$ Tet-On (~71-80% of total breakpoints) escaped cells. (red line denotes position of breakpoint)

Supplementary Table 17. Molecules displaying up-regulation in Saos2 p21$^{WAF1/Cip1}$ Tet-ON escaped cells, stemness abilities and proposed to promote carcinogenesis.

Supplementary Table 18. Molecules displaying up-regulation in Saos2 p21$^{WAF1/Cip1}$ Tet-ON escaped cells and proposed to promote carcinogenesis.

Supplementary Table 19. Molecules found expressed in Saos2 p21$^{WAF1/Cip1}$ Tet-ON escaped cells and proposed to display a bimodality in cancer promotion.

Supplementary Table 20. Molecules displaying up-regulation in Li-Fraumeni p21$^{WAF1/Cip1}$ Tet-ON escaped cells, stemness abilities and proposed to promote carcinogenesis.

Supplementary Table 21. Molecules displaying down-regulation in Li-Fraumeni p21$^{WAF1/Cip1}$ Tet-ON escaped cells.

Supplementary Table 22. Molecules found expressed in Li-Fraumeni p21$^{WAF1/Cip1}$ Tet-ON escaped cells and proposed to display a bimodality in cancer promotion.

Supplementary Table 23. List of antibodies employed in immunohistochemistry, immunofluorescence, immunoblotting, immunoprecipitation and chromatin.

Supplementary Table 24. Primers and annealing temperatures used in real time (RT)-PCR and ChIP analyses.

Supplementary Table 25. Statistics Source Data.

Supplementary Video legends

Supplementary Video 1. Dividing Saos2 p21$^{WAF1/Cip1}$ Tet-OFF cells.

Supplementary Video 2. Senescent Saos2 p21$^{WAF1/Cip1}$ Tet-ON cells.

Supplementary Video 3. Senescent and dying Saos2 p21$^{WAF1/Cip1}$ Tet-ON cells.

Supplementary Video 4. Re-replicating Saos2 p21$^{WAF1/Cip1}$ Tet-ON cells.

Supplementary Video 5. Escaped and diving Saos2 p21$^{WAF1/Cip1}$ Tet-ON cells.

ONLINE MATERIALS and METHODS

Tumour specimens

Formalin-fixed, paraffin-embedded sections from 20 head-neck carcinomas, 30 urothelial bladder carcinomas, 30 lung carcinomas and 5 dysplasia-associated lesions or masses (DALMs) from patients with ulcerative colitis, that exhibit early p53 aberrations,[17] were analyzed after local ethical committee approval and have been previously described.[14,67] Patients had not undergone any chemo-, immune- or radiotherapy.

Cell lines and culture treatments

Cell lines were maintained in DMEM (Invitrogen) with 10% FCS (Invitrogen), 2mM l-glutamine (Invitrogen), and 100μg/ml penicillin and streptomycin (Invitrogen) at 37°C and 5% CO_2.

$p21^{WAF1}$ and $p21^{PCNA}$ were subcloned from pRc-CMV vectors into the pLVXTRE3G, correspondingly. Inducible Li-Fraumeni $p21^{WAF1/Cip1}$ Tet-ON, Li-Fraumeni and Saos2 $p21^{PCNA}$ Tet-ON cells were generated by introducing the $p21^{WAF1}$- and the $p21^{PCNA}$-carrying pLVXTRE3G vectors in MDAH041 (Li-Fraumeni) fibroblasts and Saos2, respectively.[18] Clones with clear $p21^{WAF1}$ and $p21^{PCNA}$ expression were selected.

Tet-ON inducible cell lines were treated with 1μg/ml Doxycycline (Applichem) and HT1080 $p21^{WAF1}$-9 cells with 100μM IPTG (Ambion). Saos2 and MDA-MD-234 were treated with 5ng/ml TGF-β, while MCF cells with 2μM doxorubicin (Sigma).

Microphotographs were obtained with an inverted microscope (Axiovert S100; Carl Zeiss) equipped with CP-Achromat objectives and a charge-coupled device IRIS

colour video camera (SSC-C370P; Sony), using Image Pro Plus v3.0 (Media Cybernetics) software.

No cell lines used in this study were found in the database of commonly misidentified cell lines that is maintained by ICLAC and NCBI Biosample. All cell lines have been authenticated by STR profiling and are regularly tested to exclude mycoplasma contamination.

siRNA transfections and retrovirus infections

Cdc6, Cdt1, Rad52, Rad51, $p21^{WAF1}$, CDH1/FZR-1 (Thermo Scientific) and Mus81, p73 (Santa Cruz) siRNA gene silencing was performed as described, following manufacturer's instructions.[46]

Saos2 cells were transiently infected with pMSCV, pMSCV-$p21^{WAF1}$ or pMSCV-$p21^{PCNA}$ (a mutant $p21^{WAF1}$ harboring Q144, M147, F150 substitutions to A in its PIP degron motif) vectors using the Phoenix helper-free retrovirus producer cell line as previously described.[49]

Immunohistochemistry (IHC)

IHC was performed as previously published using the UltraVision LP Detection System (#TL-060-HD, Thermo Scientific) according to manufacturer's instructions.[67] Primary antibodies are described in **Supplementary Table S23**. Evaluation and controls for Ki-67 and $p21^{WAF1}$ have been previously described.[67]

Indirect Immunofluorescence (IF)

Indirect IF analysis was performed as previously published.[14] Primary antibodies are described in **Supplementary Table S23.** Secondary antibodies were Alexa Fluor® 488 goat anti-rabbit (Invitrogen, #A11034, 1:500) and Alexa Fluor® 568 goat anti-mouse (Invitrogen, #A110-31, 1:500). Image acquisition of multiple random fields was automated on a ScanR screening station (Olympus, Germany) and analyzed with ScanR (Olympus, Germany) software, or a Zeiss Axiolab fluorescence microscope equipped with a Zeiss Axiocam MRm camera and Achroplan objectives, while image acquisition was performed with AxioVision software 4.7.1.

Electron microscopy (EM) analysis of DNA RIs in human cells

The procedure was performed as previously described.[35] Images were obtained with a transmission electron microscope (Tecnai G2 Spirit; FEI; LaB6 filament; high tension ≤120 kV) equipped with a side mount charge coupled device camera (2,600×4,000 pixels; Orius 1000; Gatan, Inc), processed with DigitalMicrograph Version 1.83.842 (Gatan, Inc.) and analyzed with Image J (National Institutes of Health).

Protein extraction, cell fractionation and immunoblotting

Protein extraction and cell fractionation (**Supplementary Fig. S1di**) was performed as described before.[12,14] Primary antibodies are described in **Supplementary Table S23.** Thirty μg of protein from total extracts or 1μg of histones per sample, were adjusted with Laemmli Buffer (Sigma) and loaded on acrylamide/bis-acrylamide gels. Gel electrophoresis, transfer to PVDF membrane (Millipore) and signal development with nitro blue tetrazolium/5-bromo-4-chloro-3-indolylphosphate (NBT/BCIP) solution (Molecular Probes) or chemiluminescence were performed as previously

described.[12] Alkaline phosphatase conjugated anti-mouse or anti-rabbit secondary antibody (1:5000 dilution)(Promega) were used.

***In vivo* ubiquitin assay**

Saos2 $p21^{WAF1}$ cells were treated with MG-132 proteasome inhibitor (MERCK) for 3h at 30μM at the time points indicated **(Fig. 2d)**. Cells were lysed in RIPA buffer [50mM Tris-HCL pH 8.0, 150mM NaCl, 0.1% SDS, 1% Sodium Deoxycholate, 1% Triton X-100, protease inhibitor cocktail (Thermo Scientific), phosphatase inhibitor cocktail (Thermo Scientific), N-ethylameleimide deubiquitinase inhibitor (Applichem)]. Protein lysates were precleared with protein G agarose beads (Millipore) for 1hr and then incubated with G-protein beads bound to Cdt1 antibody (**Supplementary Table S23**) for 2 hours at 4°C. Beads were washed 3 times in RIPA buffer containing protease, phosphatase and deubiquitinase inhibitors, as above. Protein was eluted from beads with 2x SDS-β-mercaptoethanol sample buffer, boiled for 8 min and loaded on polyacrylamide gels for SDS-PAGE as described above. Blots were blocked for 1h in 5% BSA in TBS-0.1% (v/v) Tween-20 solution at room temperature (RT). Membranes were incubated overnight with Cdt1 antibody (**Supplementary Table S23**) in 5% BSA in TBS supplemented with 0.1% (v/v) Tween-20, followed by a 1h incubation with HRP- conjugated anti-mouse secondary antibody (R&D Systems) at 1:1.000 dilution at RT. Signal development was performed with NBT/BCIP solution (Molecular Probes) according to manufacturer's instructions.

CDK2 kinase activity

For each sample, 50mg of total-cell protein extract was precleared for 2h at 4°C with 5mg of rabbit immunoglobulin G (anti-Cdk2) or 5mg of mouse immunoglobulin G (anti-cyclin B1) prebound to protein A-Sepharose (Upstate-Millipore). Precleared lysates were collected and incubated with anti-Cdk2, or anti-cyclin B1with mixing for 2h at 4°C. Protein A-Sepharose was added, and the samples were mixed for 2h at 4°C. The immunoprecipitates were washed twice with TBS and twice with kinase buffer (100mM Tris [pH 7.4], 20mM MgCl2, 2mM dithiothreitol) and incubated with 5mg of histone H1 (Boehringer Mannheim), 15nM ATP for 10min at 25°C. Samples were incubated with Malachite Green Reagent for 30min (Cdk2 and cyclin B1). Kinase assay mixtures were quantified at 620nm by subtracting negative control.

Chromatin immunoprecipitation (ChIP) assay

ChIP assay was performed as previously described.[12] A 100bp fragment in the *Rad51* promoter and a 110bp amplicon, located approximately 1000bp from the transcription start site (**Fig. 5l**), were amplified. Primers and annealing temperatures are provided in **Supplemental Table S24**. PCR reactions containing 1% of the total chromatin extract used in the immunoprecipitation reactions were used as inputs.

Comet Assay

Was performed as previously described.[12] Cells were observed under a Zeiss Axiolab fluorescence microscope equipped with a monochrome CCD camera. Analysis was conducted with Cometscore software (Tritek). All experiments were performed in triplicates.

Pulsed-field gel electrophoresis (PFGE)

Has been previously described.[31]

DNA fiber spreadings

Was conducted as previously described with slight modifications.[45] Briefly, Saos2 $p21^{WAF1/}$ cells were grown in the presence or absence of doxycyclin for 4 days and then pulsed-labeled with 25μM CldU for 20min, and then labelled with 250μM IdU for 20min. Cells were then harvested and lysed on glass slides in spreading buffer. The DNA was denatured and stained with rat anti-BrdU/CldU (1:1000, OBT0030F, Immunologicals Direct) and mouse anti-IdU/BrdU (1:500, clone B44, Becton Dickinson) primary antibodies.

Isolation of nucleic acids and bisulfate treatment

DNA extraction was performed as previously described.[14] RNA was extracted with the RNeasy Mini Kit (#74104, Qiagen). For assessing DNA methylation levels of p73 promoter, 1 μg DNA was bisulphite-converted using the EZ-DNA Methylation Gold kit (ZymoResearch) as per supplier's guidelines and eluted in 30 μl of elution buffer.

cDNA preparation and real time (RT)-PCR

cDNA generation and real-time reverse transcription PCR (RT-PCR) analysis was run as described before.[67] DNA methylation levels for p73-promoter were assessed by high-resolution-melting (HRM) analysis. The reaction was performed in a StepOne Real time machine (Life Technologies) using Universal Master Mix II w/o UNG containing SYBR (Life Technologies) and 200nM primers. A dissociation (melt)

curve programme followed at the end of 40 cycles. Signal analysis was carried out using the StepOne v2.3 software. SssI methylated and unmethylated DNA was run in parallel as positive and negative controls, respectively. Primer sequences and annealing temperatures are provided in **Supplemental Table S24**. Results are presented as n-fold changes for the various time points after $p21^{WAF1}$ induction versus the values of the non-induced sample. Mean value was calculated from three independent measurements.

Flow cytometric analysis (FACS)

Cell cycle analysis was assessed on a FACS Calibur (Becton-Dickinson) as described before.[14]

For BrdU pulse-chase proliferation assays, cells were pulse-labeled with 10μM BrdU (Roche) for 1h, fixed in 70% ethanol, and incubated in 2M HCl for 30min. Cells were incubated with mouse antibody against BrdU (1:100) for 1h. For EdU analysis, cells were either pulsed for 10min or 24h with 10μM EdU. Cells were fixed in 70% ethanol and incubated with mouse anti–γ-H2AX (1:100, Millipore) or mouse anti-$p21^{WAF1}$ (1:100, SantaCruz) for 30 min, followed by further 15 min incubation with Alexa Fluor 488 anti–mouse IgG (1:100, Invitrogen) or anti-mouse E-Phycoerythrin (1:100, Invitrogen). EdU was detected with a Click-iT EdU Cell Proliferation Assay kit (Invitrogen).

For MCM2 staining, cells were washed once in wash buffer (1% (w/v) BSA in PBS), while unbound MCM2-7 was extracted in freshly prepared CSK buffer (10mM HEPES, 100mM NaCl, 3mM MgCl2, 1mM EGTA, 300mM sucrose, 1% (w/v) BSA, 0.2% (w/v) Triton-X100, 1mM DTT, 1mM PMSF, 10ng/ml Pepstatin, 10ng/ml

Leupeptin and 10ng/ml Aprotinin) on ice for 10min. Extracted cells were then fixed in 2% (v/v) paraformaldehyde in PBS for 10min at 37°C, washed twice in wash buffer and stored in wash buffer at 4°C until staining. CSK extracted fixed cells were permeabilised in ice cold 70% (v/v) ethanol for 10min at RT, washed in wash buffer and incubated for 1h at RT with mouse monoclonal anti-human MCM2 (BM28 #610700, BD Biosciences) diluted 1:500 in wash buffer. Cells were then washed once in wash buffer and incubated for 30min at RT in the dark with Alexa Fluor 488 goat anti-mouse secondary antibody (#A-11029, Life Technologies) diluted 1:500 in wash buffer, before being washed twice in wash buffer and re-suspended in 50µg/ml 7-AAD (7-aminoactinomycin D, Life Technologies) diluted in wash buffer. Samples were analysed using FACS Canto (Becton Dickinson) and the BD FACS DIVA software (BD Biosciences). Data analysis was performed using Flowjo (version 7.6.5, Tree Star Inc.). To quantify G1 MCM levels, the Flowjo software was used to gate on cells with a G1 DNA content and then the mean, median, 95th and 99th percentiles of the Alexa Fluor 488 levels in the G1 cells were calculated for each replicate; the data is presented with the background mean, median, 95th percentile or 99th percentile subtracted to correct for the increase in auto-fluorescence.

Senescence staining

Control (OFF) and induced (ON) Saos2 $p21^{WAF1}$ Tet-ON or MDAH041 $p21^{WAF1}$ Tet-ON cells were fixed in 1% paraformaldehyde and then processed for Sa-β-gal or Sudan Black B staining and counterstained with nuclear fast red, as described elsewhere.[66] Only cytoplasmic staining was scored as positive signal.

MTT Assay

Cytotoxicity was estimated by the MTT (3-[4,5-dimethylthiazol-2-yl]-2,5-diphenyltetrazolium bromide) assay.[12] Data from three independent measurements were averaged and corresponding s.d. is also reported.

Soft agar and invasion assays

Soft agar and invasion assays were performed as described elsewhere.[12] Experiments were performed in three independent replicates.

***In vitro* tumoursphere formation assays**

Saos2 Tet-On $p21^{WAF1}$ (10^4) cells were suspended in sphere formation medium [serum-free DMEM/F12 medium (Invitrogen) supplemented with 20ng/ml epidermal growth factor (EGF, Sigma), 20ng/ml basic fibroblast growth factor (bFGF, Sigma) and 1×B27 supplement (Invitrogen)] in ultra-low attachment 6-well plates (Corning). Cells were cultured under 5% CO_2 at 37°C for 15 days. Number of generated spheres were counted and sized under an inverted microscope (Axiovert S100; Carl Zeiss) equipped with CP-Achromat objectives. Subsequently, medium with spheres were aspirated, treated with trypsin to dissociate cells from spheres and centrifuged **(Fig. 8k)**. Cell pellets were resuspended in fresh medium, counted and plated on soft agar, as previously described.[12] Data from three independent measurements from this combined procedure were averaged and corresponding s.d. is reported.

Molecular Cytogenetics

Molecular cytogenetics analyses were conducted as previously reported.[12] Cytogenetic analyses were performed using a 63× magnification lens on a fluorescent Axio-Imager Z1, Zeiss microscope, equipped with a MetaSystems charge-coupled device (CCD) camera and the MetaSystems Isis software.

High-throughput analyses

Proteomics

Total protein was extracted from 2 biological replicates of non-induced and 12h, 48h and 96h induced Saos2-p21^{WAF1} Tet-ON cells (n=2 epxeriments), where protein Digestion and 8plex-iTRAQ Labeling was performed as previously described.[16] The pooled whole sample was split in two equal parts lyophilized and stored at -20^{o}C. To the first half of the aforementioned iTRAQ labeled sample High-pH Reverse Phase (RP) Peptide Fractionation was performed as previously described.[16] The second half of the iTRAQ labeled peptides was fractionated with Hydrophilic Interaction Chromatography as previously described.[68]

The individual high-pH RP and HILIC peptide fractions were analysed by LC-MS/MS followed by database searching as previously described.[69]

High-throughput whole genome analyses

aCGH analysis. Genomic DNA from 30 days induced and non-induced Saos2- and Li-Fraumeni-p21^{WAF1} Tet-ON cells was extracted using the BioRobot® M48 System (Qiagen) and the MagAttract® DNA Blood Midi M48 Kit (Qiagen). Quality and quantity of the DNA samples was determined on a NanoDrop ND-1000 UV-VIS spectrophotometer.

Agilent Human Genome CGH 4x180K [to analyze Saos2-p21^{WAF1} escaped and non-induced, each comprising 2 biological replicates, (n=2)] and 1x1MK [to analyze i. Saos2-p21^{WAF1} escaped and non-induced, each comprising 2 biological replicates, (n=2) and ii. Li-Fraumeni-p21^{WAF1} escaped and non-induced, each comprising 3 biological replicates, (n=3)] microarrays were used. Labelling and hybridization was carried out according to manufacturer's guidelines. Data were processed using Feature Extraction 10.7.3.1 and analysed using Cytogenomics 2.7.22.0 software (Agilent) with the following settings: Algorithm: ADM-1, Threshold: 6.7, with a minimum of 4 probes for a region to be included. Centralization and fuzzy zero corrections were applied to remove putative variant intervals with small average $\log_2$ ratios as compared to the noise-level which was determined by the system.

Whole genome sequencing (WGS). Genomic DNA from two biological replicates (n=2) obtained at 30 days induction and non-induction of Saos2- and Li-Fraumeni-p21^{WAF1} Tet-ON cells, respectively, was used for WGS. The library preparation and the WGS were carried out in the Greek Genome Center (GGC) of Biomedical Research Foundation of Academy of Athens (BRFAA) and in EMBL Genecore facility.

WGS was performed achieving 20-30x coverage of the human genome with paired-end sequencing (2x150 and 2x100 bp). Quality control was performed with fastqc software[70] and alignment to the human genome (GRCh37/hg19 version) was performed with bowtie2 algorithm.[71] Samtools[72] was used to convert sam files to bam and for sorting bam files. Breakdancer software[73] (breakdancer-1.1-2011_02_21 version) was utilized in order to identify SV (intra- and inter-chromosomal translocations, deletions, insertions and inversions).

Use of breakdancer with default parameters led to identification of new inter-chromosomal translocations in "ON" versus "OFF" cells in both cell types (**Supplementary Fig. S7)**. In order to identify microhomology regions in the inter-chromosomal translocations observed in both systems we used the coordinates from the breakdancer output and extended 30bp on both sides of the breakpoint-junction. Clustal W was used for aligning the regions around the breakpoint junctions. Microhomology regions identified on the breakpoint spanned from 2-38bp.

RNA-seq analysis. RNA was collected from non-induced, 10 days (10d) and "escaped" Li-Fraumeni p21$^{WAF1/Cip1}$ Tet-ON cells [six biological replicates for escaped (n=6) and four biological replicates for non-induced (n=4)]. RNA-seq library preparation and analysis procedure was performed as described before.[8]

Expression microarray analysis. Total RNA was isolated from three biological replicates of non-induced and 12h, 48h and 96h induced Saos2-p21^{WAF1} Tet-ON cells (n=3), using RNeasy Total RNA kit (Qiagen) following the manufactures instructions. Microarray analysis was performed by the microarray unit of CBM Core Facility Italy (http://www.cbm.fvg.it) using Illumina's Whole-Genome Expression Beadchip. Integrity of total RNA was evaluated using capillary electrophoresis (Bioanalyzer 2100, Agilent) and quantified using a Nanodrop 1000. Aliquots of RNA (250 ng) samples were amplified according to specifications of the Illumina® TotalPrep™ RNA Amplification Kit (Ambion) to produce a pool of biotin-labeled RNA corresponding to the polyadenylated (mRNA) fraction. The cRNA samples were applied to whole-genome HumanHT-12 v4.0 arrays (Illumina) and hybridized according to manufacturer's specification. The hybridization images signal intensities were extracted and background subtracted using Illumina Inc. BeadStudio (v3.3.7). Data were checked for the Illumina internal quality control.

Total RNA was extracted from the non-induced and "escaped" Saos2-p21^{WAF1} Tet-ON cells using Trizol (Life Technologies) and choloroform/isoamyl alcohol (49:1) [four biological replicates for escaped (n=4) and three biological replicates for non-induced (n=3)]. Targets were prepared using the GeneChip Whole Transcriptome (WT) Plus reagent kit and hybridized to Affymetrix GeneChip Human Transcriptome array 2.0 (HTA 2.0). The obtained Saos2-p21^{WAF1} transcriptome profile was compared with the Li-Fraumeni p21^{WAF1} transcriptome profile obtained by RNA-seq.

Bioinformatic analysis

Transcriptome and Proteome analyses from non-induced, 12h, 48h and 96h induced Saos2-p21^{WAF1} Tet-ON cells. Protein and gene ratios (time-point/time-0) were log(2) transformed and centered. Statistically significant differentially expressed genes and proteins ($p<0.05$) where determined by the log-2 ratios normal distributions and ANOVA plus Kruskal-Wallis (Kruskal Wallis only for the transcriptome data-set where n=3) since there were more than one time-points. All calculations were performed with R. The "Gene-Set Enrichment Analysis" on the Gene-Ontology Biological-Process set was performed as previously described.[16] Pathway visualization for all data-sets was performed with Ariadne Genomics Pathway Studio v9.0. Proteomics dataset were deposited at ProteomeXchange Consortium via the PRIDE partner repository with the dataset identifier PXD001289.

Transcriptome analysis from non-induced and "escaped" Saos2-p21^{WAF1} Tet-ON cells. Affymetrix .CEL files were normalized with the Robust Multi-array Average (RMA) algorithm. Data were further analyzed by Principal Component Analysis and one-way ANOVA ($p<0.05$). Differentially expressed transcripts were analyzed using

the Ingenuity Pathway Analysis software considering all direct and indirect relationships obtained only from experimentally verified information.

WGS and aCGH data comparison. To compare the WGS data with the aCGH one regarding DNA copy number aberrations in "escaped" (ON) cells versus control (OFF) cells (both in Saos2 and Li-Fraumeni systems), the WGS data were processed as follows: a) Genomic regions presenting less than 10-times coverage were filtered out to ensure data high-quality, b) The log2 of the ratio of the normalized reads in the "escaped" cells over the normalized number of reads in the control-cells was calculated, c) For each chromosome the aforementioned log2-ratios underwent DNA copy-number segmentation analysis utilizing the circular binary segmentation algorithm through the Bioconductor package "DNAcopy".[74]

Assessment of randomness in the overlap between the transcriptomics and aCGH data through Monte-Carlo simulation. To access the probability of the observed overlap between the transcriptionally affected genes (DNA-microarray for Saos2 and RNA-Seq for Li-Fraumeni p21 Tet-ON systems) and the genes present in the significantly affected genomic regions (aCGH data) being due to chance, a Monte-Carlo simulation approach was utilized. Specifically, the genes present on the corresponding transcriptomics analysis platform (DNA-microarray for Saos2 and RNA-Seq for Li-Fraumeni) were randomly sampled 10^4 times with a sample size equal to the number of significantly regulated genes. For each random sampling the overlap with the genes present in regions exhibiting genomic aberrations according to aCGH was calculated. The distribution of the number of overlaps was found to be normal according to the Kolmogorov-Smirnov test for normality; hence the p-value of the observed overlap in our data was calculated. That p-value represents the probability of the observed overlap to belong to the distribution of the randomly

generated overlaps, therefore being due to chance alone. All statistical analysis was carried out with R. All datasets were deposited at: http://www.ncbi.nlm.nih.gov/geo/query/acc.cgi?token=oxcrwqcsppktped &acc=GSE62166, with GSE62166 dataset identifier for Affymetrix transcriptomics and aCGH, while SRP045212 identifier corresponds to WGS dataset.

Pathway Analysis. Proteomics and transcriptomics data were analyzed with Ariadne Pathway Studio v9.0 as previously described.[16]

Statistics and Reproducibility

Parametric (*t*-test and one-way ANOVA) and non-parametric tests (Mann–Whitney and Kolmogorov-Smirnov test for normality), were used for hypothesis testing with p-values <0.05 considered as significant.

ONLINE REFERENCES

67. Evangelou, K. *et al*. The DNA damage checkpoint precedes activation of ARF in response to escalating oncogenic stress during tumorigenesis. *Cell Death Differ* **20,** 1485-1497 (2013).

68. Delehouzé, C. *et al*. CDK/CK1 inhibitors roscovitine and CR8 downregulate amplified MYCN in neuroblastoma cells. *Oncogene* **33**; 5675-5687 (2014)

69. Papachristou, E.K. *et al*. The shotgun proteomic study of the human ThinPrep cervical smear using iTRAQ mass-tagging and 2D LC-FT-Orbitrap-MS: the detection of the human papillomavirus at the protein level. *J Proteome Res* **12,** 2078-2089 (2013).

70. Ramirez-Gonzalez, R.H. *et al*. StatsDB: platform-agnostic storage and understanding of next generation sequencing run metrics. Version 2. *F1000Res*. **2,** 248 (2013).

71. Langmead, B. & Salzberg, S.L. Fast gapped-read alignment with Bowtie 2. *Nat Methods* **9,** 357-359 (2012).

72. Li, H. *et al*. 1000 Genome Project Data Processing Subgroup. The Sequence Alignment/Map format and SAMtools. *Bioinformatics* **25,** 2078-2079 (2009).

73. Chen, K. *et al*. BreakDancer: an algorithm for high-resolution mapping of genomic structural variation. *Nat Methods* **6,** 677-681 (2009).

74. Venkatraman, E.S. & Olshen, A.B. A faster circular binary segmentation algorithm for the analysis of array CGH data. *Bioinformatics* **23,** 657-663 (2007).

Figure 1

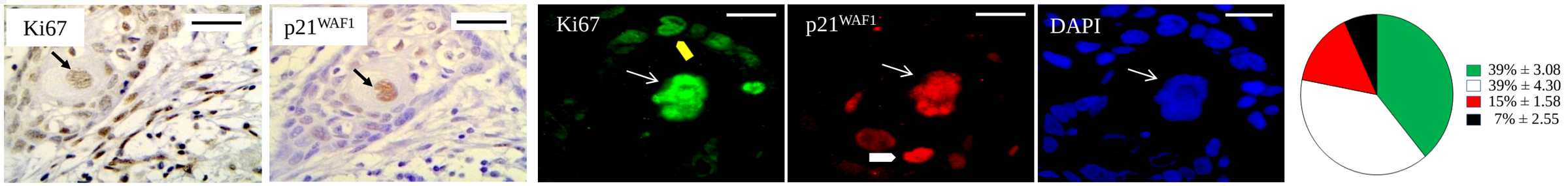
Serial section IHC analysis

IF analysis

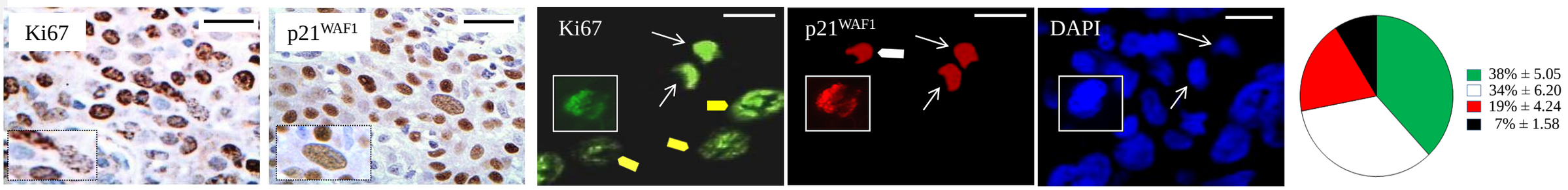
Cumulative data

p21WAF1-/Ki67+
p21WAF1-/Ki67-
p21WAF1+/Ki67-
p21WAF1+/Ki67+

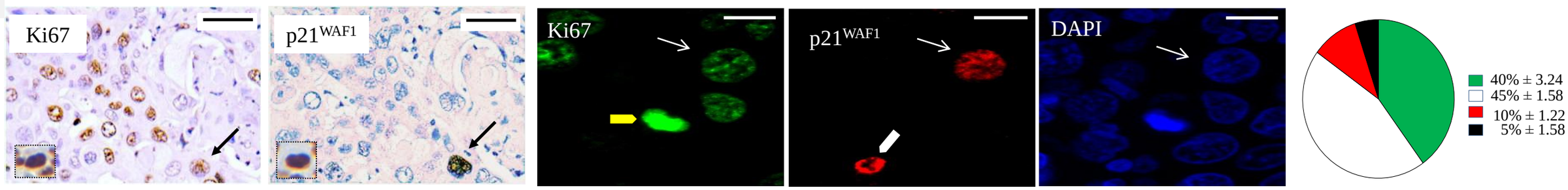
a. Head&Neck Ca



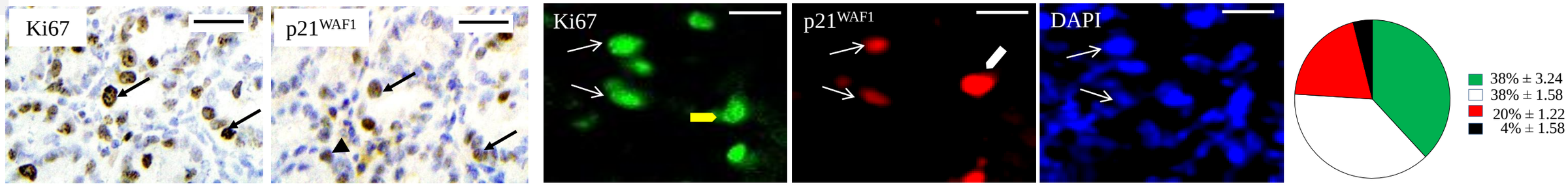
b. Lung Ca



c. Urothelial Ca



d. Precancerous



e.

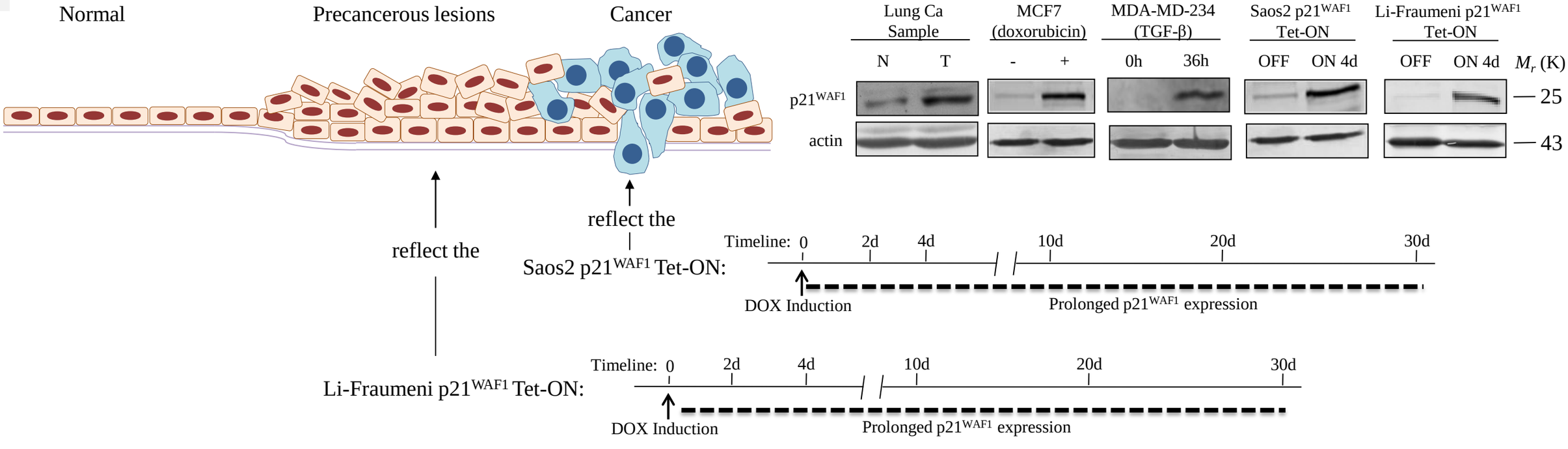
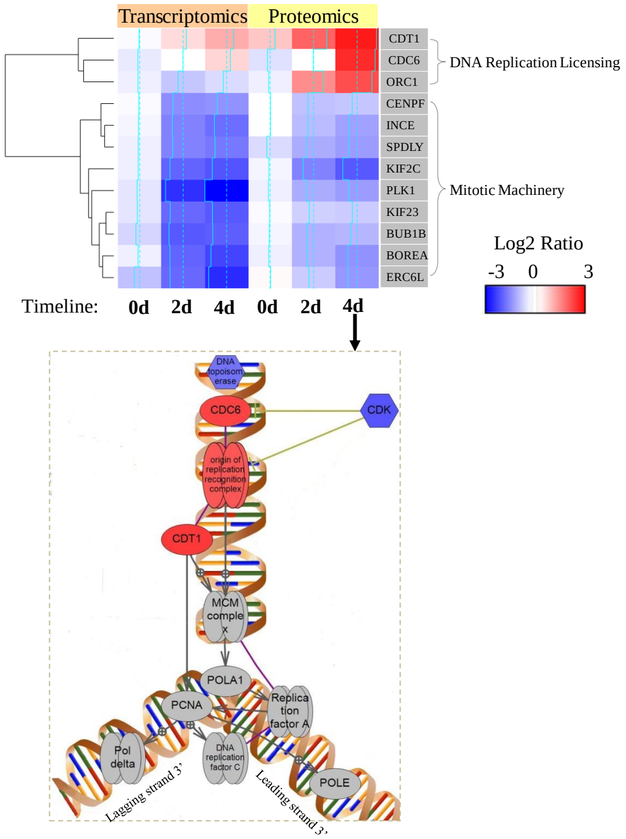


Figure 2

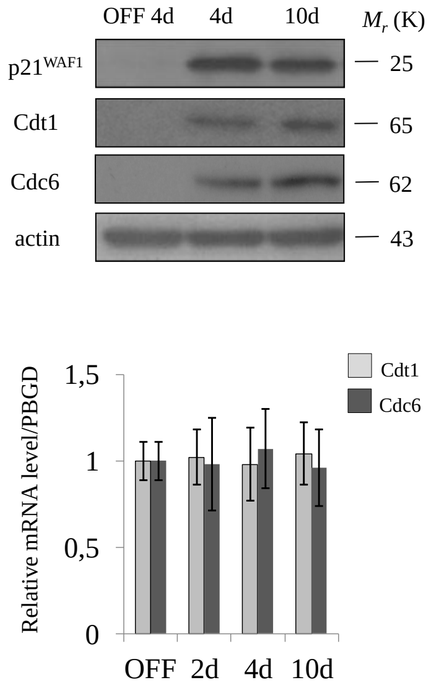
Saos2 p21^{WAF1} Tet-ON

a.



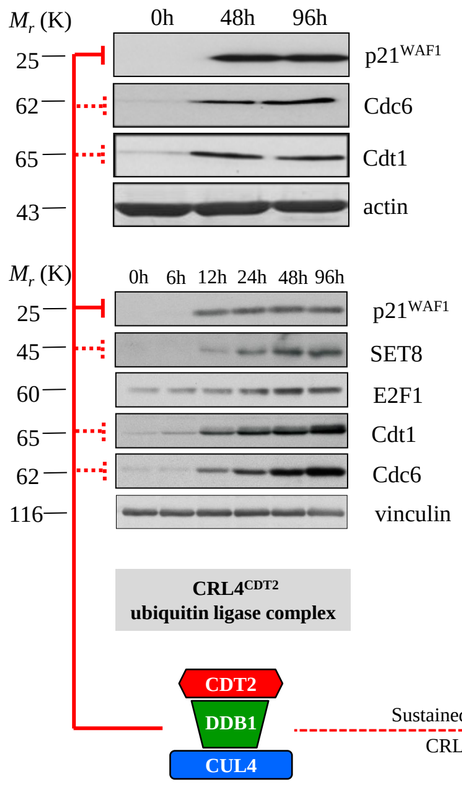
Li-Fraumeni p21^{WAF1} Tet-ON

b.

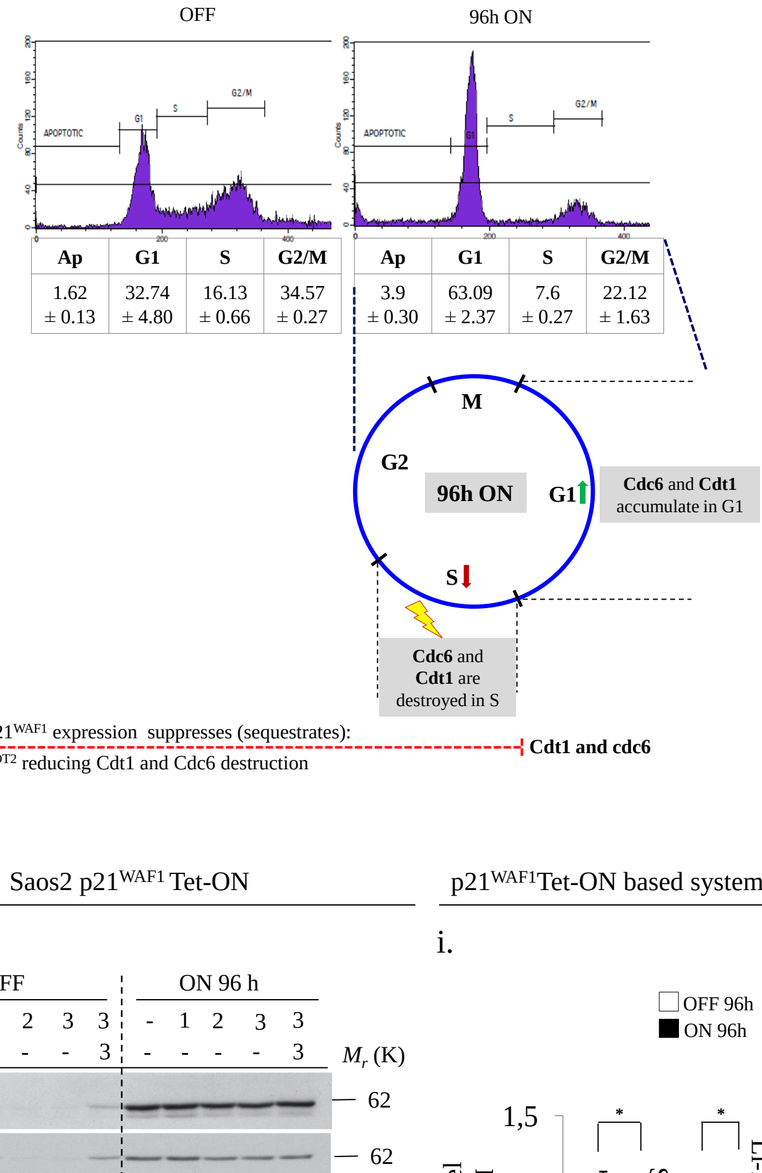


Saos2 p21^{WAF1} Tet-ON

c.

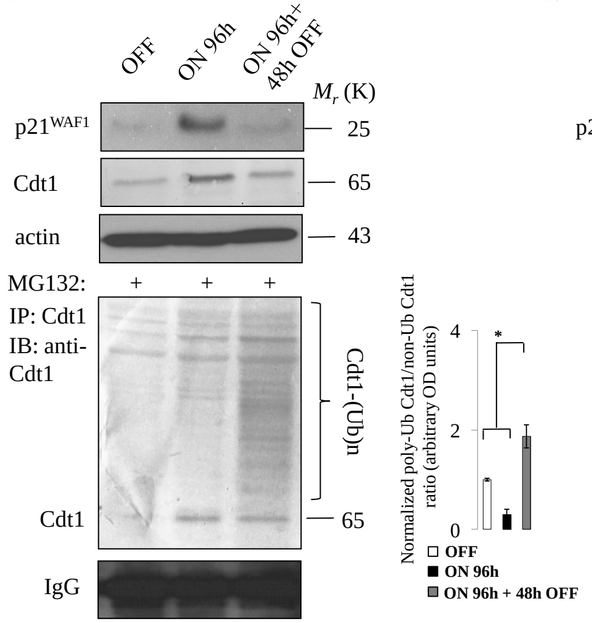


g.



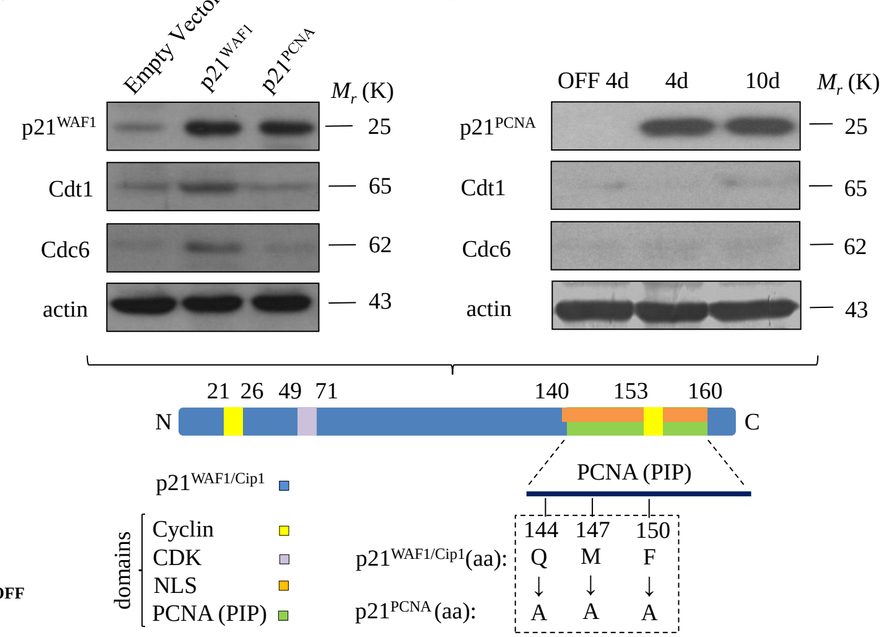
Saos2 p21^{WAF1} Tet-ON

d.



Saos2 (transient transfection)

e.

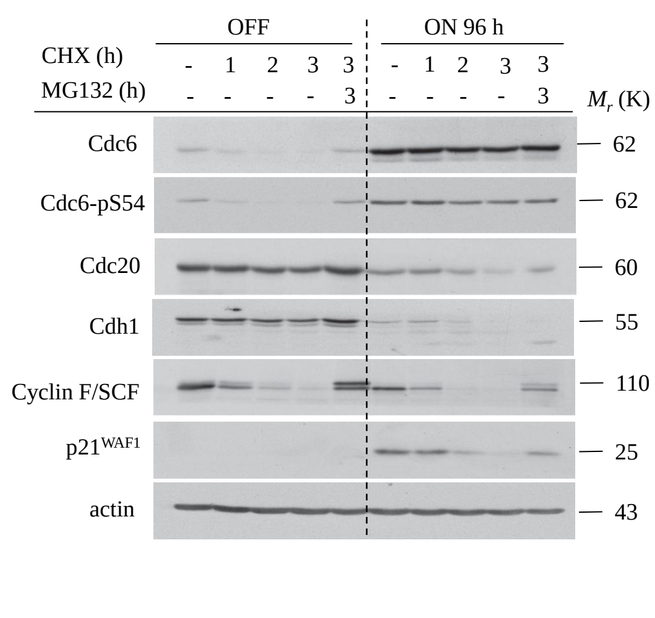


Li-Fraumeni p21^{PCNA} Tet-ON

f.

Saos2 p21^{WAF1} Tet-ON

h.



p21^{WAF1}Tet-ON based systems

i.

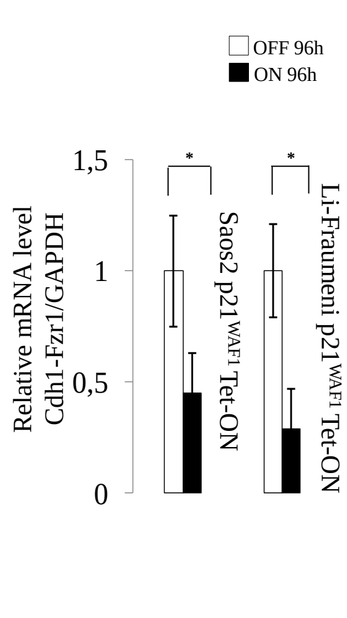


Figure 3

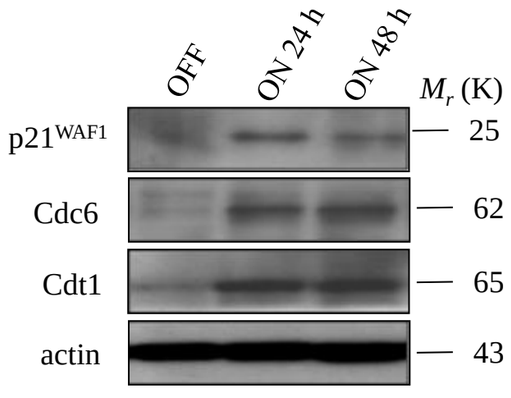
H1299 p21^{WAF1} – Ponasterone-ON (p53null)

HT1080 p21^{WAF1} – IPTG-ON (wt p53)

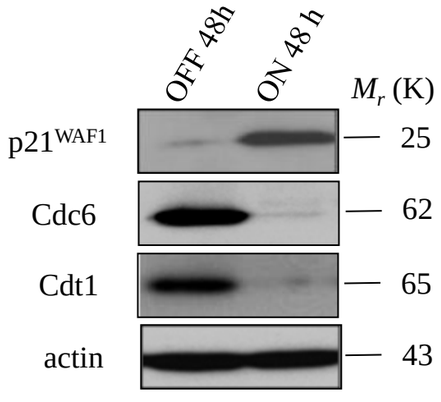
Saos2 p53 Tet-ON (p53null)

Saos2 + TGF-β (p53null)

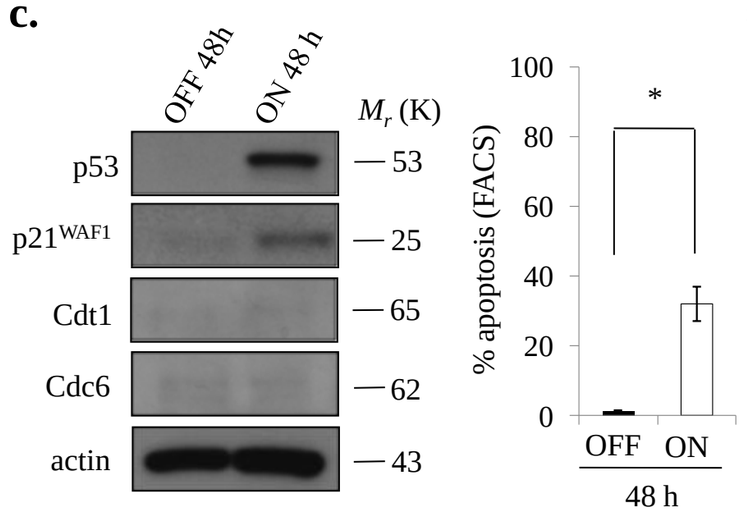
a.



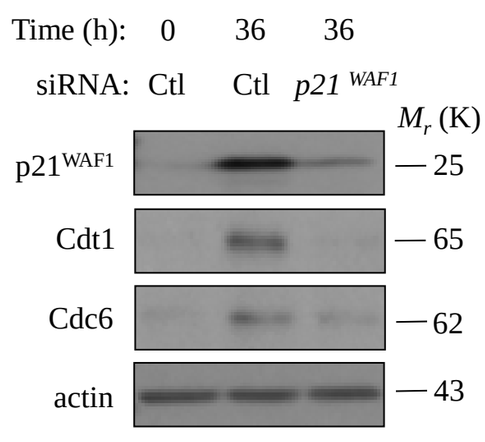
b.



c.



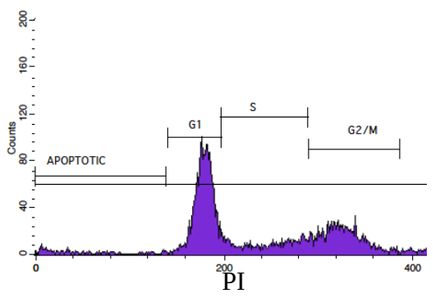
d.



HT1080 p21^{WAF1} –IPTG-ON

e.

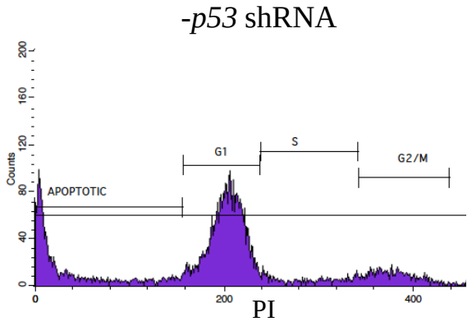
OFF 96h



Ap	G1	S	G2/M
2.53 ± 0.53	45.19 ± 5.35	17.51 ± 1.54	28.25 ± 1.42

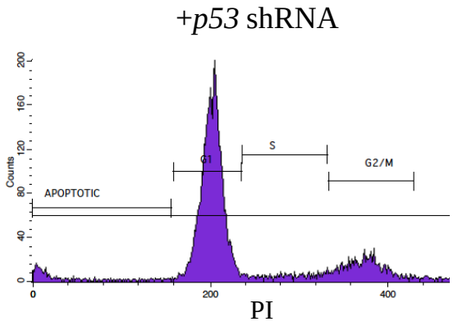
ON 96h

-p53 shRNA



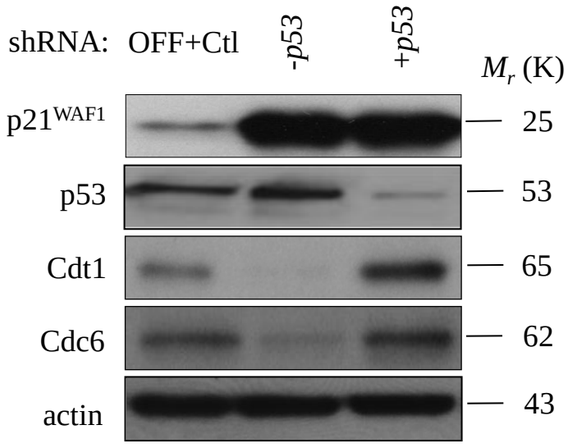
Ap	G1	S	G2/M
26.07 ± 1.49	55.03 ± 2.23	6.06 ± 0.52	10.14 ± 1.93

+p53 shRNA



Ap	G1	S	G2/M
4.14 ± 0.62	70.54 ± 3.47	5.65 ± 0.53	15.95 ± 1.34

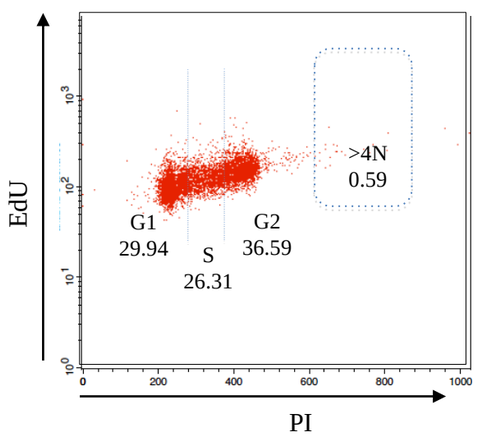
ON 96h



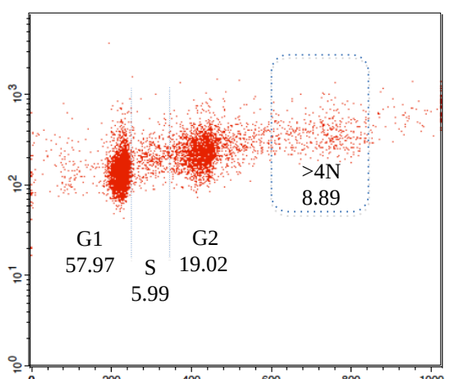
Saos2 p21^{WAF1} Tet-ON

f.

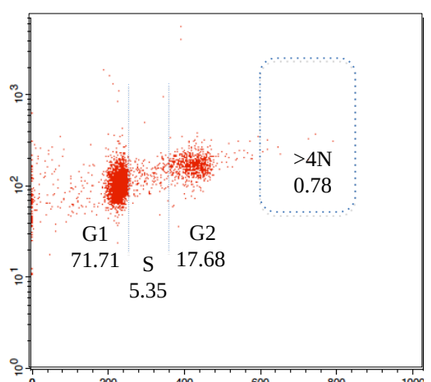
OFF 4d + Ctl siRNA

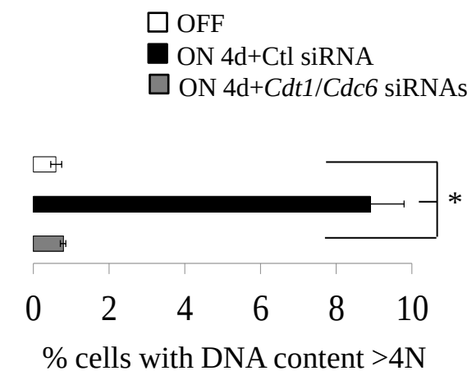


ON 4d + Ctl siRNA



ON 4d + *Cdt1*/*Cdc6* siRNAs

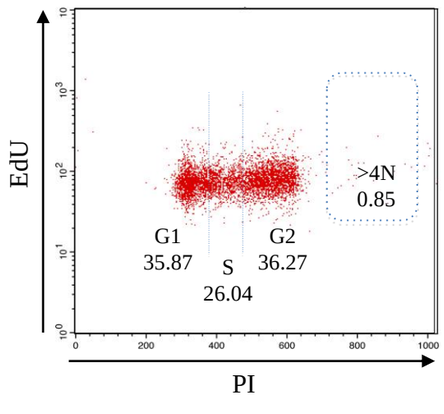




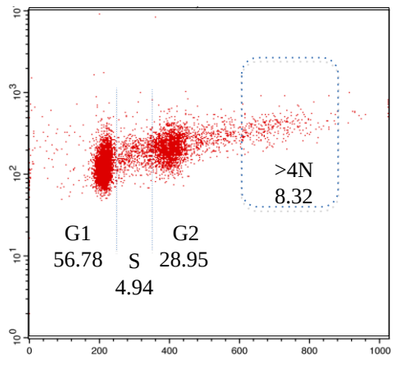
Li-Fraumenip21^{WAF1} Tet-ON

g.

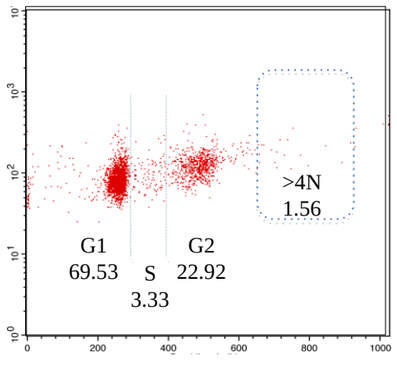
OFF 4d +Ctl siRNA

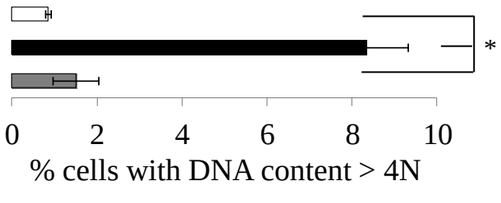


ON 4d+Ctl siRNA



ON 4d+ *Cdt1/Cdc6* siRNA

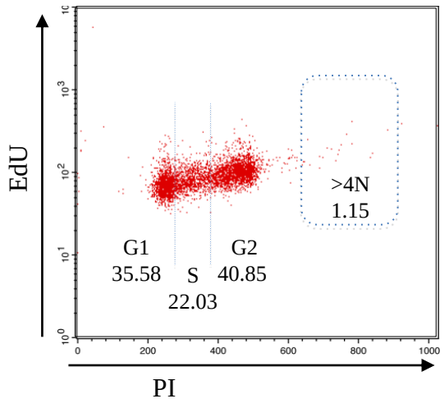




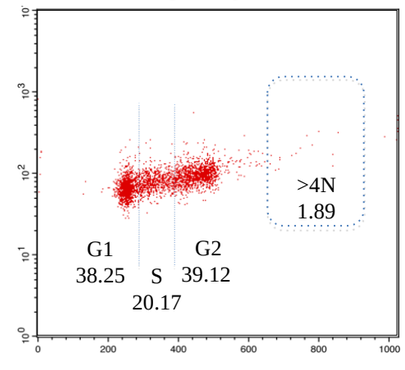
Li-Fraumeni p21^{PCNA} Tet-ON

h.

OFF 4d



ON 4d



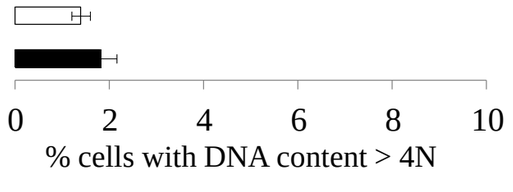
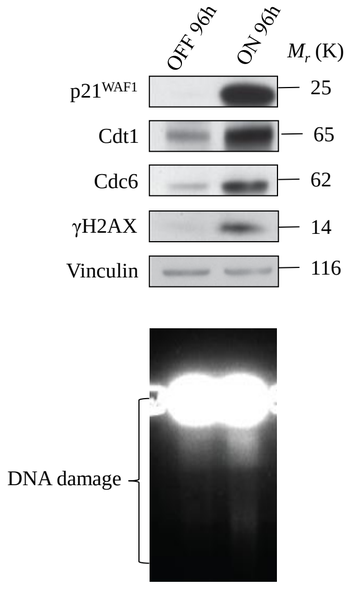


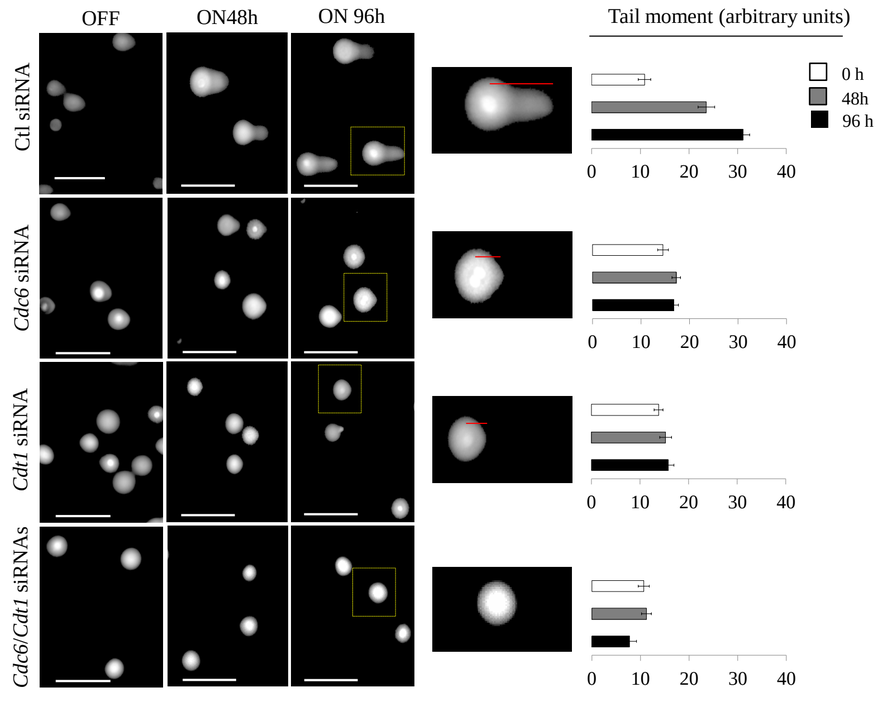
Figure 4

Saos2 p21^{WAF1} Tet-ON

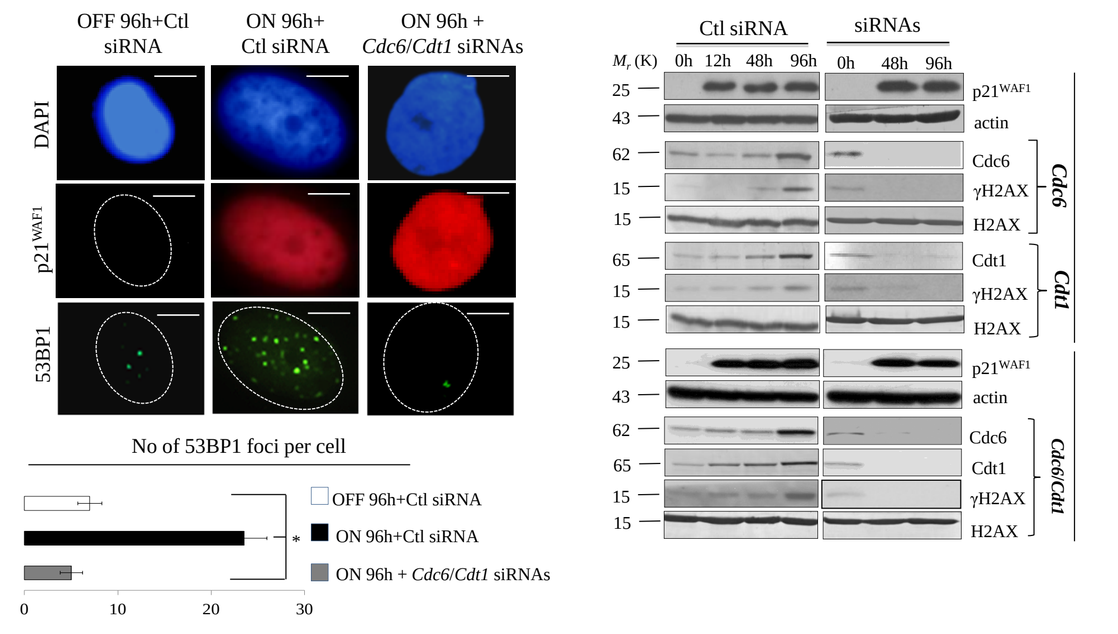
a.



b.

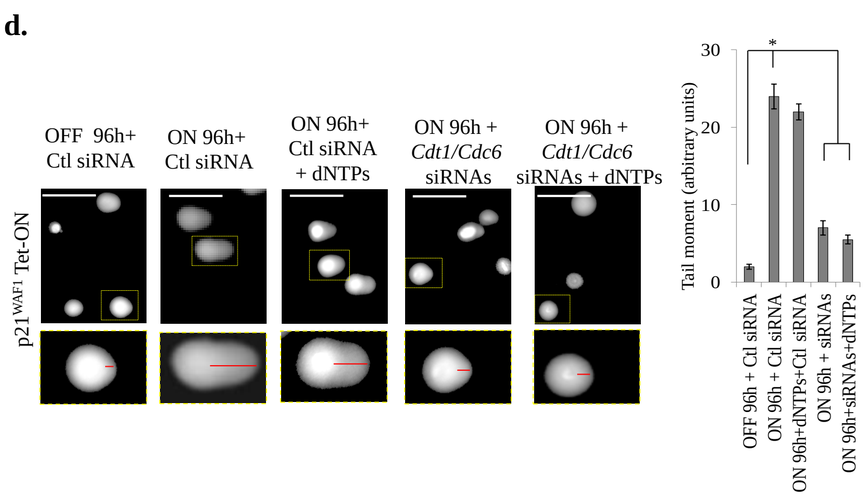


c.

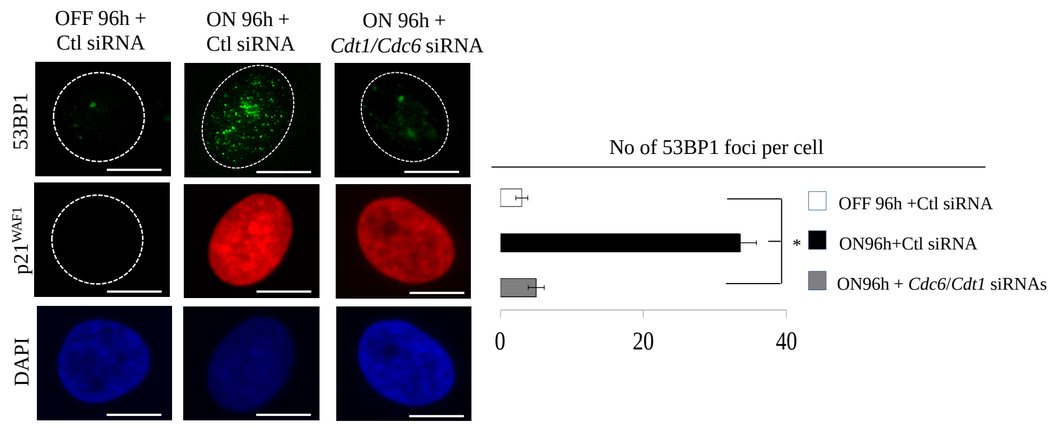


Li-Fraumeni p21^{WAF1} Tet-ON

d.

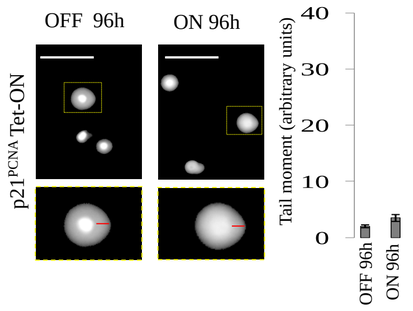


e.



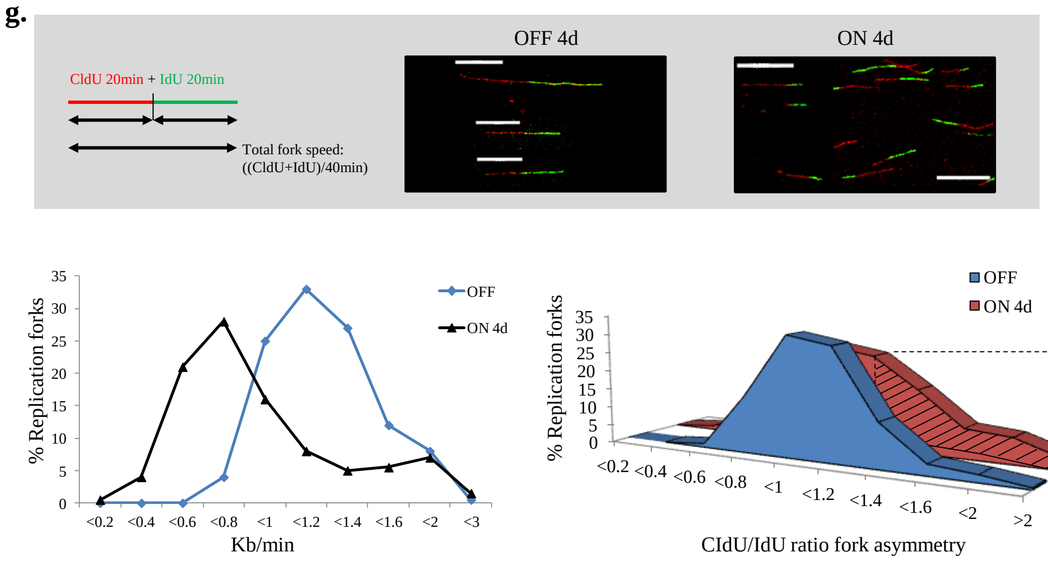
Li-Fraumeni p21^{PCNA} Tet-ON

f.



Saos2 p21^{WAF1} Tet-ON

g.



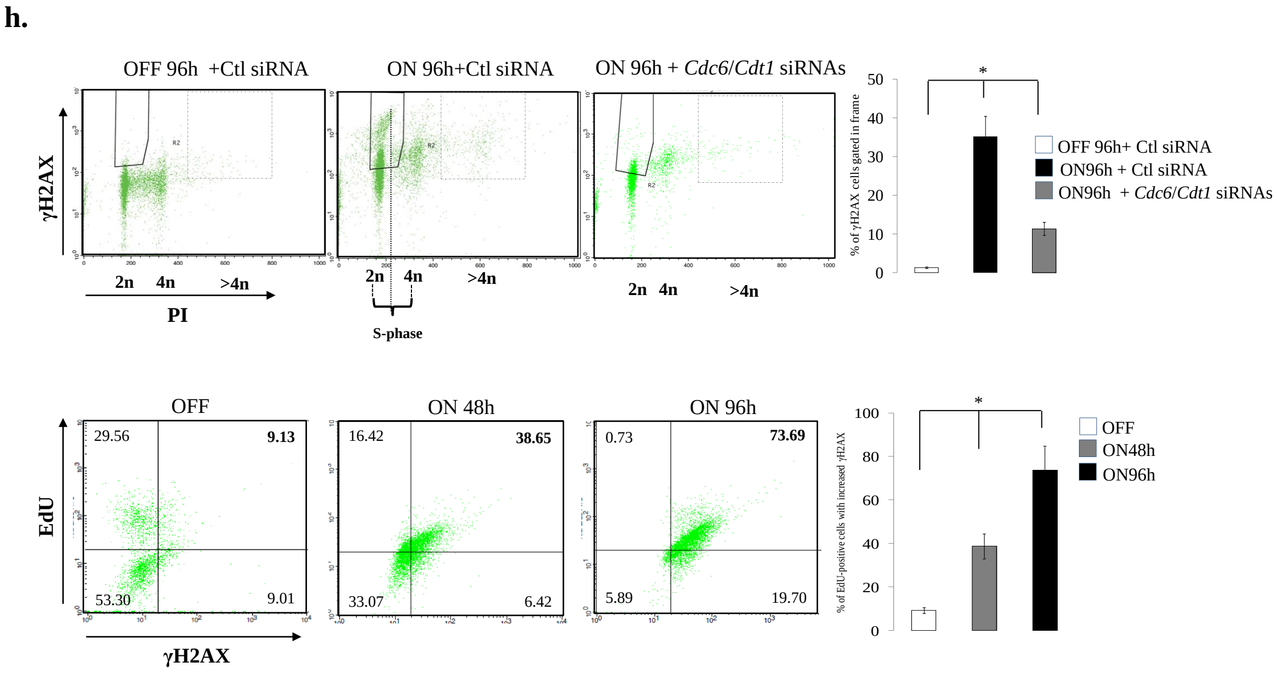
Replication fork speed

	CldU kb/min	Idu Kb/min	Total speed	*p* (T-test)	n
OFF 4d	1.16 ± 0.26	1.17 ± 0.33	1.16 ± 0.27		498
ON 4d	0.9 ± 0.43	0.88 ± 0.47	0.89 ± 0.43	7.50E-24	377

Replication fork asymmetry

	CldU/IdU	*p (T-test)	n
OFF 4d	1.03 ± 0.24		498
OFF vs ON 4d	1.09 ± 0.36	0.001885	377

h.



Li-Fraumeni p21^{WAF1} Tet-ON

i.

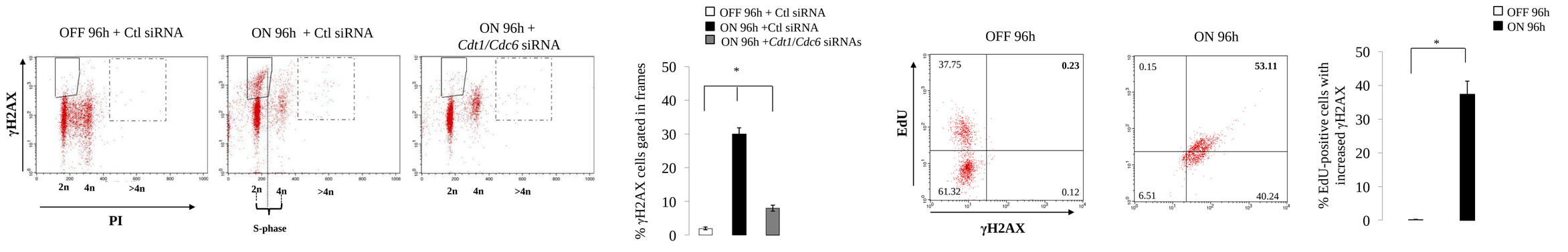


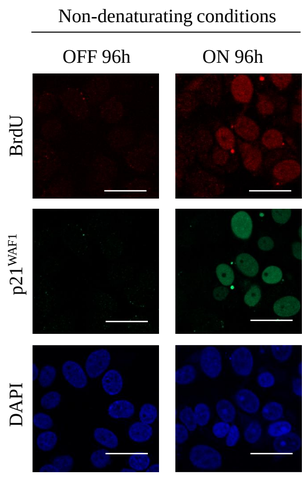
Figure 5

Saos2 p21^{WAF1} Tet-ON

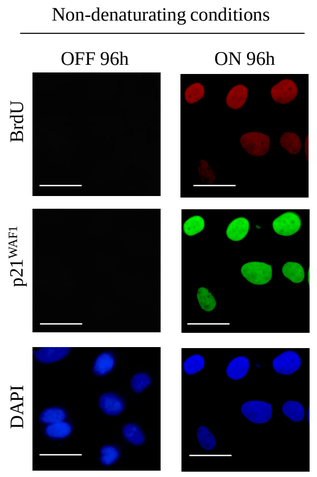
Li-Fraumeni p21^{WAF1} Tet-ON

Saos2 p21^{WAF1} Tet-ON

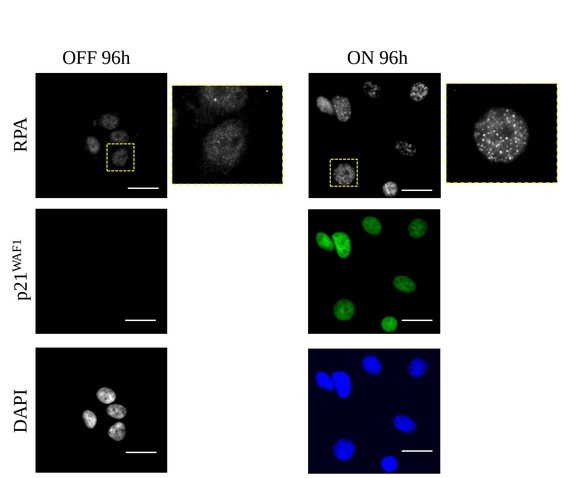
a.



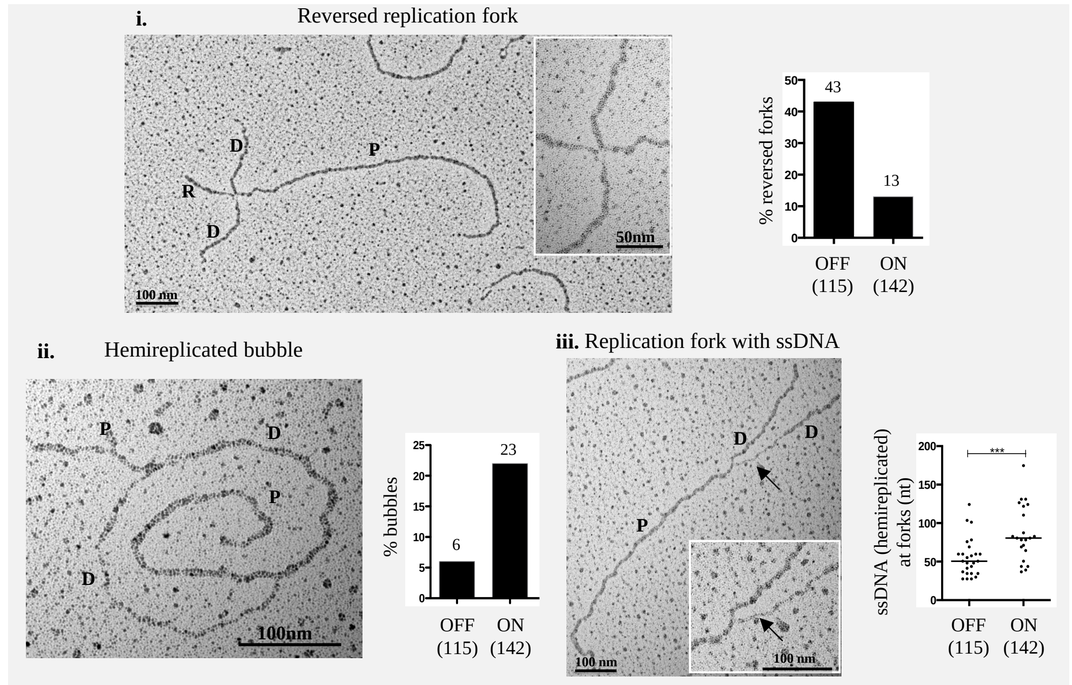
b.



c.



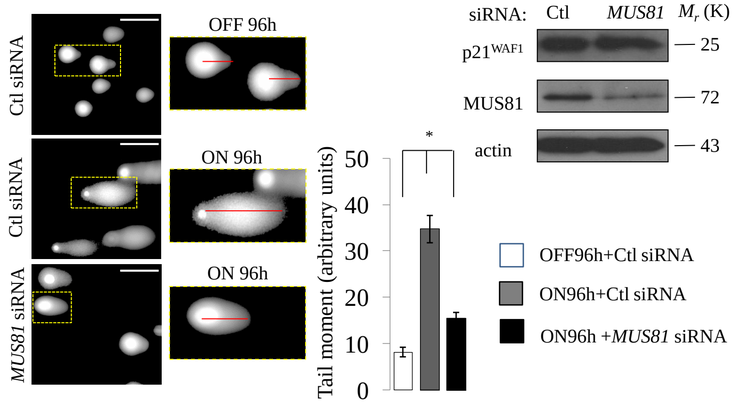
d.



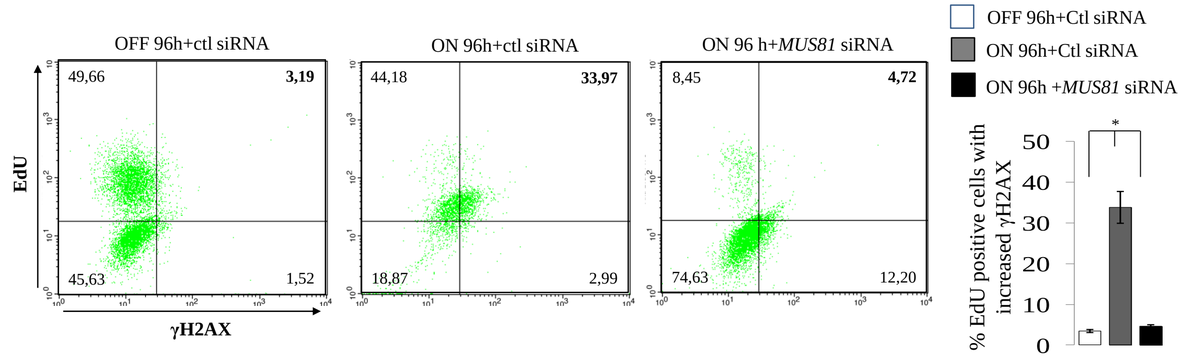
Saos2 p21^{WAF1} Tet-ON

Li-Fraumeni p21^{WAF1} Tet-ON

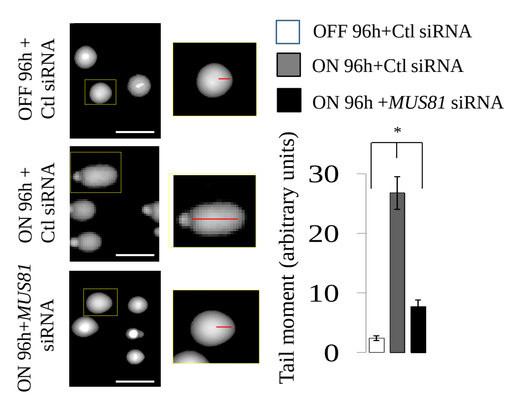
e.



f.

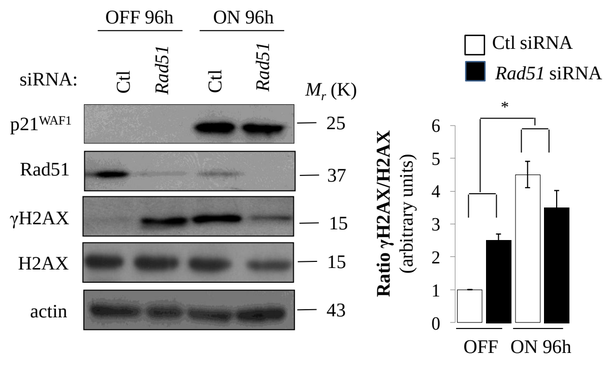


g.

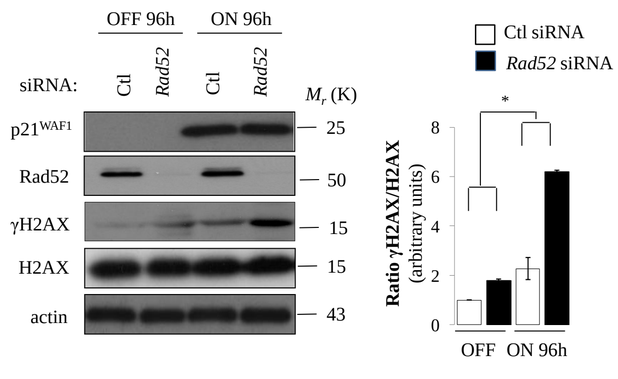


Saos2 p21^{WAF1} Tet-ON

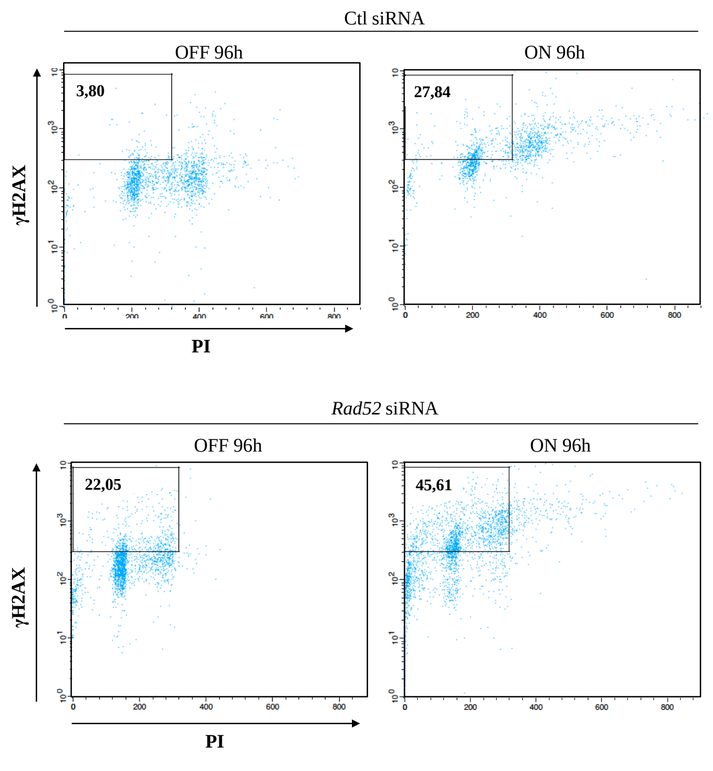
h.

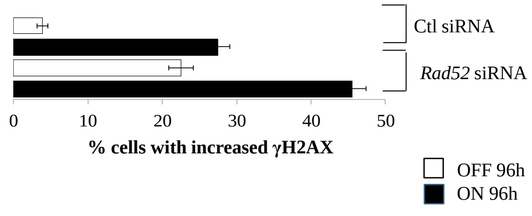


i.



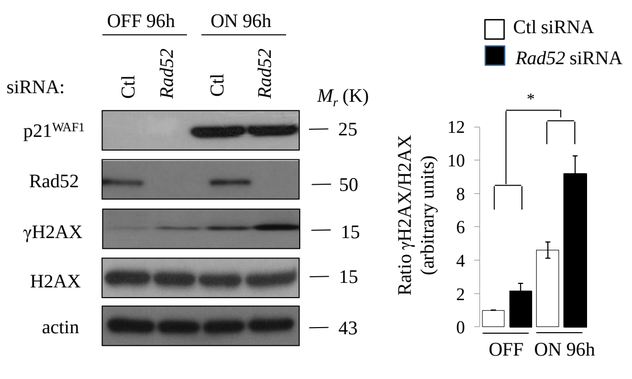
j.





Li-Fraumeni p21^{WAF1} Tet-ON

k.



Saos2 p21^{WAF1} Tet-ON

l.

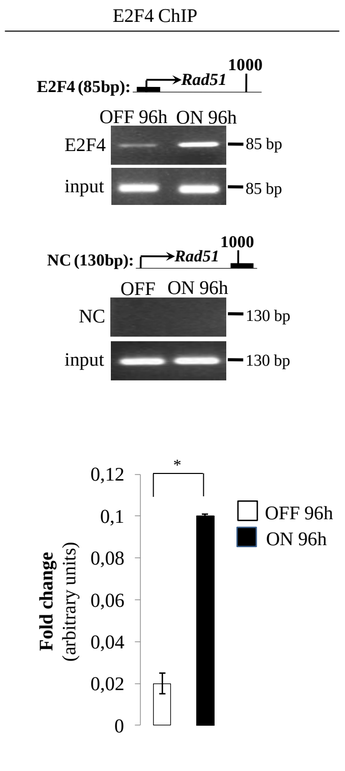
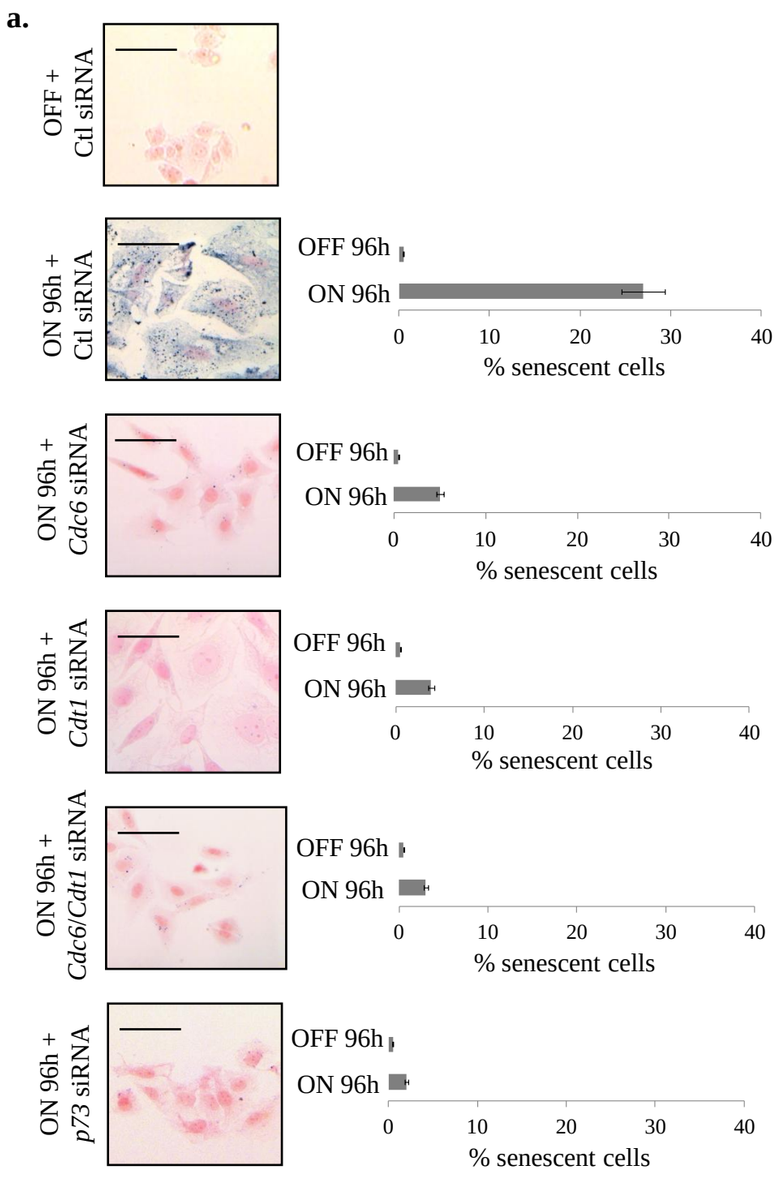
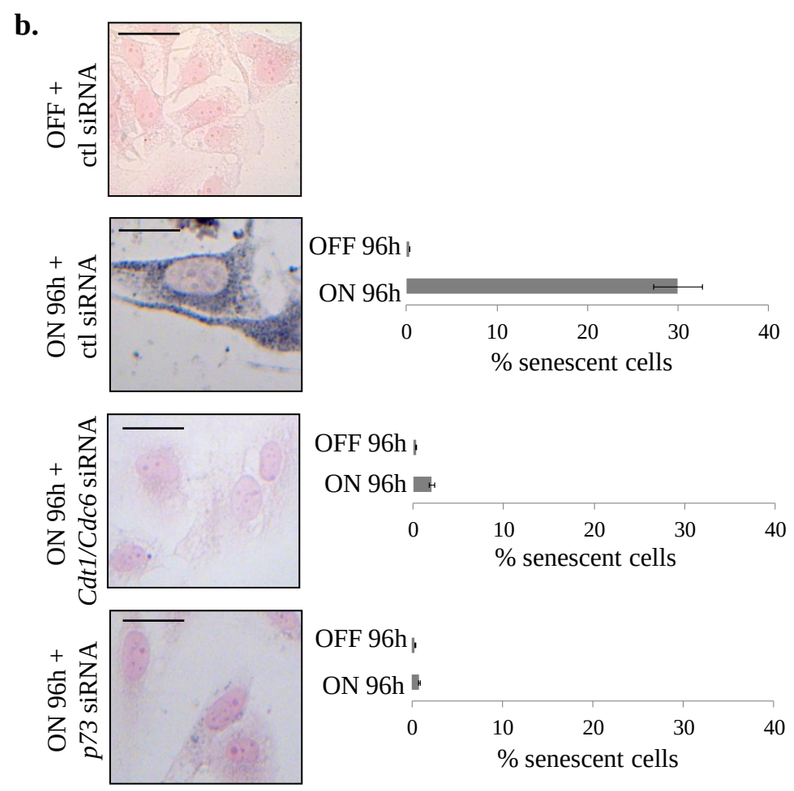
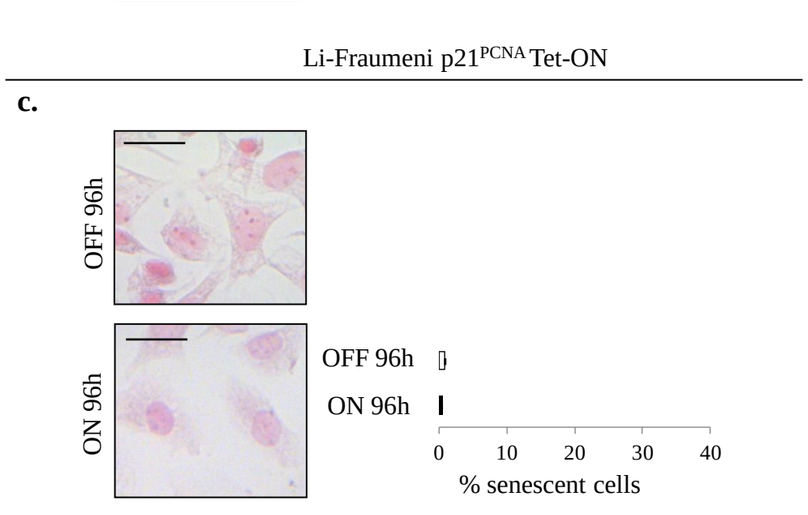
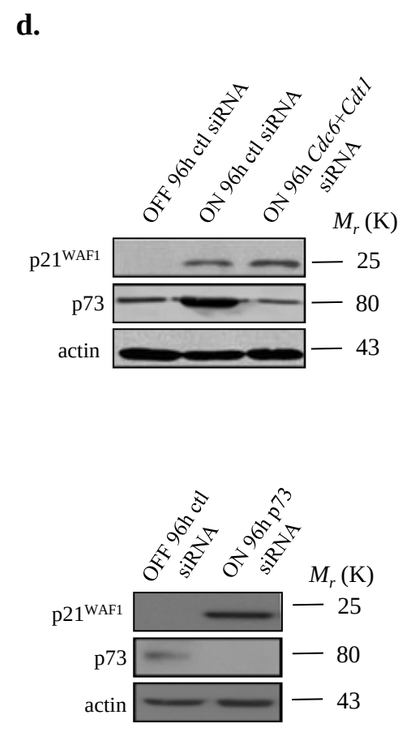


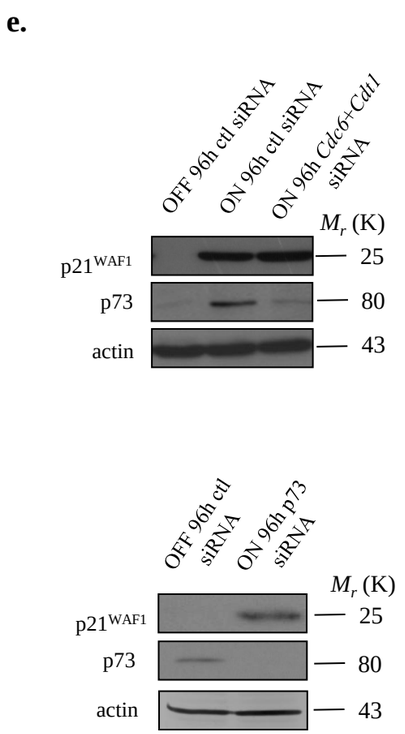
Figure 6

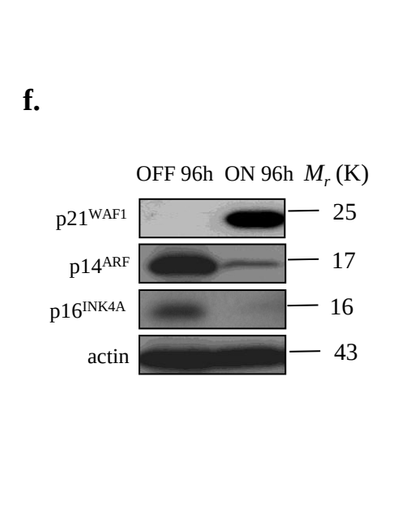

Saos2 p21WAF1 Tet-ON
a.
OFF + Ctl siRNA
ON 96h + Ctl siRNA
ON 96h + Cdc6 siRNA
ON 96h + Cdt1 siRNA
ON 96h + Cdc6/Cdt1 siRNA
ON 96h + p73 siRNA
OFF 96h
ON 96h
0
10
20
30
40
% senescent cells

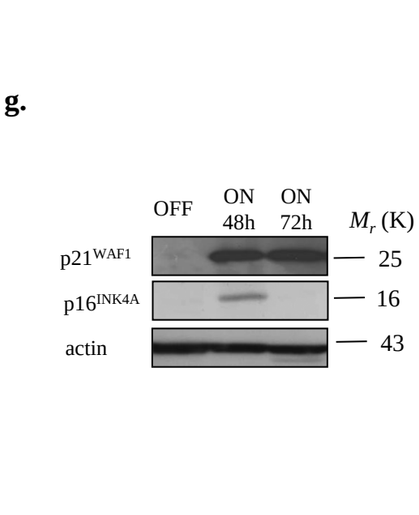

Li-Fraumeni p21WAF1 Tet-ON
b.
OFF + ctl siRNA
ON 96h + ctl siRNA
ON 96h + Cdt1/Cdc6 siRNA
ON 96h + p73 siRNA
OFF 96h
ON 96h
0
10
20
30
40
% senescent cells


Li-Fraumeni p21PCNA Tet-ON
c.
OFF 96h
ON 96h
0
10
20
30
40
% senescent cells


Saos2 p21WAF1 Tet-ON
d.
OFF 96h ctl siRNA
ON 96h ctl siRNA
ON 96h Cdc6+Cdt1 siRNA
Mr (K)
p21WAF1
p73
actin
25
80
43


Li-Fraumeni p21WAF1 Tet-ON
e.
OFF 96h ctl siRNA
ON 96h ctl siRNA
ON 96h Cdc6+Cdt1 siRNA
Mr (K)
p21WAF1
p73
actin
25
80
43

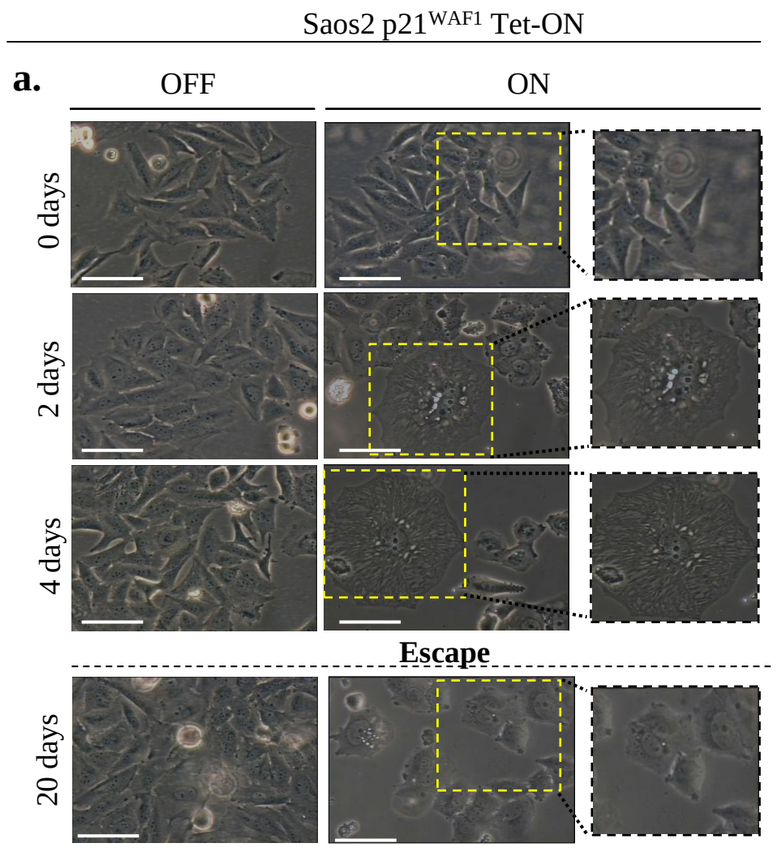

f.
OFF 96h ctl siRNA
ON 96h p73 siRNA
Mr (K)
p21WAF1
p73
actin
25
80
43

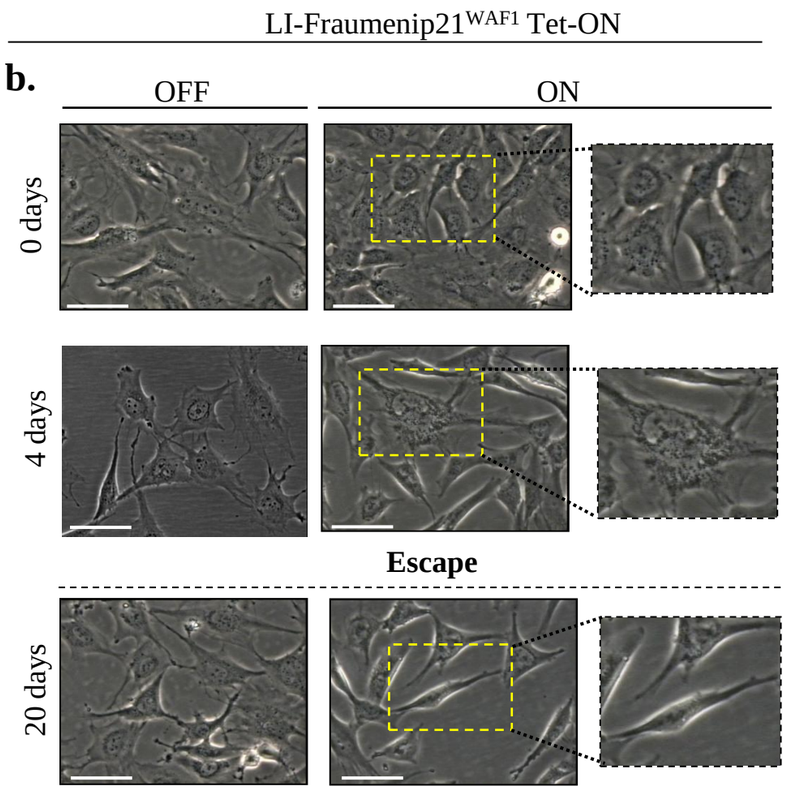

OFF 96h ctl siRNA
ON 96h p73 siRNA
Mr (K)
p21WAF1
p73
actin
25
80
43

OFF 96h
ON 96h
Mr (K)
p21WAF1
p14ARF
p16INK4A
actin
25
17
16
43

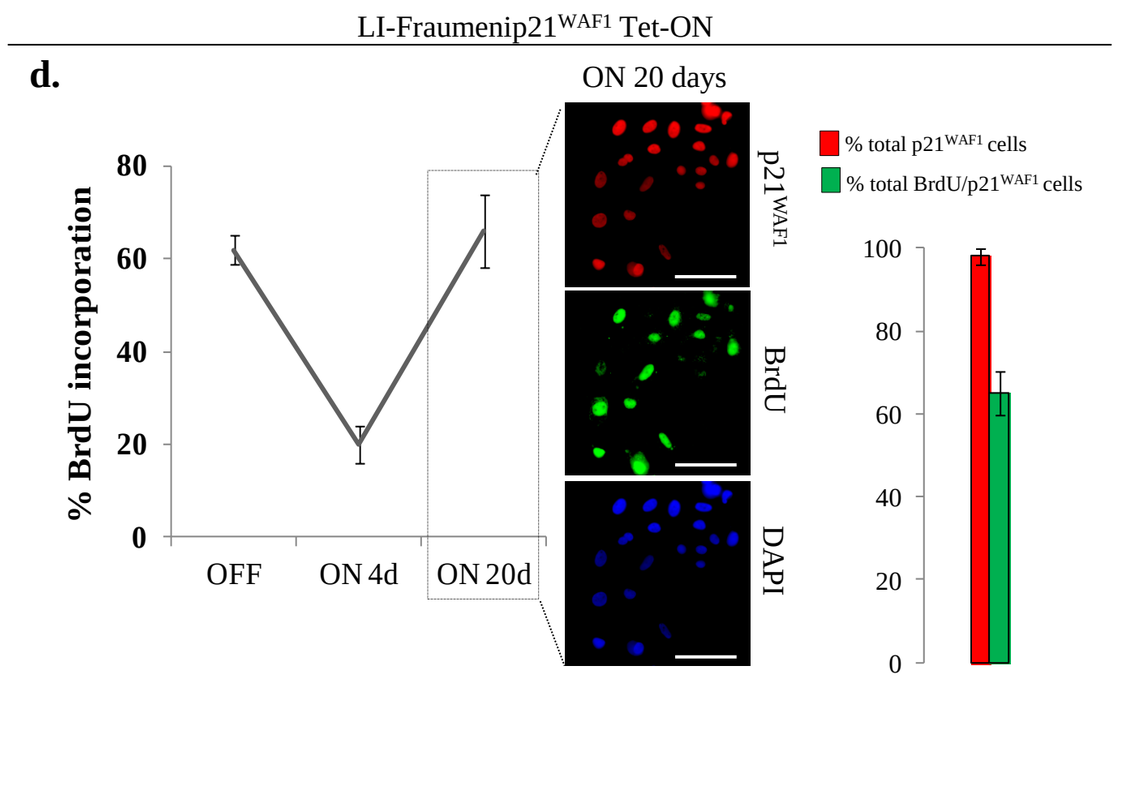
g.
OFF
ON 48h
ON 72h
Mr (K)
p21WAF1
p16INK4A
actin
25
16
43

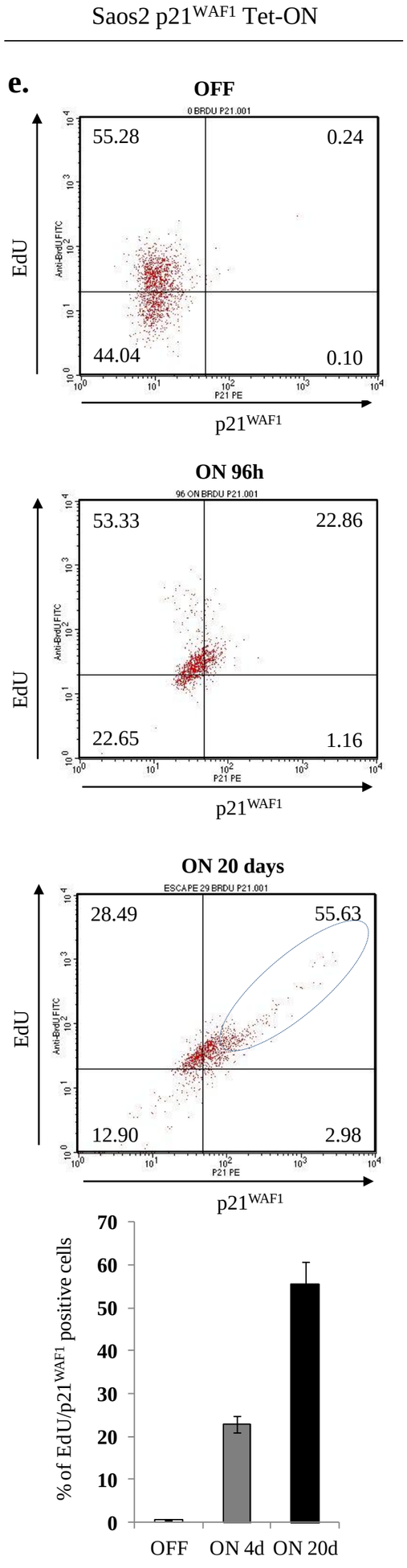
Figure 7

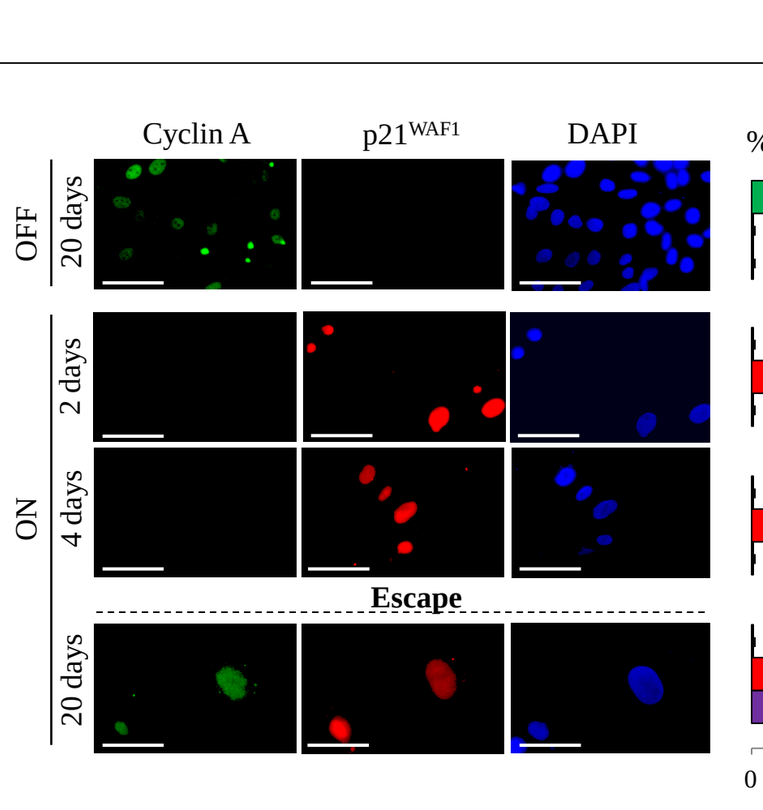

Saos2 p21WAF1 Tet-ON
a.
OFF
ON
0 days
2 days
4 days
Escape
20 days

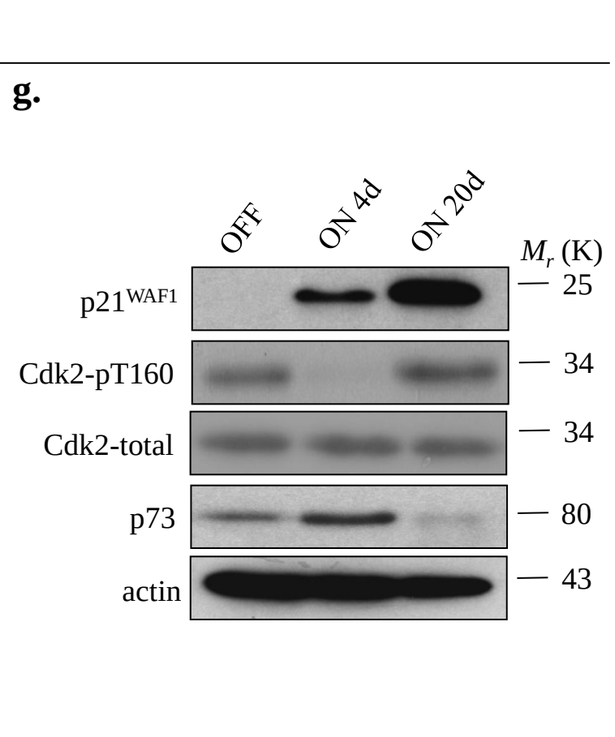

LI-Fraumenip21WAF1 Tet-ON
b.
OFF
ON
0 days
4 days
Escape
20 days

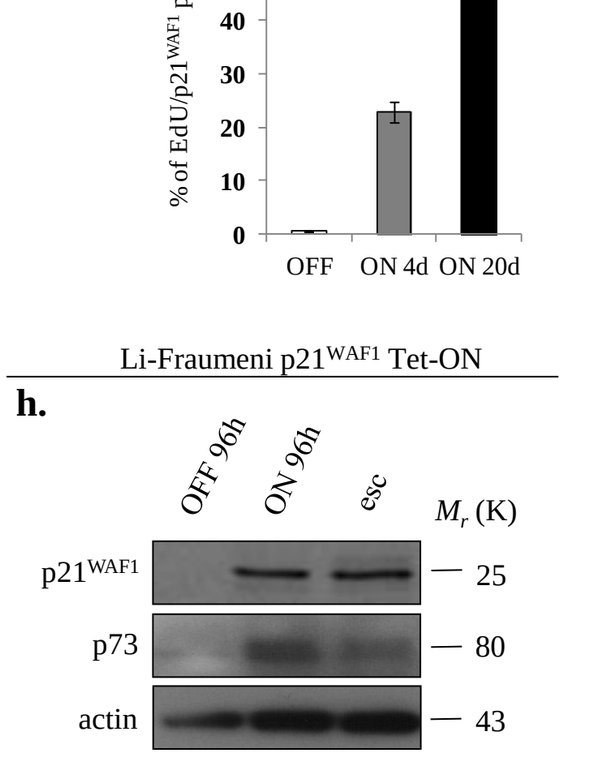
Saos2 p21WAF1 Tet-ON
c.
ON 20 days
% BrdU incorporation
80
60
40
20
0
OFF
ON 2d
ON 4d
ON 20d
p21WAF1
BrdU
DAPI
% total p21WAF1 cells
% total BrdU/p21WAF1 cells
100
80
60
40
20
0

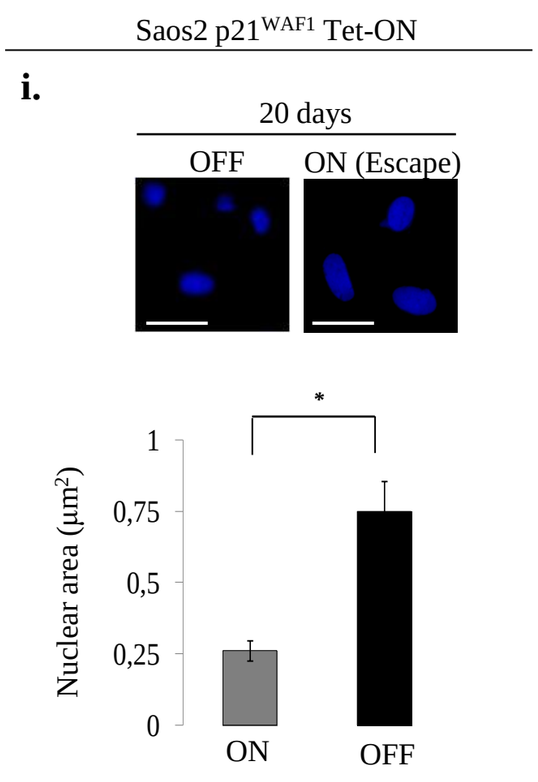

LI-Fraumenip21WAF1 Tet-ON
d.
ON 20 days
% BrdU incorporation
80
60
40
20
0
OFF
ON 4d
ON 20d
p21WAF1
BrdU
DAPI
% total p21WAF1 cells
% total BrdU/p21WAF1 cells
100
80
60
40
20
0

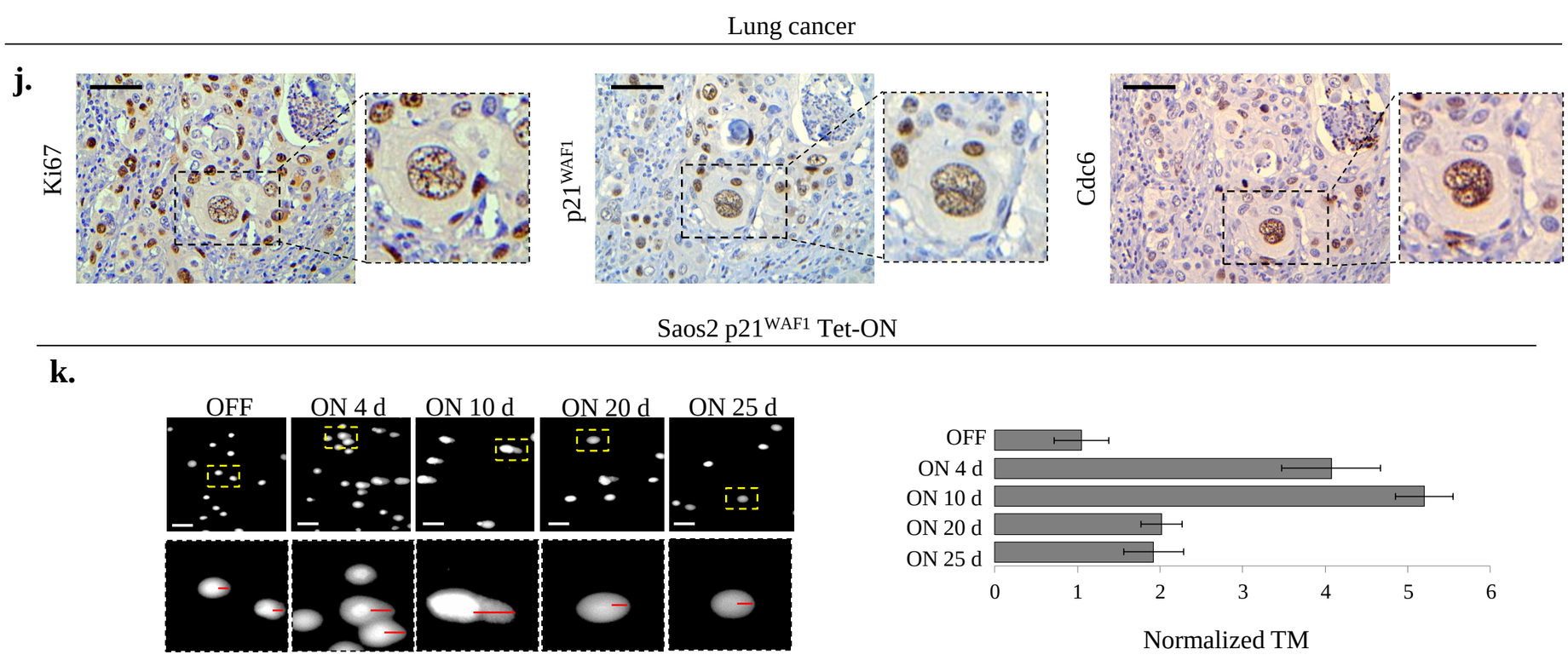

Saos2 p21WAF1 Tet-ON
e.
OFF
55.28
0.24
44.04
0.10
EdU
p21WAF1
ON 96h
53.33
22.86
22.65
1.16
ON 20 days
28.49
55.63
12.90
2.98
% of EdU/p21WAF1 positive cells
70
60
50
40
30
20
10
0
OFF
ON 4d
ON 20d


Saos2 p21WAF1 Tet-ON
f.
Cyclin A
p21WAF1
DAPI
% of CyclinA/p21WAF1 cells
OFF
ON
20 days
2 days
4 days
Escape
+/-
-/+
+/+
0
50
100


g.
OFF
ON 4d
ON 20d
Mr (K)
p21WAF1
Cdk2-pT160
Cdk2-total
p73
actin
25
34
34
80
43


Li-Fraumeni p21WAF1 Tet-ON
h.
OFF 96h
ON 96h
esc
Mr (K)
p21WAF1
p73
actin
25
80
43


Saos2 p21WAF1 Tet-ON
i.
20 days
OFF
ON (Escape)
*
Nuclear area (µm2)
1
0,75
0,5
0,25
0
ON
OFF


Lung cancer
j.
Ki67
p21WAF1
Cdc6

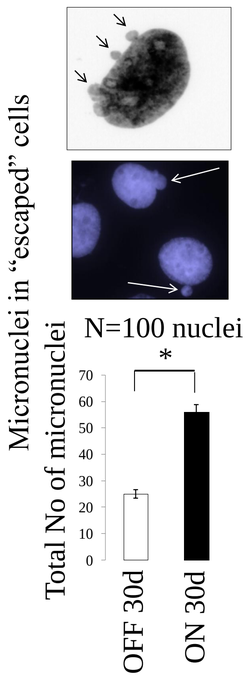
Saos2 p21WAF1 Tet-ON
k.
OFF
ON 4 d
ON 10 d
ON 20 d
ON 25 d
Normalized TM
0
1
2
3
4
5
6

Figure 8

Saos2 p21^{WAF1} Tet-ON

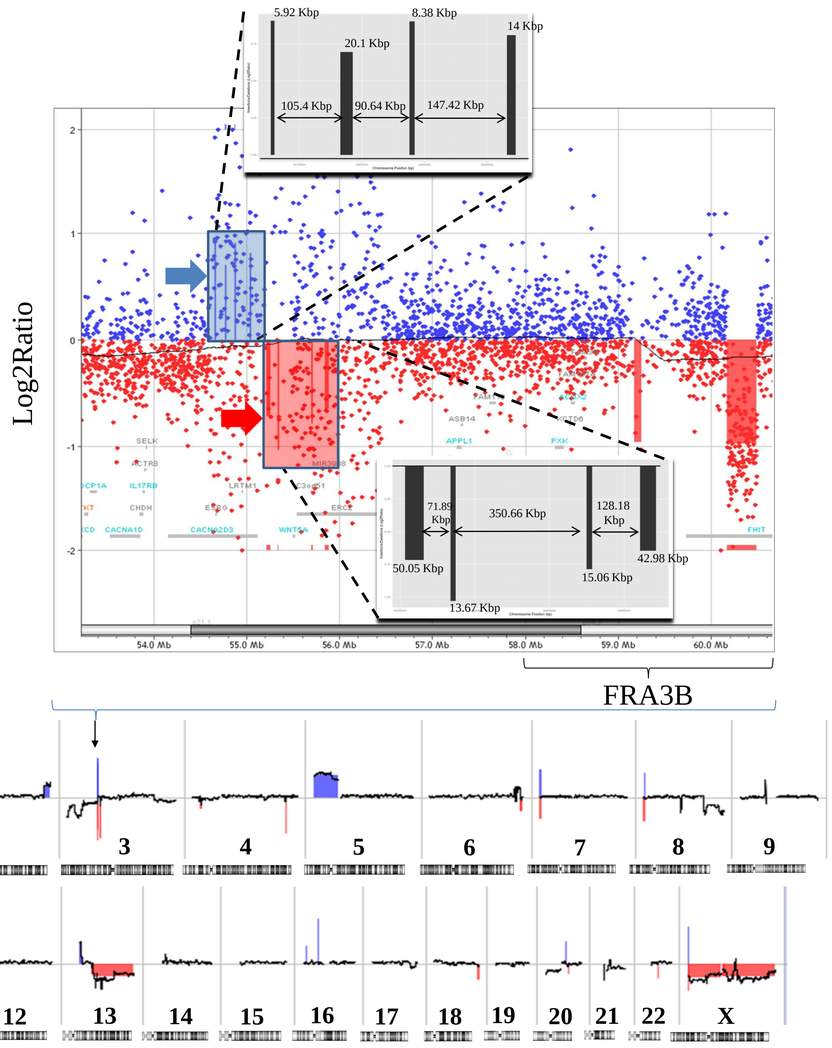
Li-Fraumeni p21^{WAF1} Tet-ON

a.



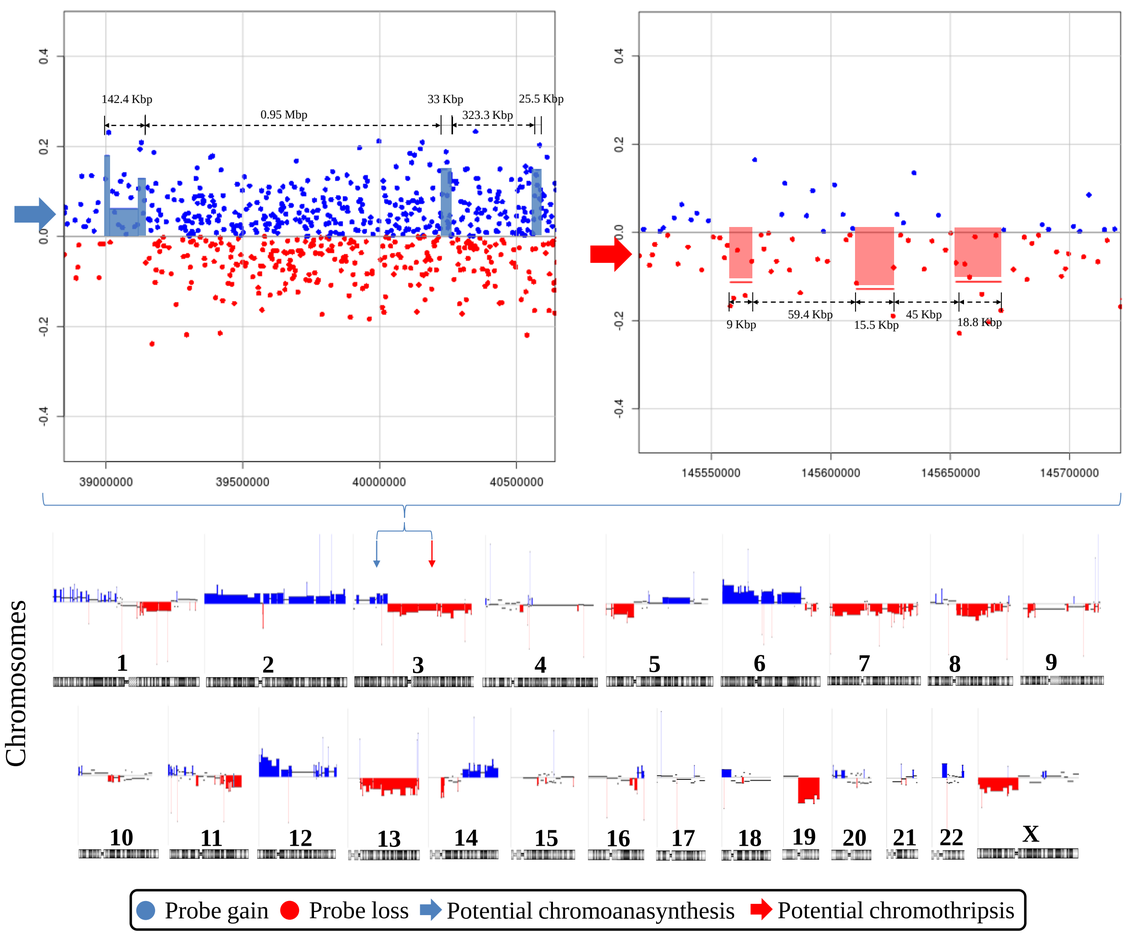
b.

aCGH analysis of "escaped" vs OFF cells



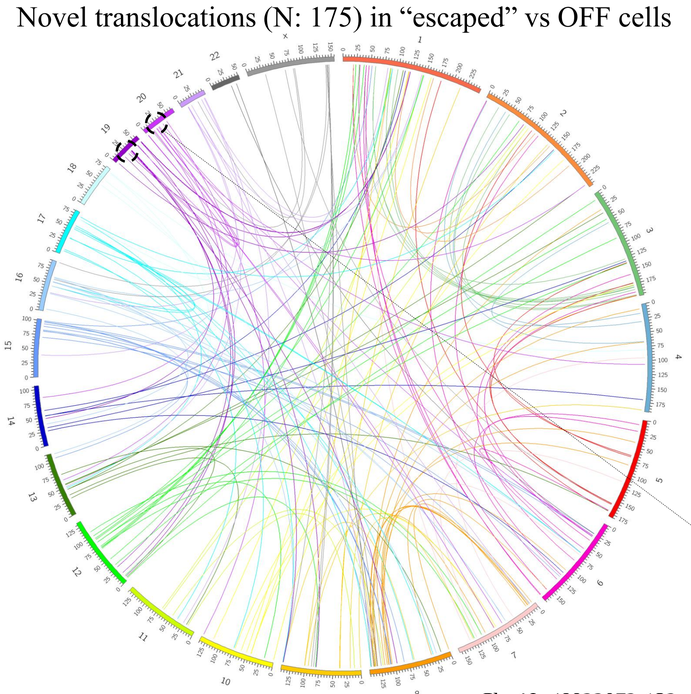
c.

aCGH analysis of "escaped" vs OFF cells



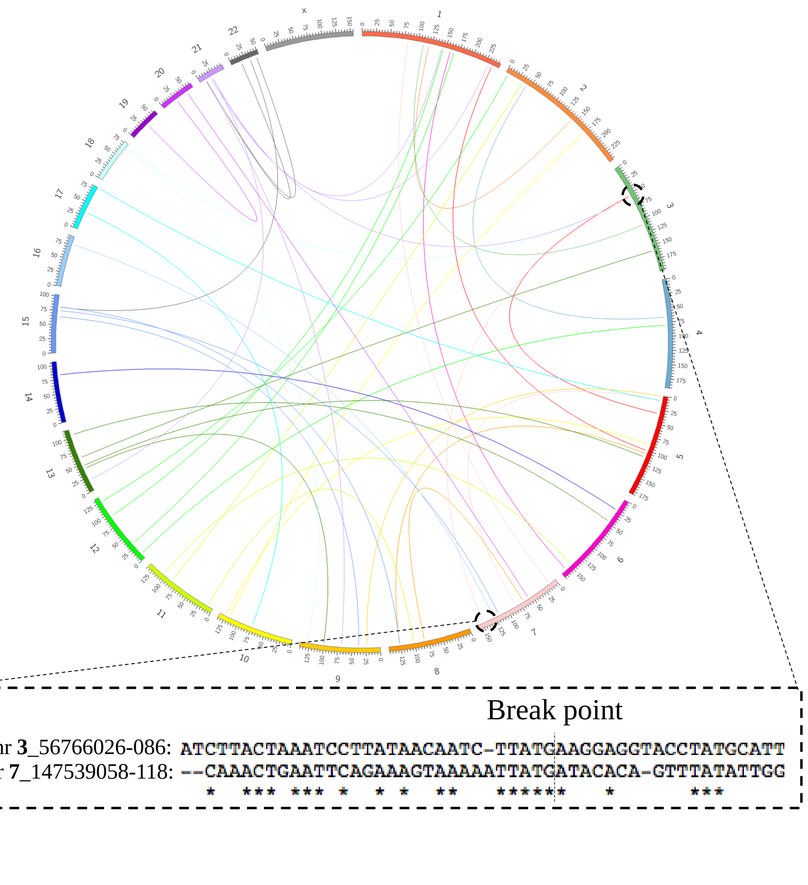
d.

Novel translocations (N: 175) in "escaped" vs OFF cells



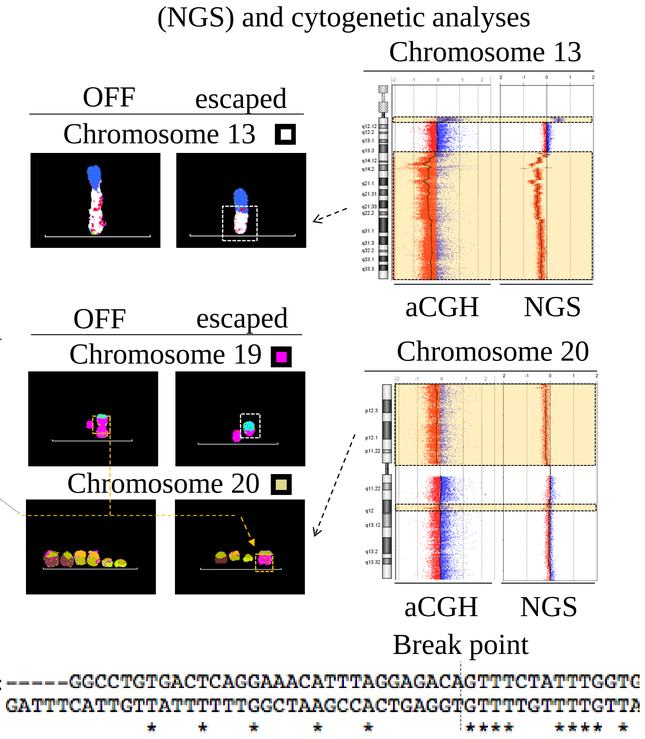
e.

Novel translocations (N: 44) in "escaped" vs OFF cells



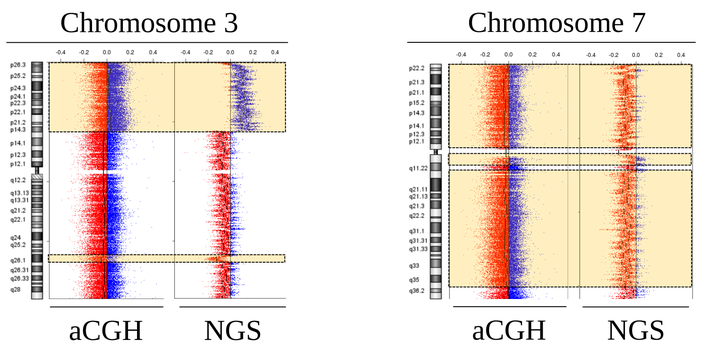
f.

Concordance between aCGH, deep sequencing (NGS) and cytogenetic analyses

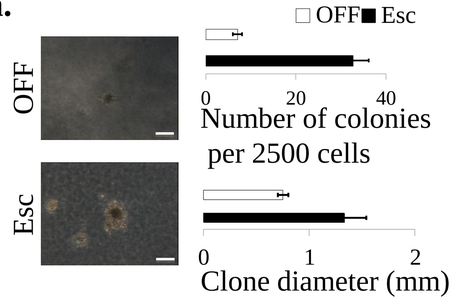


g.

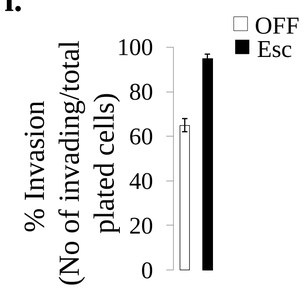
Concordance between aCGH and deep sequencing (NGS) analyses



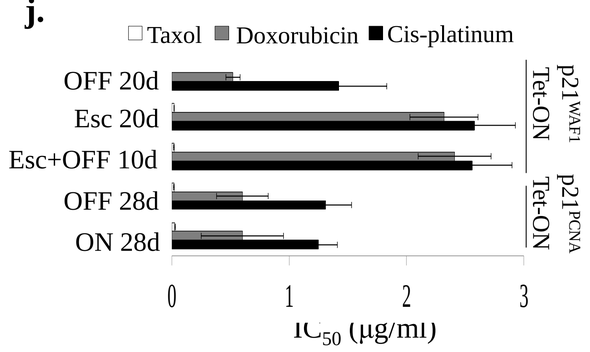
h.



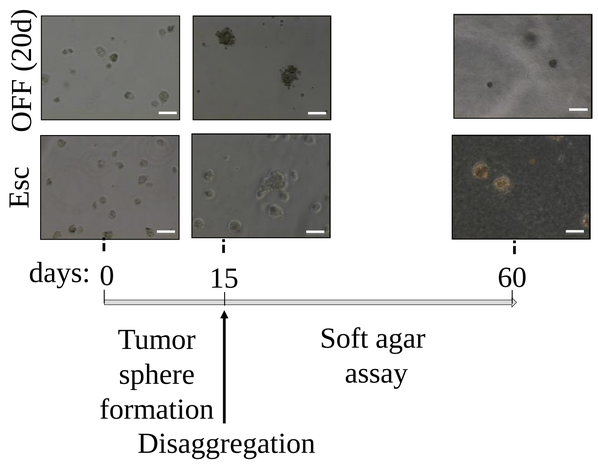
i.

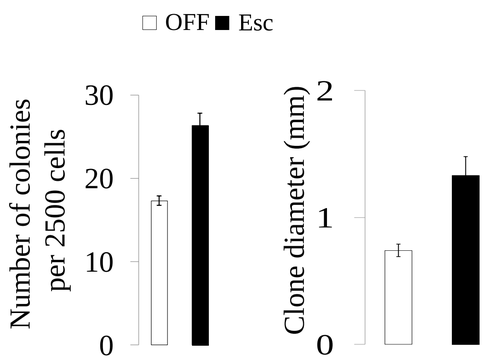


j.

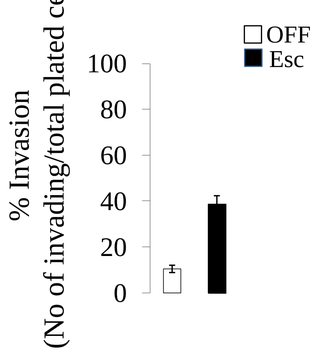


k.

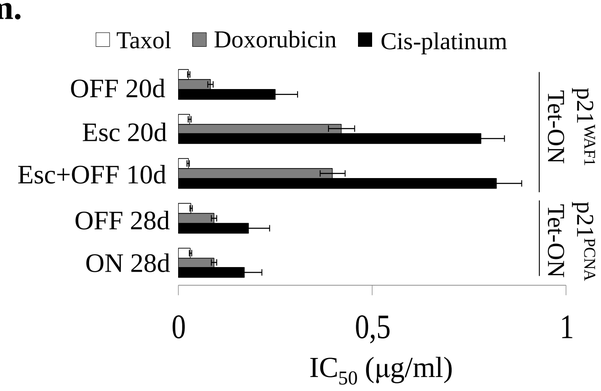




l.



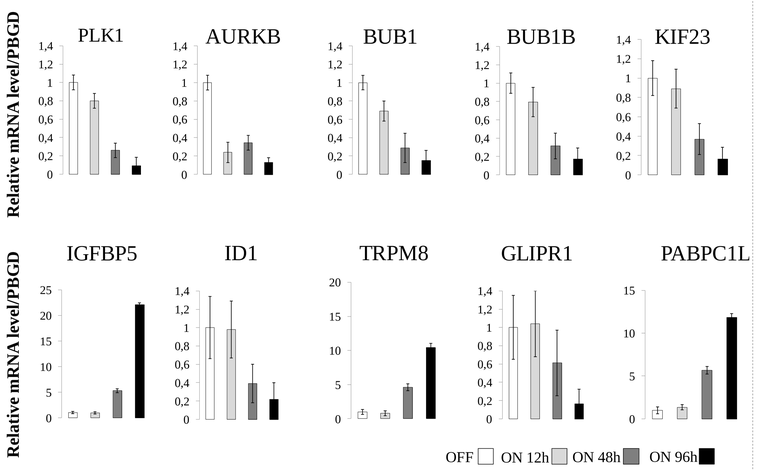
m.



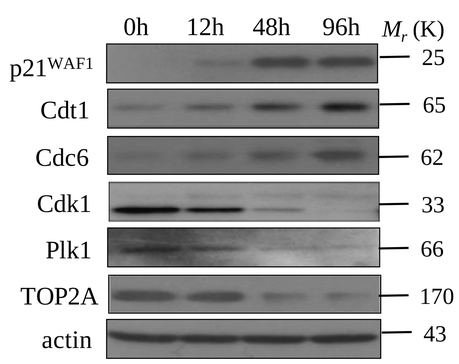
Suppl. Figure 1

ai.

Saos2 p21^{WAF1} Tet-ON

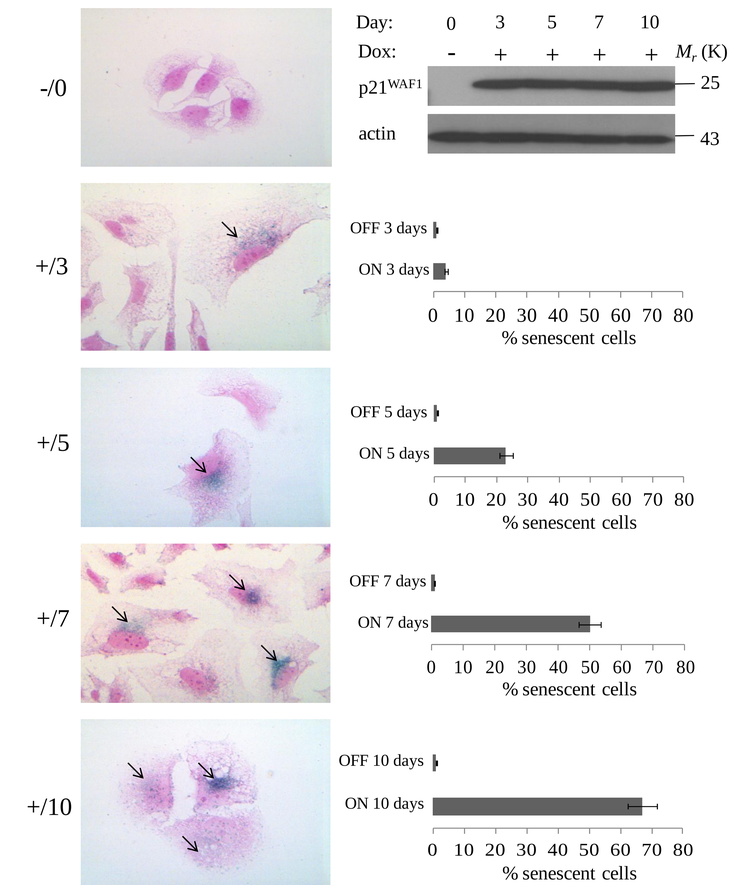


aii.



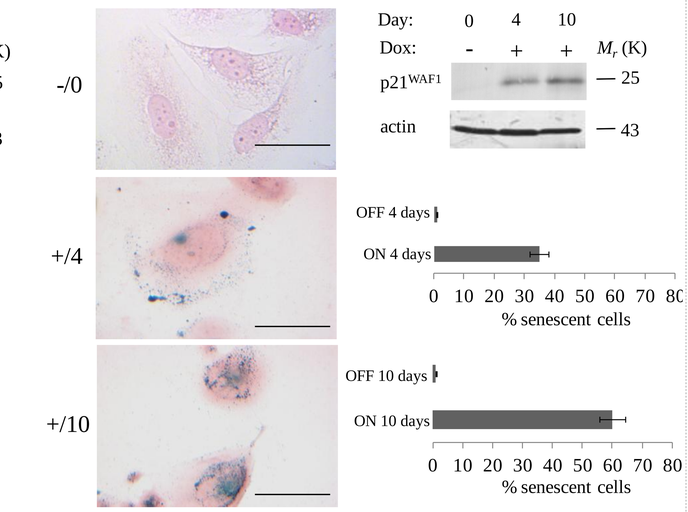
bi.

Saos2 p21^{WAF1} Tet-ON



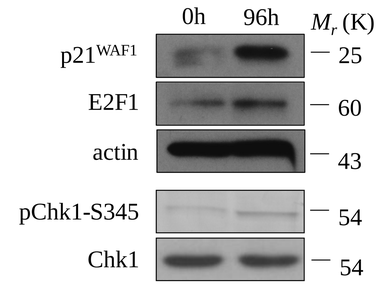
bii.

Li-Fraumeni p21^{WAF1} Tet-ON



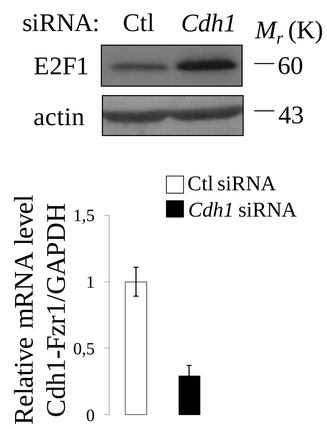
ci.

Saos2 p21^{WAF1} Tet-ON



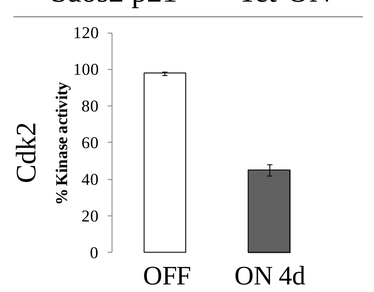
cii.

H1299



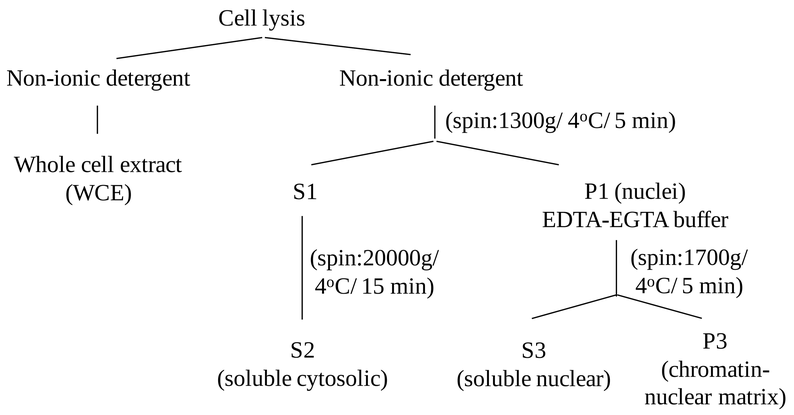
ciii.

Saos2 p21^{WAF1} Tet-ON



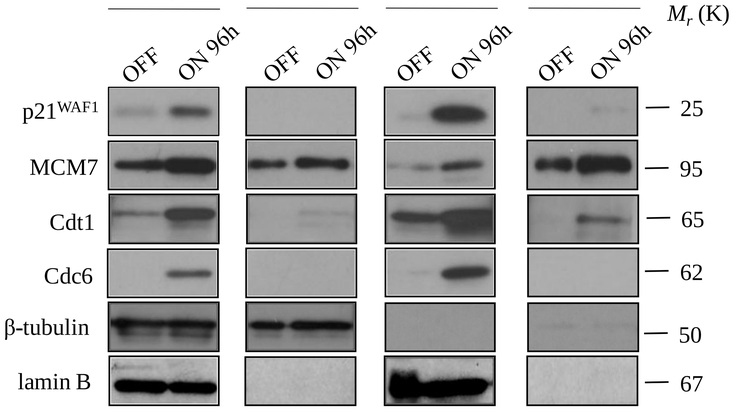
di.

Saos2/Li-Fraumeni p21^{WAF1} Tet-ON



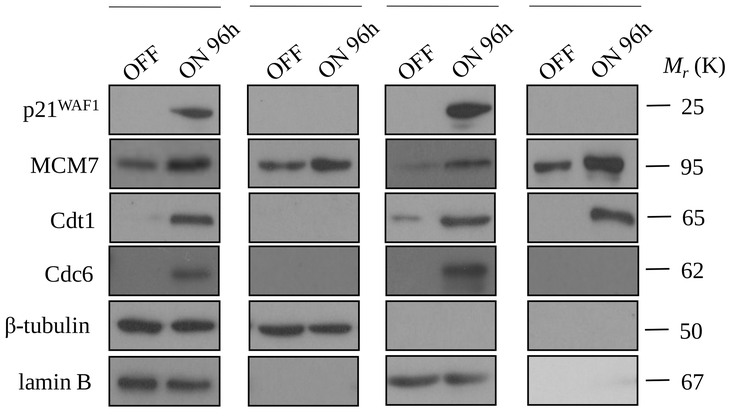
dii.

Saos2 p21^{WAF1} Tet-ON



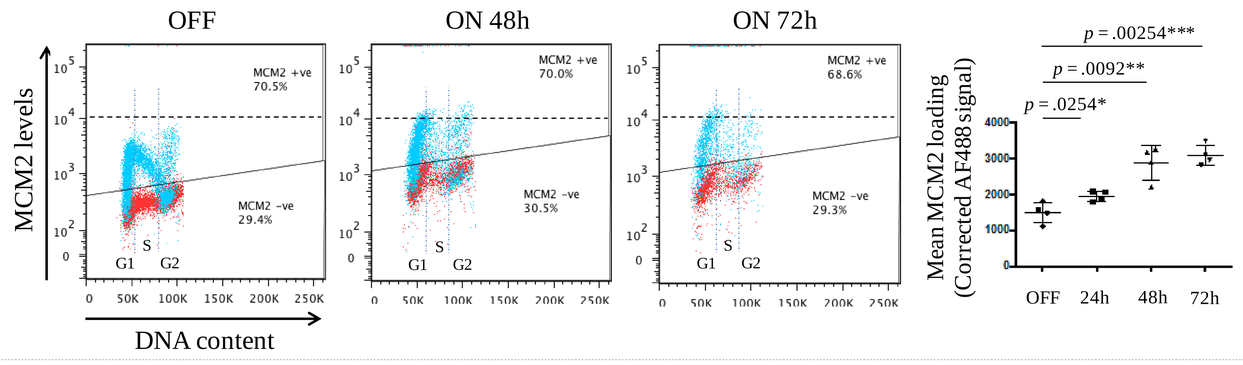
diii.

Li-Fraumeni p21^{WAF1} Tet-ON



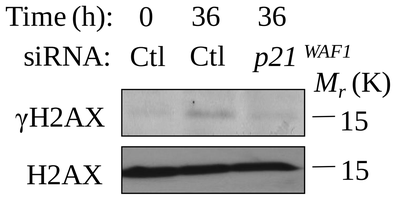
div.

Saos2 p21^{WAF1} Tet-ON



eiii.

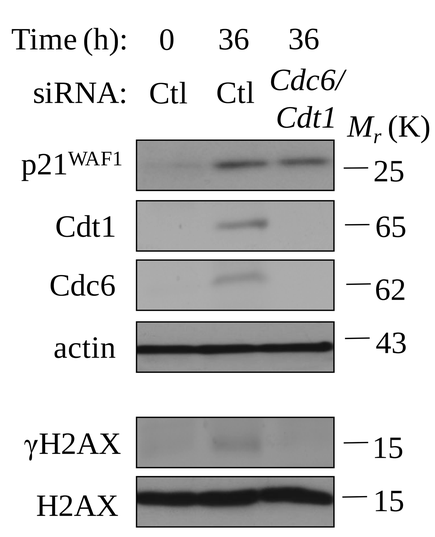
Saos2 + TGF-β



* This panel is complementary to panel **d** of **Figure 3**

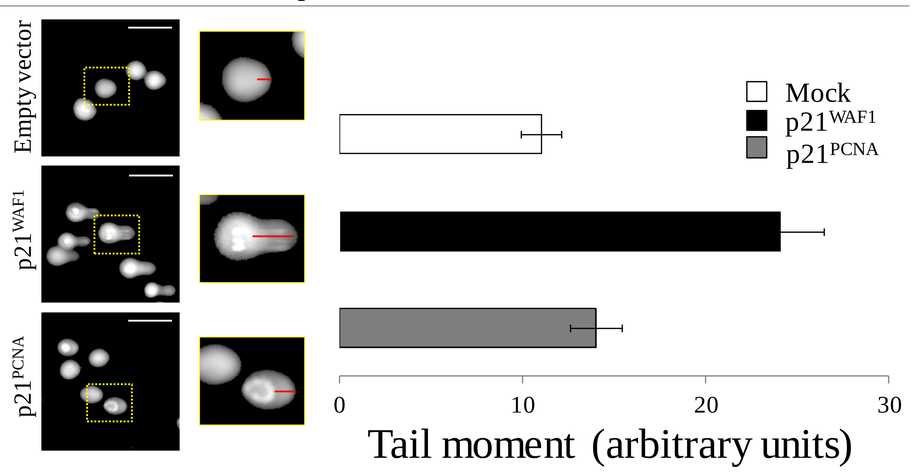
eiv.

Saos2 + TGF-β

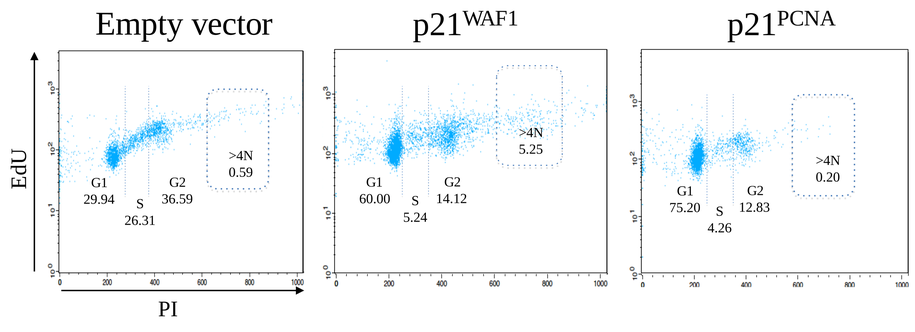


ei.

Saos2 p21^{WAF1} Tet-ON



eii.



Suppl. Figure 2

ai.

Time-line and manipulations

p21^{WAF1} siRNA: 1st round 2nd round 3rd round

p21^{WAF1} inductions (day): 0 1 4 7 10

aii.

Saos2 p21^{WAF1} Tet-ON

Cell collection and immunoblot analysis: 0 d OFF ctr si; 0 d OFF si p21; 1 d ON no si; 1 d ON ctr si; 4d ON si p21; 10 d ON si p21

p21^{WAF1}, Cdt1, Cdc6, actin

0 d OFF ctl si; 1 d ON ctl si; 10 d ON si p21

p21^{WAF1}, 53BP1, DAPI

10d OFF ctr si; 10d ON si p21

Tail moment (arbitrary units)

% senescent cells

Taxol; Doxorubicin; Cis-platin

IC$_{50}$ (µg/ml)

aiii.

Li-Fraumenip21^{WAF1} Tet-ON

Cell collection and immunoblot analysis: 0 d OFF ctr si; 0 d OFF si p21; 1 d ON no si; 1 d ON ctr si; 4d ON si p21; 10 d ON si p21

p21^{WAF1}, Cdt1, Cdc6, actin

0 d OFF ctl si; 1 d ON ctl si; 10 d ON si p21

p21^{WAF1}, 53BP1, DAPI

10d OFF ctr si; 10d ON si p21

Tail moment (arbitrary units)

% senescent cells

Taxol; Doxorubicin; Cis-platin

IC$_{50}$ (µg/ml)

b.

Saos2 p21^{WAF1} Tet-ON

PCNA Patterns

Early S-Phase; Mid S-Phase; Late S-Phase; G1/G2 phases

OFF: PCNA, p21^{WAF1}, DAPI

ON 96h: PCNA, p21^{WAF1}, DAPI

% PCNA positive cells

OFF; ON 96h

early-S; mid-S; late-S; G1-G2

c.

Saos2 p21^{WAF1} Tet-ON

OFF; ON 96 h; OFF HU, ATRi

BrdU; p21^{WAF1}; DAPI

Tail moment (arbitrary units)

OFF; 8 days; 30 days

di.

Saos2 p21^{WAF1} Tet-ON

96h ON

53BP1; p21^{WAF1}; DAPI

Ctl siRNA; *Mus81* siRNA

γH2AX; p21^{WAF1}; DAPI

Ctl siRNA; *Mus81* siRNA

ON96h+Ctl siRNA

ON96h +*MUS81* siRNA

dii.

OFF; 8 days; 30 days

diii.

Li-Fraumenip21^{WAF1} Tet-ON

OFF 96h; ON 96h

siRNA: Ctl; *Rad51*; Ctl; *Rad51*

M_r (K)

p21^{WAF1}, Rad51, γH2AX, H2AX, actin

Ctl siRNA

Rad51 siRNA

Ratio γH2AX/H2AX (arbitrary units)

OFF ON 96h

dv.

Li-Fraumeni p21^{WAF1} Tet-ON

TP73; EGR-1

OFF; Esc; M_r (K)

EGR-1, actin

OFF; "escaped" (ON)

Relative mRNA level/PBGD

dvi.

Li-Fraumeni p21^{WAF1} Tet-ON

TP73; *EGR-1*

OFF; Esc; M_r (K)

EGR-1, actin

OFF; "escaped" (ON)

Relative mRNA level/PBGD

dvii.

Potential mechanism for p73 down-regulation

OFF: EGR-1 → P1-*TP73α* → **p73** → *PRKACB*; HECW2 → p73

Esc (ON): EGR-1 ✕ → P1-*TP73α* ✕ → p73 → *PRKACB*; HECW2 → p73

ei.

Saos2 p21^{WAF1} Tet-ON

% Kinase activity

OFF; ON 4d; ON 20d (escaped)

ON

OFF; 1d; 2d; 4d; 20d (escaped)

p21^{WAF1}, actin

M_r (K)

eii.

Li-Fraumenip21^{WAF1} Tet-ON

ON

OFF; 10d; 20d (escaped)

p21^{WAF1}, actin

M_r (K)

fi.

Saos2 p21^{WAF1} Tet-ON

TP73 promoter methylation

Saos2: OFF; Esc

Ctl DNA: Methylated; Unmethylated

Melt Curve

Temperature (°C)

fii.

EGR1; TP73; HECW2; PRKACB

fiii.

a; b; c; d; e(←EGR-1 binding sites)

P1

TP73α 5' 1 2 3 14 3'

HECW2; 636 aa

TDA; DBD; OD; SAM

PRKACB; PRKACB

fiv.

Saos2 p21^{WAF1} Tet-ON

OFF; "escaped" (ON)

TP73; *EGR-1*; *HECW2*; *PRKACB*

Relative mRNA level/PBGD

fv.

Saos2 p21^{WAF1} Tet-ON

OFF; Esc; M_r (K)

EGR-1, actin

HECW2, actin

PRKACB, p-CREB, actin

fvi.

Li-Fraumeni p21^{WAF1} Tet-ON

TP73; *EGR-1*

OFF; Esc; M_r (K)

EGR-1, actin

OFF; "escaped" (ON)

Relative mRNA level/PBGD

g.

Ki67; p21^{WAF1}; Cdt1

Head&Neck Ca; Urothelial Ca

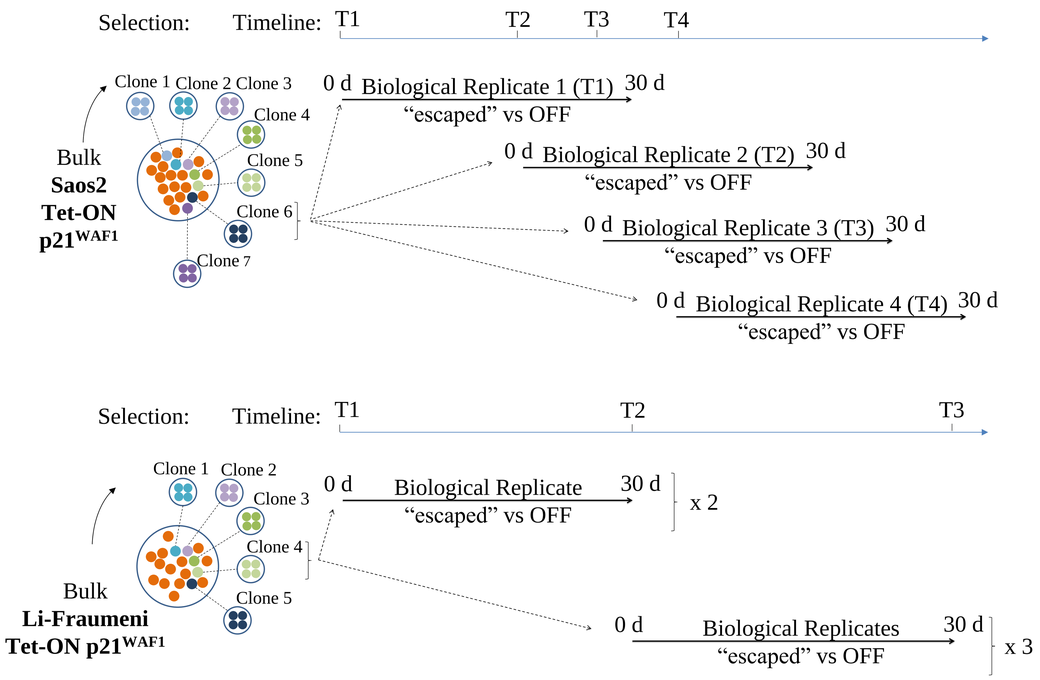
Ki67; p21^{WAF1}; Cdc6

Precancerous

Supplementary Figure 3

a.

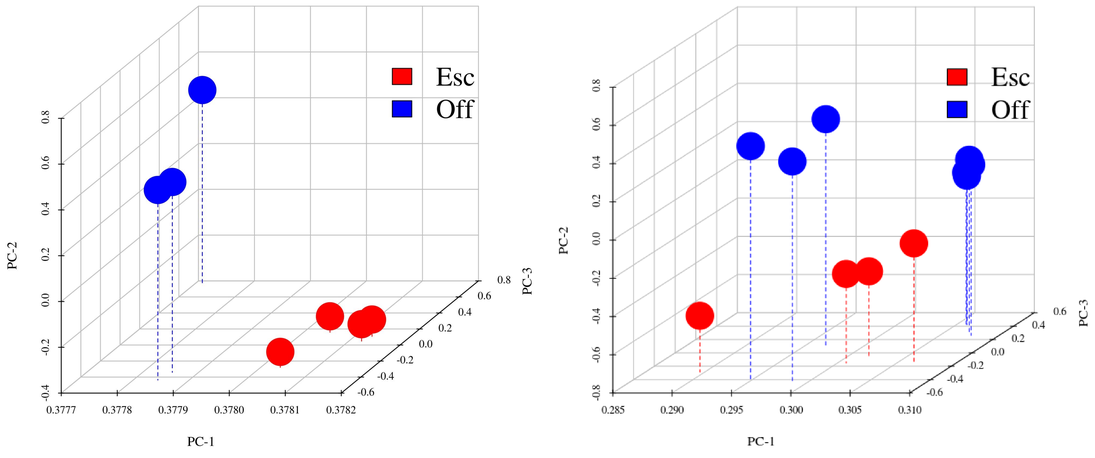
Experimental plan of transcriptomic analyses



Notes:
i. T(1-4): initiation time–point for each independent biological replicate
ii. Experimental duration of each biological replicate: 30 d

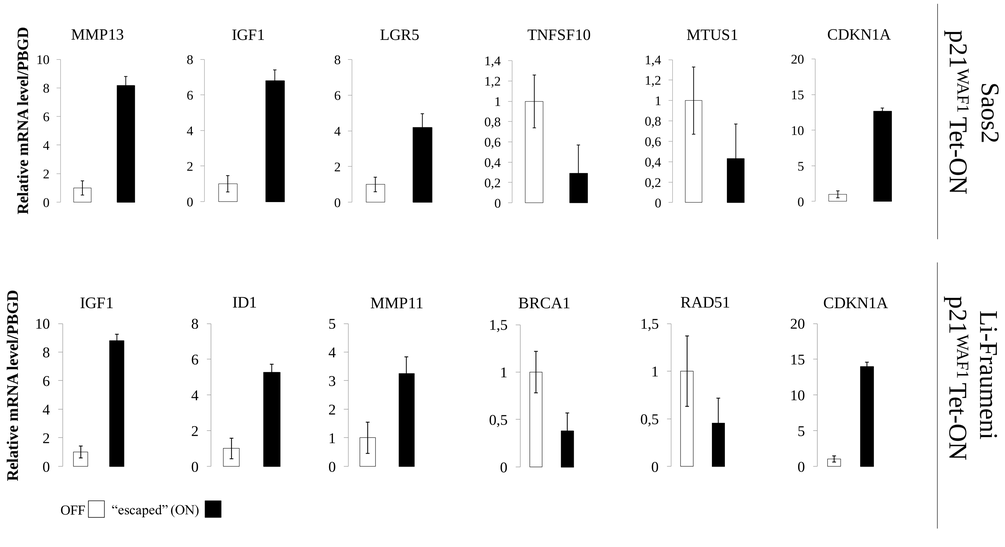
b.

Principal component analysis (PCA):
Majorly different gene expression signatures



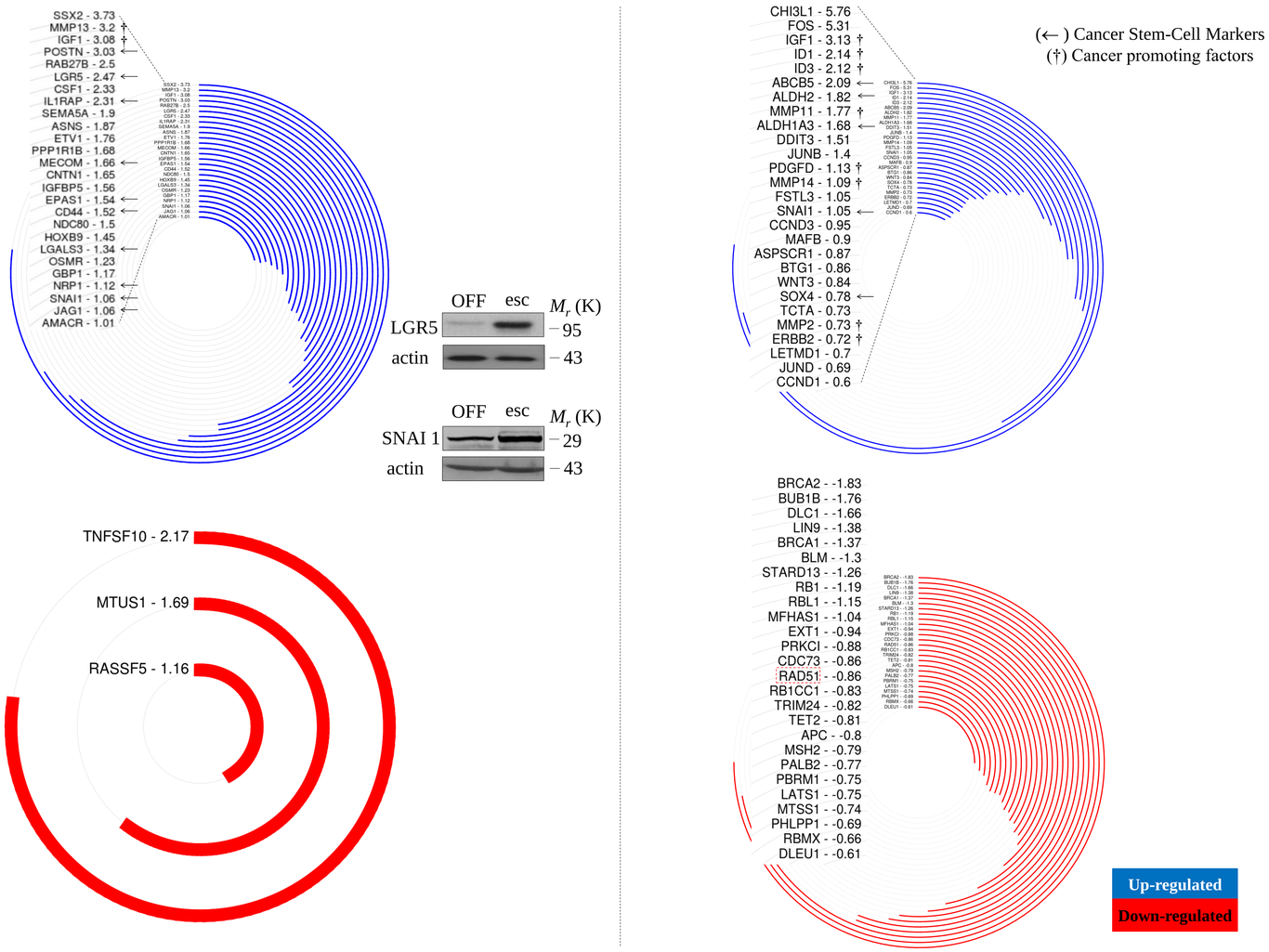
c.

Representative gene validations



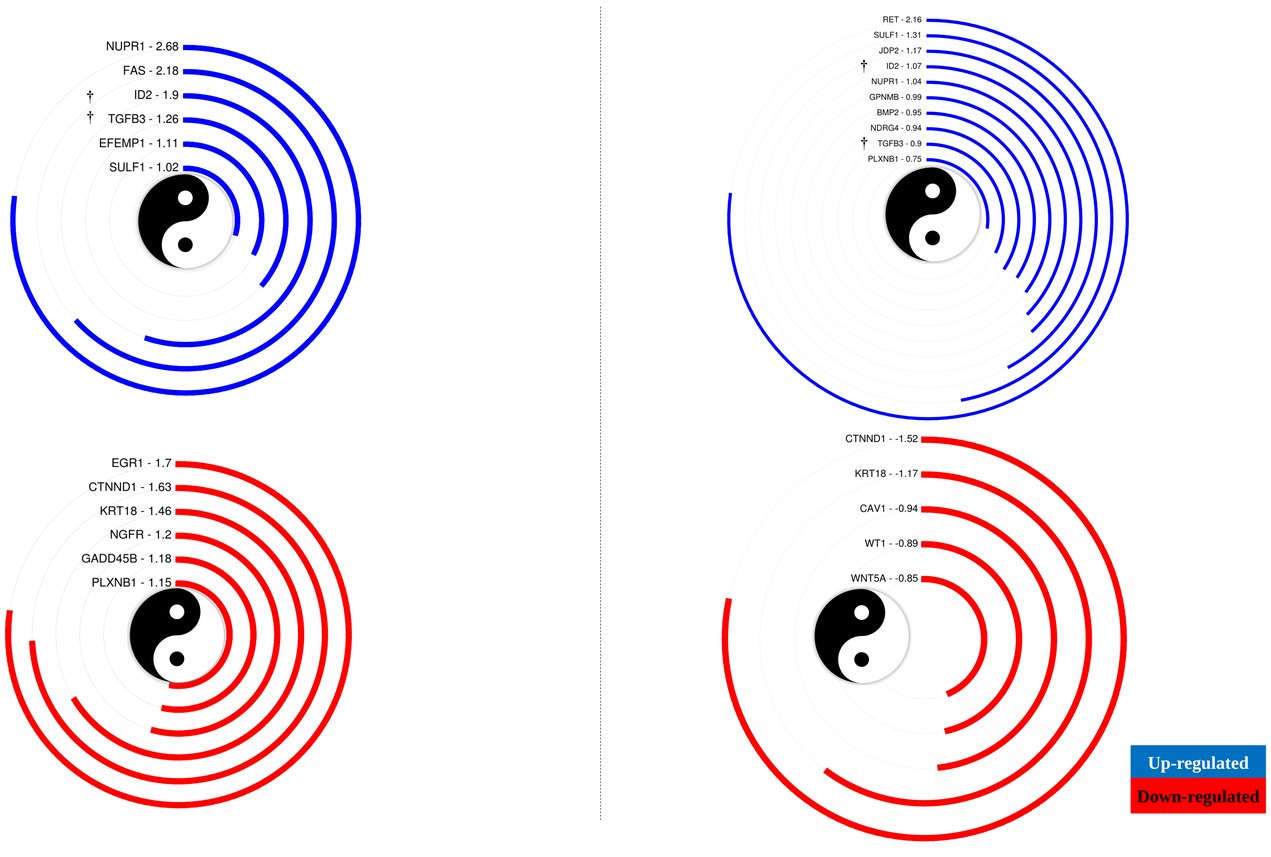
d.

Expression status of genes linked with cancer progression



e.

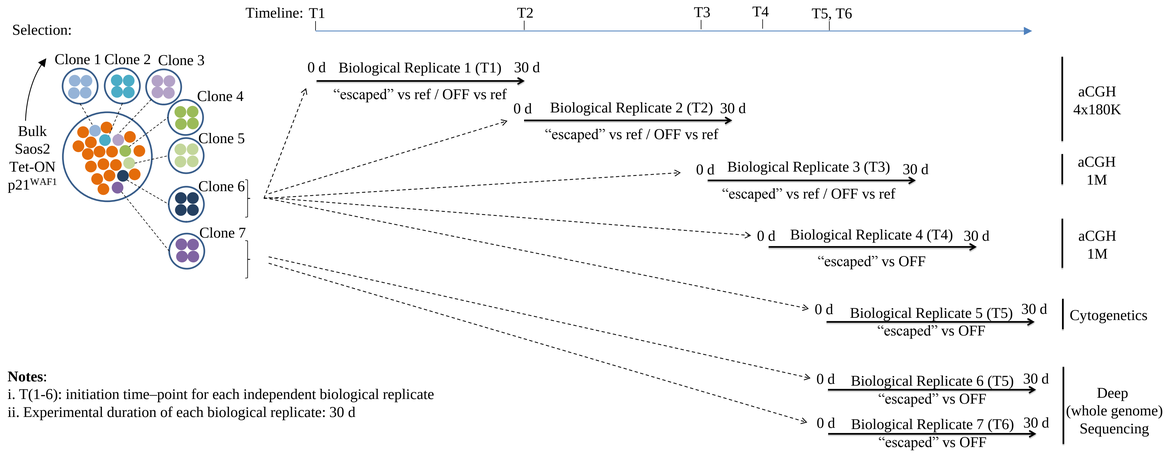
Yin-Yang Genes. Expression status either promotes or suppresses cancer



Suppl. Figure 4

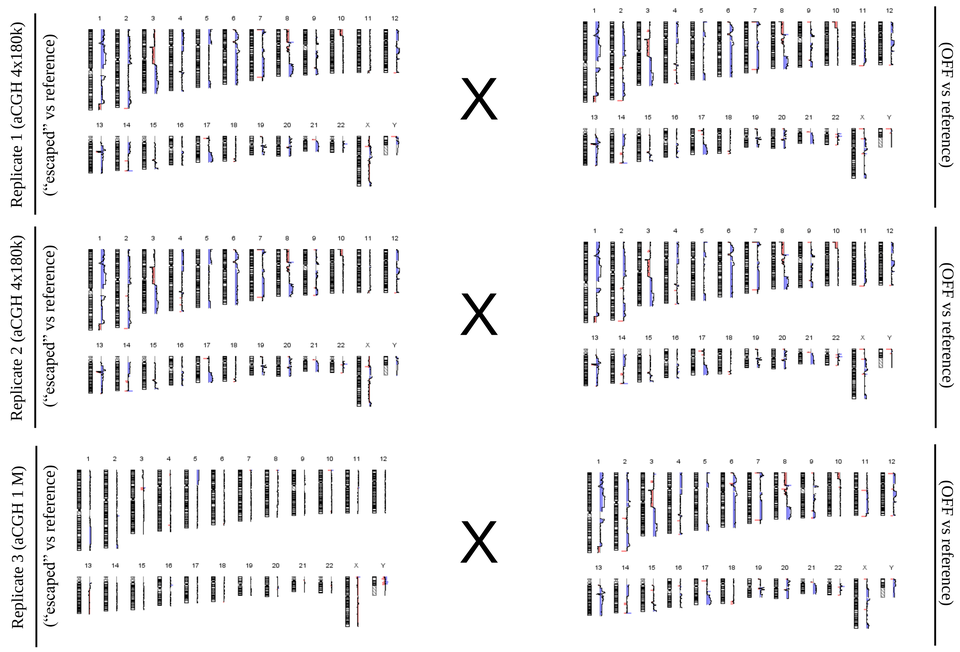
Saos2 Tet-ON p21^{WAF1}

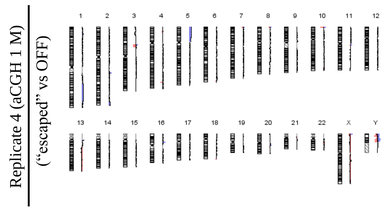
a. Experimental plan of genomic analyses



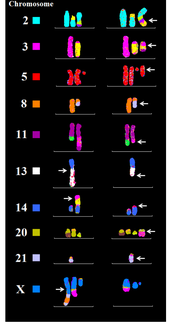
Notes:
i. T(1-6): initiation time–point for each independent biological replicate
ii. Experimental duration of each biological replicate: 30 d

b. aCGH biological replicates (see panel a)

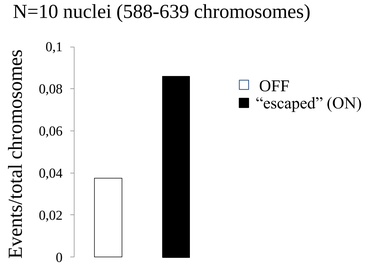




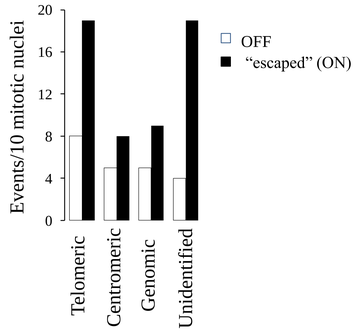
c. Novel clonal rearrangements



d. Cytogenetically defined aberrations

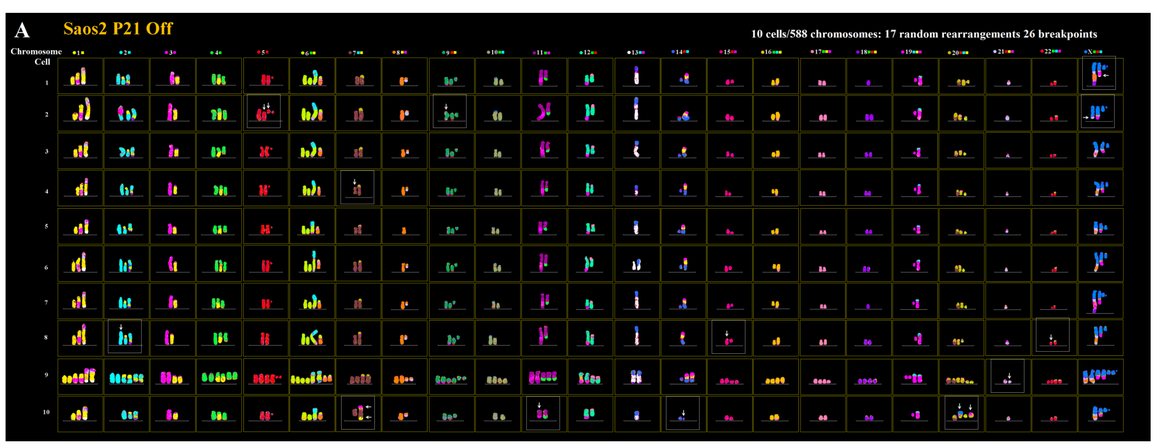


e.

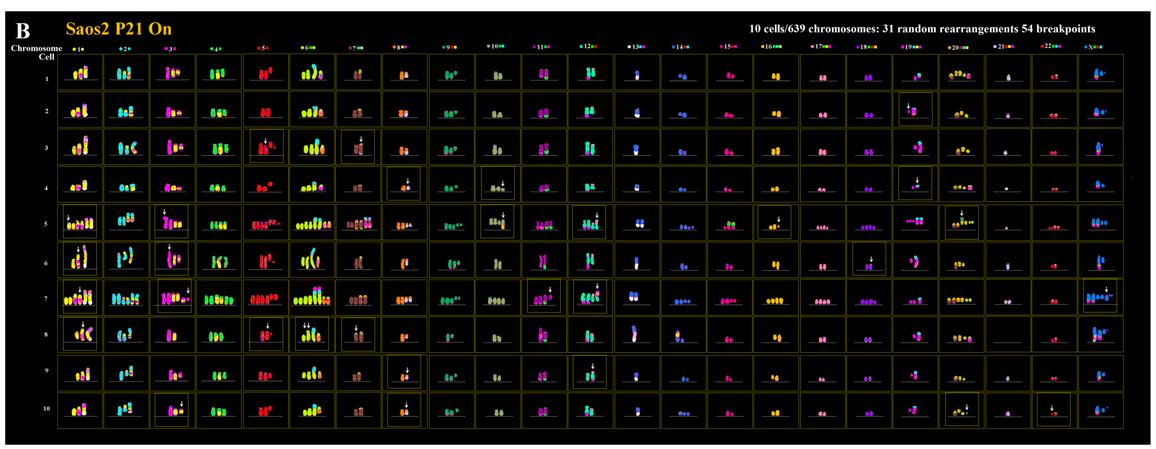


f. Novel random cytogenetic aberrations

Saos2 p21^{WAF1} Tet-ON: OFF



Saos2 p21^{WAF1} Tet-ON: "escaped" (ON)

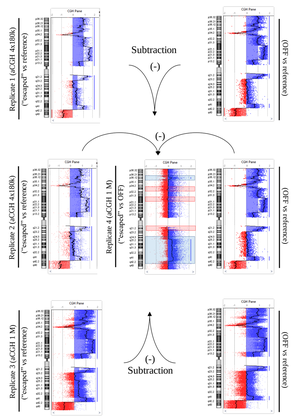


Suppl. Figure 5

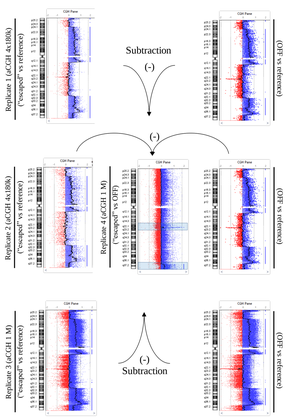
Correlation between aCGH replicates and corroboration with cytogenetically detectable novel clonal alterations in Saos2 p21^{WAF1} Tet-ON*

Gaines
Losses

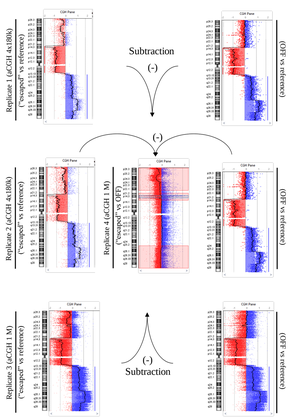
Chromosome 1



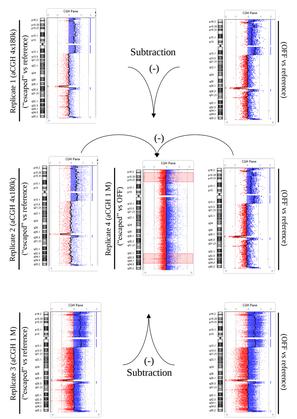
Chromosome 2



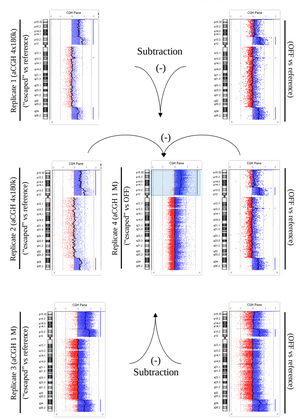
Chromosome 3



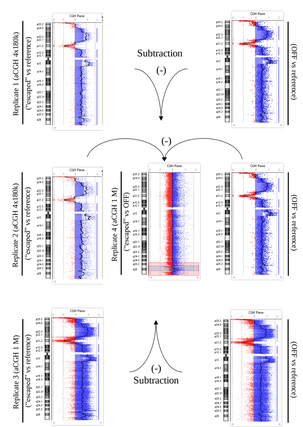
Chromosome 4



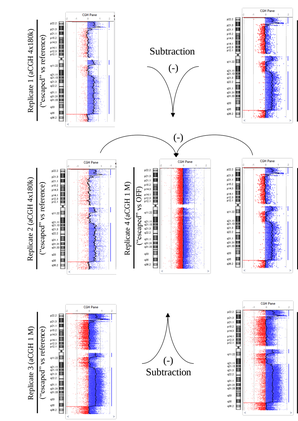
Chromosome 5



Chromosome 6

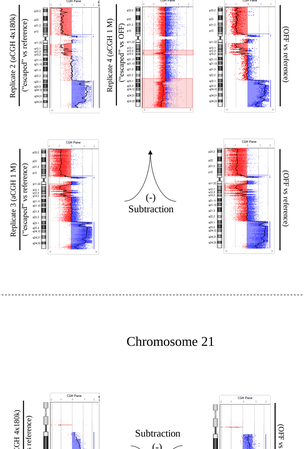


Chromosome 7

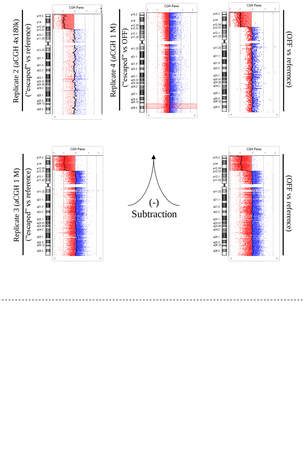


Submicroscopic changes:
7p22.3

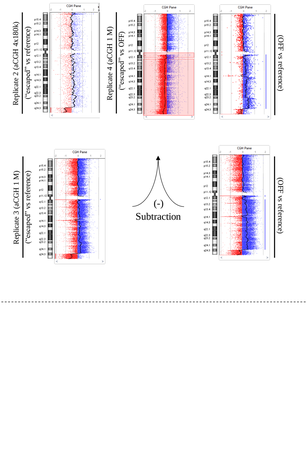
Chromosome 8



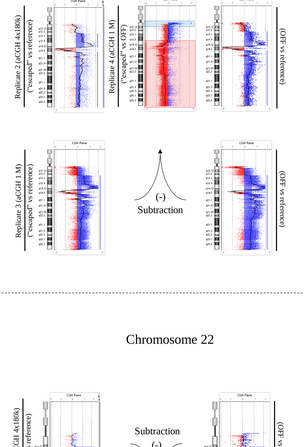
Chromosome 10



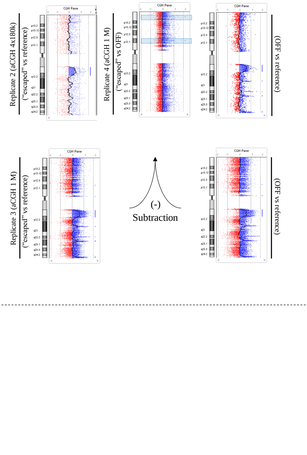
Chromosome 11



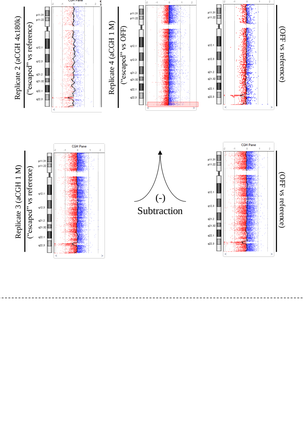
Chromosome 13



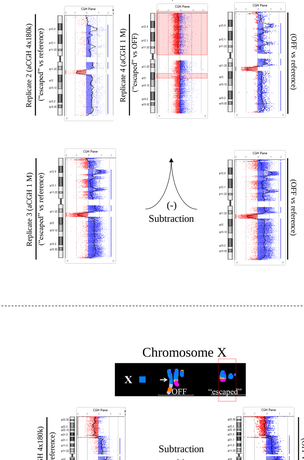
Chromosome 16



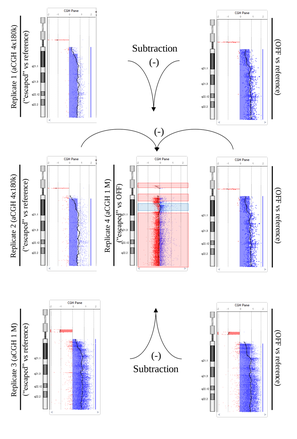
Chromosome 18



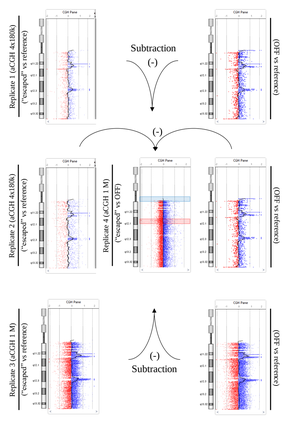
Chromosome 20



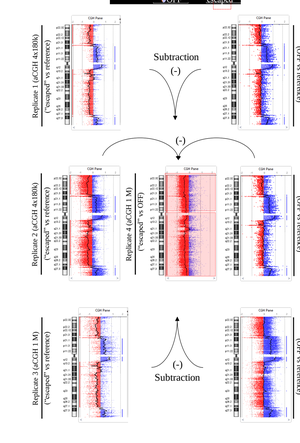
Chromosome 21



Chromosome 22



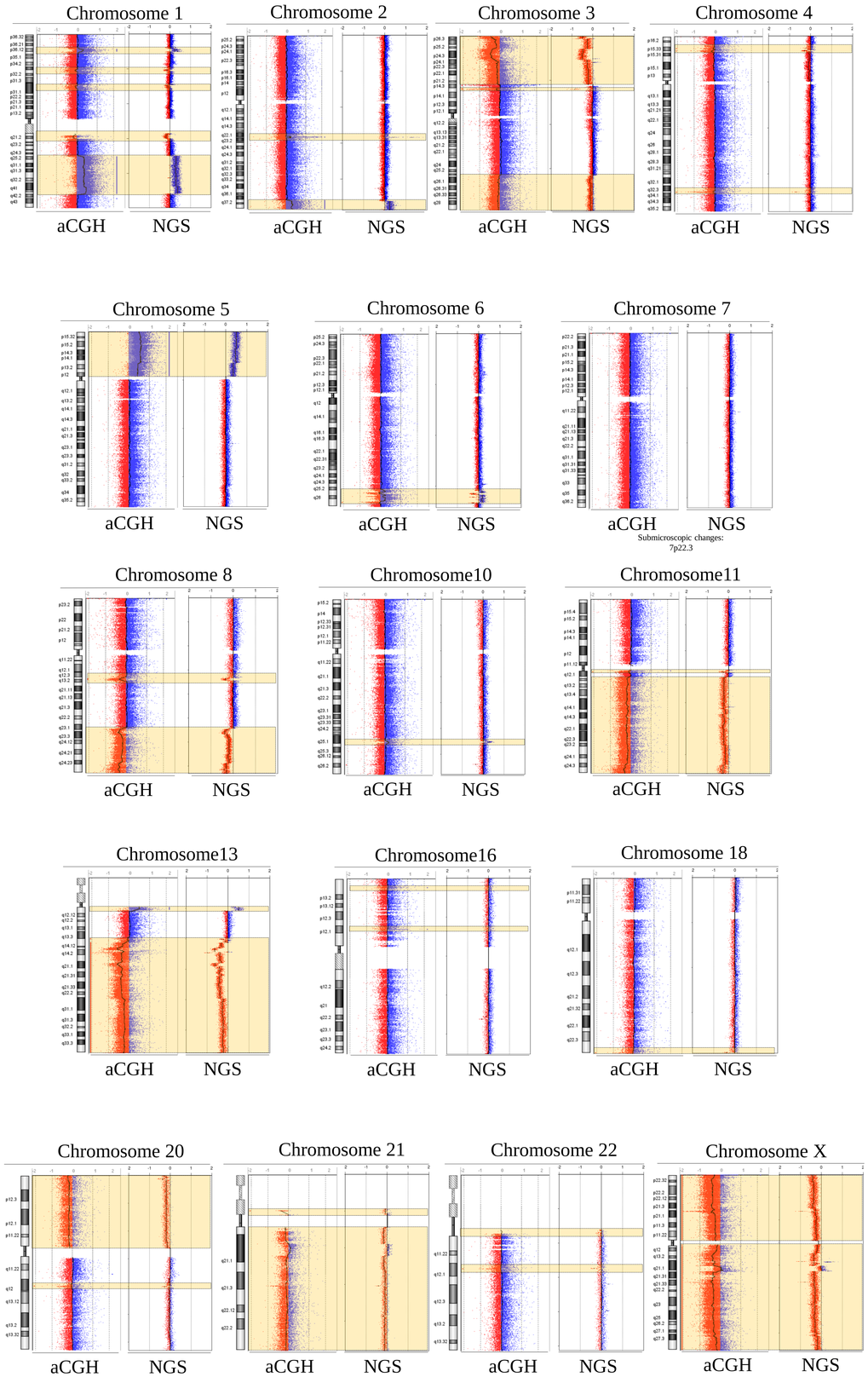
Chromosome X



Suppl. Figure 6

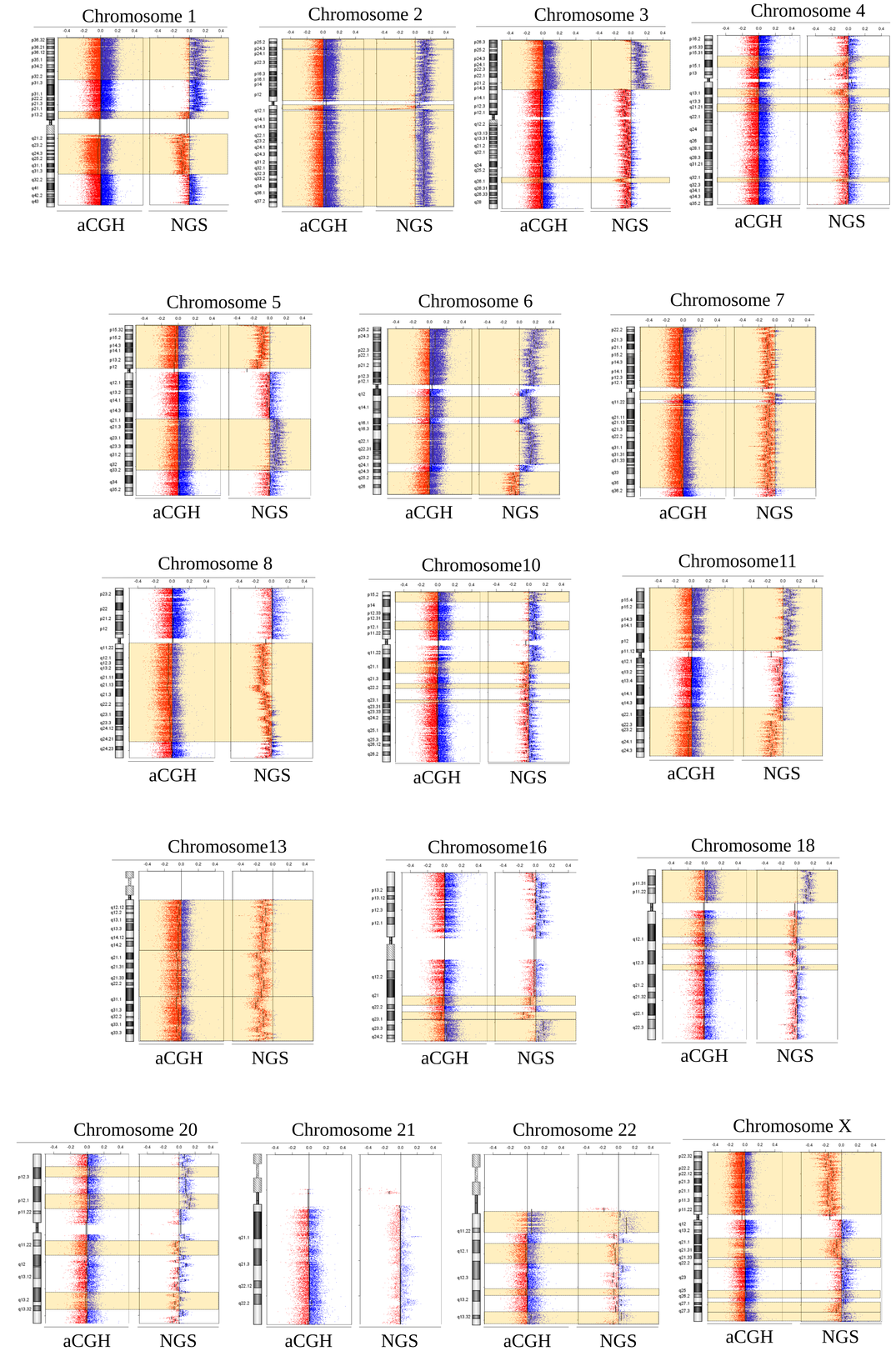
a.

Concordance between aCGH and NGS analyses in Saos2 p21^{WAF1} Tet-ON cells



b.

Concordance between aCGH and NGS analyses in Li-Fraumeni p21^{WAF1} Tet-ON cells



Suppl. Figure 7

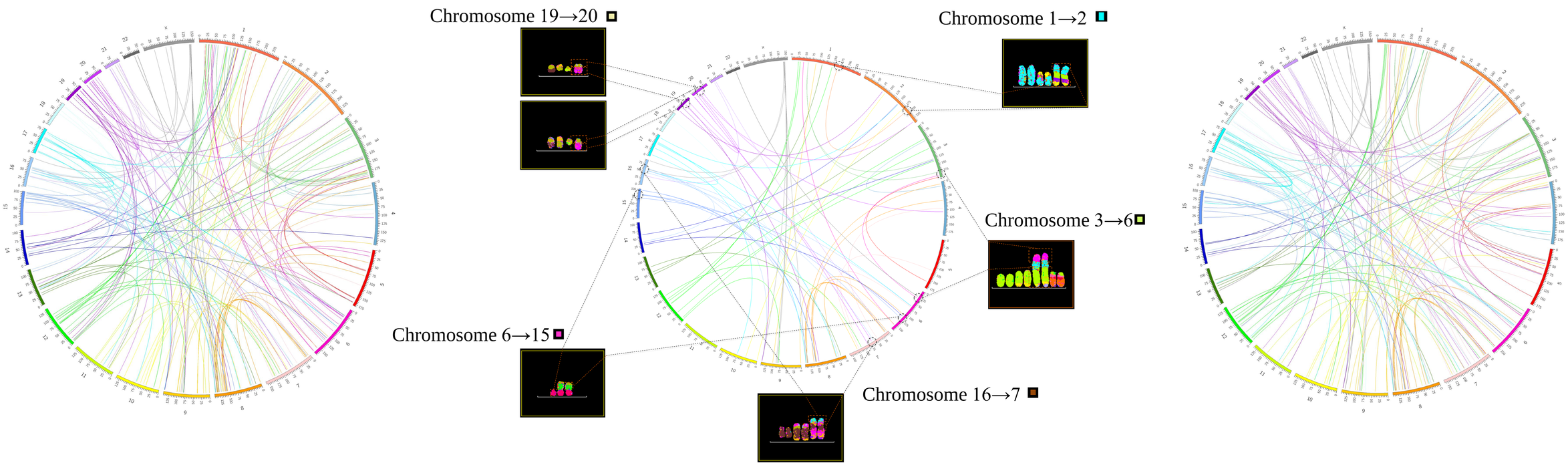
a.

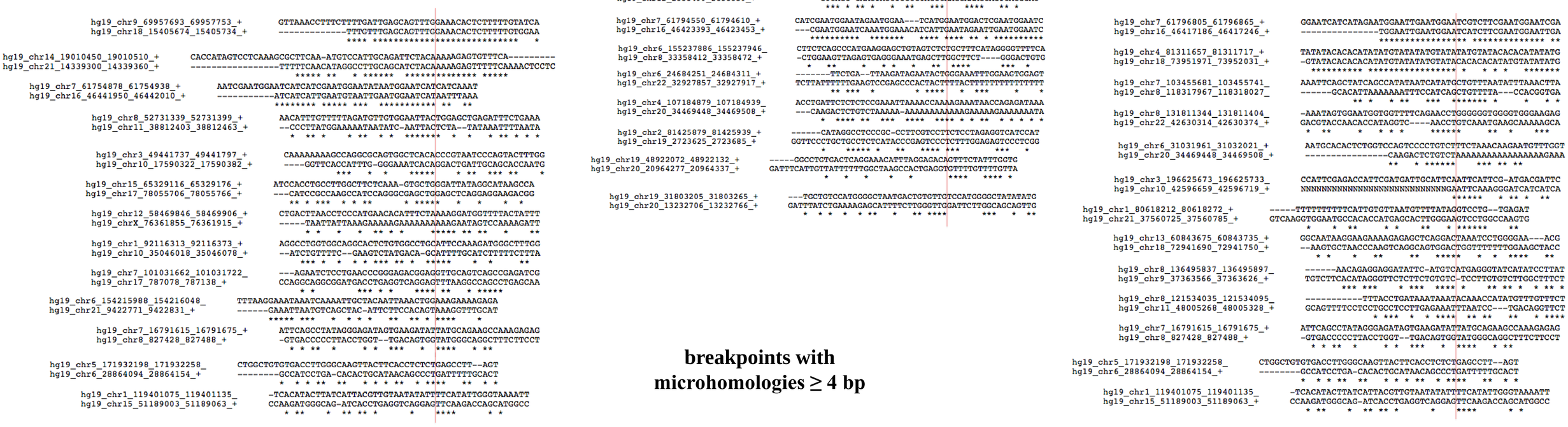
Saos2 p21^{WAF1} Tet-ON

175 breakpoints – 1st replicate (102 fragile sites)
breakpoints with microhomologies: 120 (68.57%)

71 common breakpoints (40 fragile sites)
breakpoints with microhomologies: 50 (70.42%)

152 breakpoints – 2nd replicate (78 fragile sites)
breakpoints with microhomologies: 105 (69.08%)





breakpoints with microhomologies ≥ 4 bp

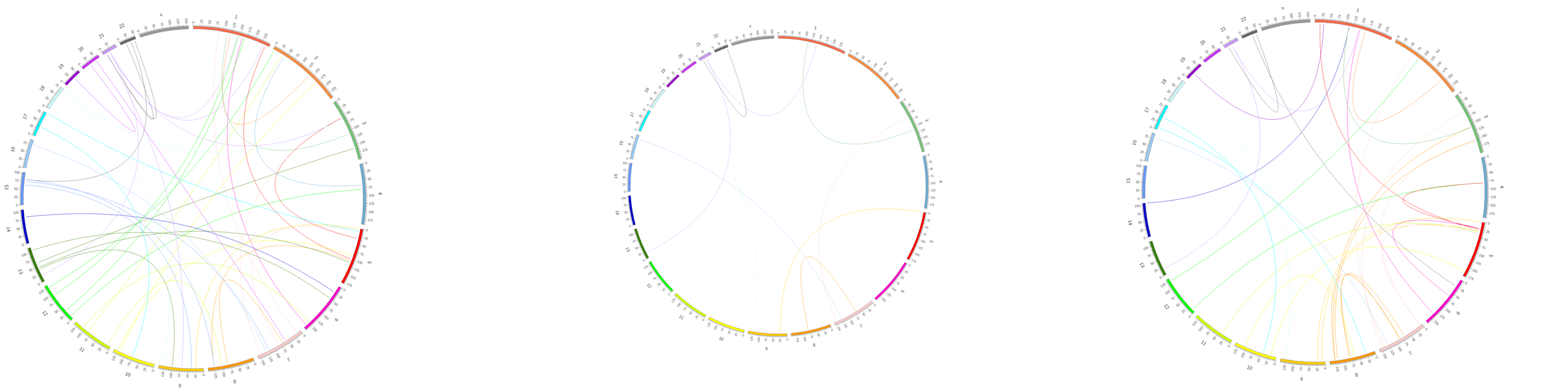
b.

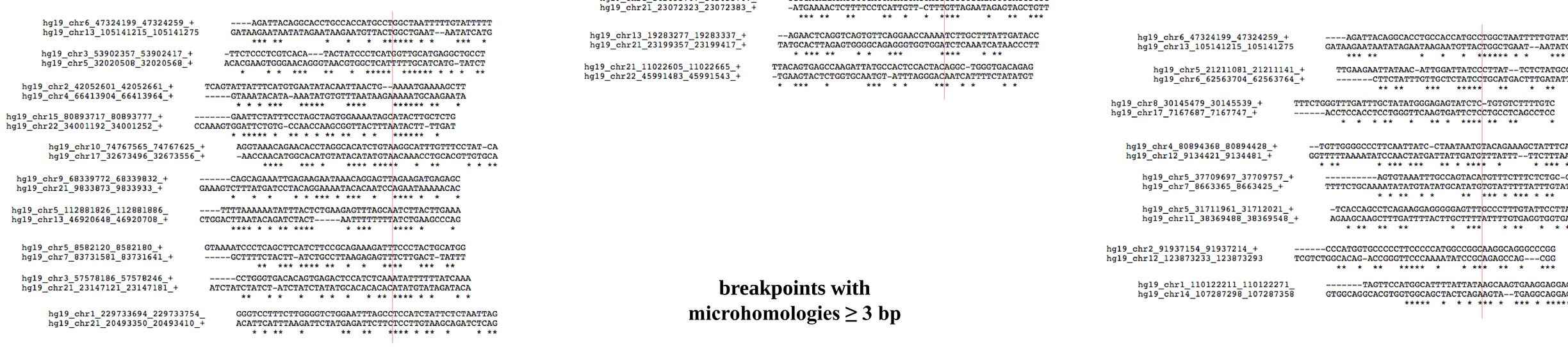
Li-Fraumeni p21^{WAF1} Tet-ON

44 breakpoints – 1st replicate (24 fragile sites)
breakpoints with microhomologies: 35 (79.55%)

9 common breakpoints (4 fragile sites)
breakpoints with microhomologies: 7 (77.77%)

34 breakpoints – 2nd replicate (19 fragile sites)
breakpoints with microhomologies: 24 (70.59%)

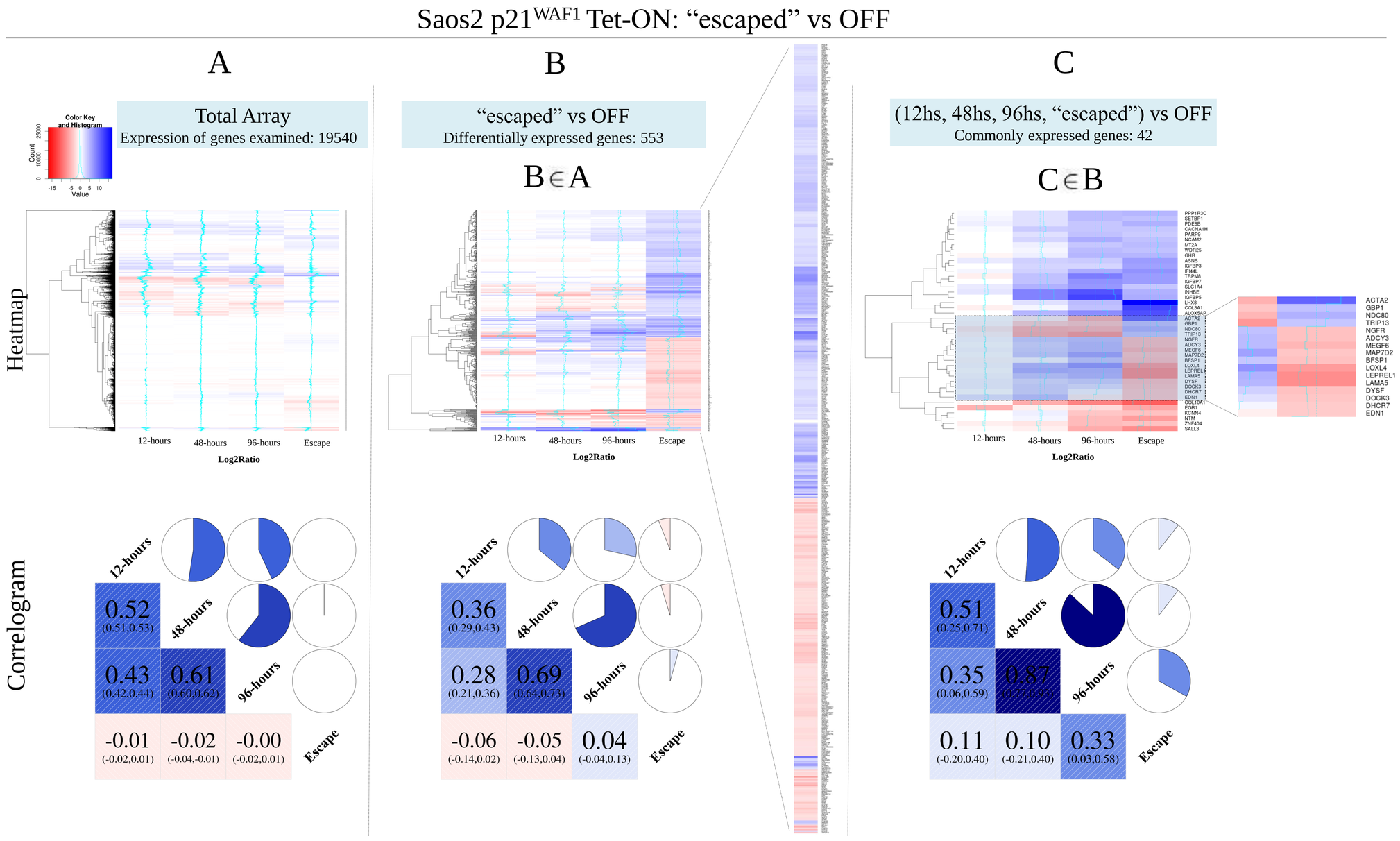




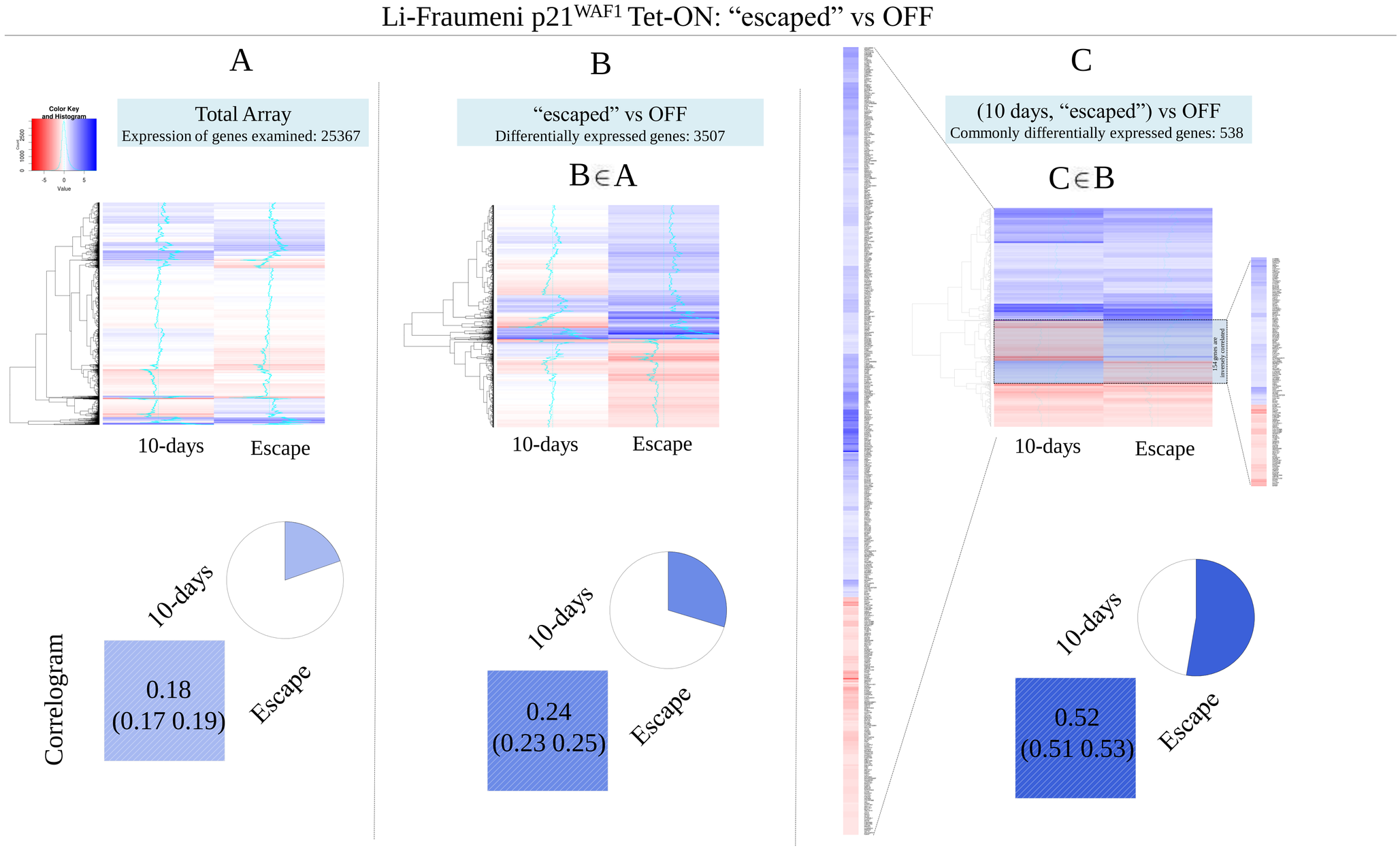
breakpoints with microhomologies ≥ 3 bp

Suppl. Figure 8

a.



b.



c.

